UNIVERSITY OF SOUTHAMPTON

FACULTY OF ENGINEERING AND APPLIED SCIENCE

ELECTRONICS AND COMPUTER SCIENCE

FIBRE-OPTIC PRESSURE SENSOR FOR DOWNHOLE MONITORING IN THE OIL INDUSTRY

by

JOHN REDVERS CLOWES

A Thesis submitted for the degree of
Doctor of Philosophy.

January 2000

UNIVERSITY OF SOUTHAMPTON

ABSTRACT

FACULTY OF ENGINEERING AND APPLIED SCIENCE

ELECTRONICS AND COMPUTER SCIENCE

Doctor of Philosophy

FIBRE OPTIC PRESSURE SENSOR FOR DOWNHOLE MONITORING IN THE OIL INDUSTRY

by John Redvers Clowes

Cost-effective oil and gas production is becoming more important than ever. The availability of downhole information is seen to be the key to increasing oil-recovery efficiency, currently estimated to be 35% on average for North Sea oil-wells.

Fibre-optic sensors have the potential to measure many downhole parameters. However, high-temperature, high-pressure (HTHP) fluids are shown to have adverse effects on fibre pressure-sensors and cables. All unprotected, silica-fibre, pressure sensors drift in HTHP fluids. Furthermore, optical-fibre cables fail in HTHP fluids.

Diffusion of molecular water from HTHP fluids into silica fibres is shown to be the root cause of drift and damage to fibre sensors and cables. Ingress of molecular water into the fibre causes expansion of the silica and results in highly stressed regions of the fibre.

A carbon and polyimide coating process is identified as a suitable hermetic coating for fibre-optic cables in downhole conditions. However, this coating is shown to be inadequate for protecting optical-fibre pressure sensors.

A novel coating technology is developed, in which the sensor is sleeved in a silica capillary, which is filled with a liquid metal. The packaging technique improves the stability of side-hole-fibre pressure sensors to better than 0.1psi per month at temperatures up to 300°C.

The pressure sensor developed in this thesis (the SD-series sensor) is tested in a field trial at Chevron's Coalinga test facility in California.

The SD-series pressure sensor out-performs any existing downhole pressure gauge in the world and is to be made commercially-available to the global oil industry in the year 2000.

Contents

Chapter 1

Introduction

1.1 Downhole Monitoring in the Oil Industry.

1.1.1 The Global Oil Crisis: Oil Production in the 21st Century.

In 2010, according to forecasts, the world's economies will demand about 10 billion more barrels of oil than the global oil industry will be able to produce [1, 2].

Cost-effective oil production is becoming more important than ever, not only to the profit- making oil corporations and nations, but also to the individual people of the world.

Advances in technology are required in key areas of the oil industry, most notably in reservoir exploration and in oil-well production-management, to increase yield and profit. The application of new technology in oil refinery processes and in monitoring and preventing leaks in oil and gas transport pipelines will also have an impact on future global oil production.

In the early days of the oil industry, oil explorationists would guess the location of sub-surface reservoirs by recognising surface features that marked their presence [3]. Today, however, the majority of these shallow oil traps have been exploited and explorationists must now seek oil in deep and offshore reservoirs.

The rock beneath the North Sea is seen to be a rich source of such oil reservoirs. However, until recently, only one in three of the exploration wells drilled there found oil or gas [4]. Considering the remote locations of such reservoirs and the logistics and expense of offshore drilling, these "missed wells " add significant cost to the development of successfully located reserves.

The application of new technology in the form of seismic surveying, 3-dimensional imaging and virtual reality can now allow geologists to pin point where to drill for oil with high accuracy [1]. This significantly reduces the number of exploration wells that need to be drilled and allows for more careful planning and drilling of development wells.

On average, the recovery from typical North Sea wells is estimated to be between 35% and 40% of the original oil in place. This leaves the majority of reserves behind

irretrievably. The vision of the reservoir engineer is to be able to recover as much of the hydrocarbon in place until production ceases to be cost-effective. Experts now predict that this value can be increased to 60% or 70% by improving reservoir management techniques.

One of the key elements to improved reservoir management, is seen to be the availability of permanent downhole information. The key is better prediction and control of the distribution and movement of oil, gas and water within the reservoir.

1.1.2 Oil Field Development

1.1.2.1 The Completed Development Well.

Figure 1.1.1 is a schematic of a simplified, vertical, completed well showing the key components.

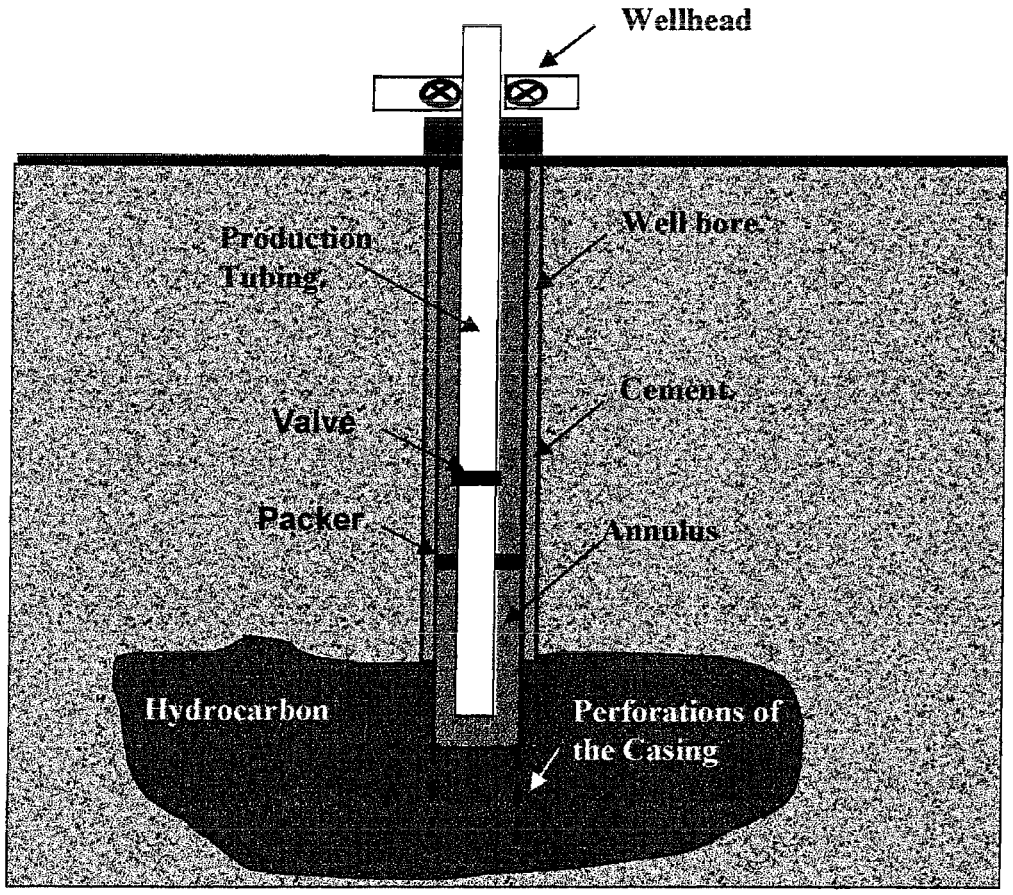

Figure 1.1.1: Schematic of a simplified, vertical, completed well showing the major components and construction.

The generalised structure and construction stages are as follows:

- The well bore is drilled.
- The casing is lowered (section by section) into the well bore and is set in place by pouring cement into the annulus surrounding the casing.
- The production tubing is lowered (section by section) into the casing.
- A packer is positioned in the annulus between the production tubing and casing (referred to as the annulus) at a point above the intended production zone. A packer is a solid unit of rubber that expands when the weight of the production tubing is set down onto it. This forms a seal and isolation between the production zone and the annulus.
- A test valve is positioned within a section of the production tubing somewhat above the packer. This valve can be operated either by a wireline lowered into the production tubing or annulus, or by pressure applied on the annulus.
- The casing is perforated in the production zone. Flow of wellbore fluid from the formation into the production tubing is achieved via the perforated section of the casing.

In many cases, particularly in modern, deep reservoirs, the reservoir is "over pressure" and production is driven by the pressure differential between the well and atmospheric surface pressure. As the well is produced, the downhole pressure falls and eventually the well will become "under pressure".

In "under pressure" wells and in heavy-oil wells, where fluid flow is extremely slow, production is assisted by injecting high-pressure water, steam or a miscible gas into the reservoir from a nearby injector well. Production is also often assisted by gas lift (methane is injected into the production string to lift the hydrocarbon), or by pumping the hydrocarbon with a downhole pump.

1.1.2.2 Well Testing

During the phases of a field's exploration and appraisal and throughout the production lifetime, well testing is a vital activity.

The first stage of well testing after the discovery of a potential reservoir is Well Logging. This is the fundamental method of analysis of the reservoir formation [5]. Well Logging involves the drilling of exploration wells and open-hole analysis to determine

properties such as: rock porosity, hydrocarbon presence and saturation, and general well-productive capacity. They provide the initial analysis that governs whether to develop a reservoir and if so, where to drill initial development wells.

Once a development well has been drilled and completed, there are two major categories of downhole testing, initial and long-term. Initial tests occur immediately after, or during perforation of the casing and long-term tests occur throughout the production lifetime of the well.

Both initial and long-term well tests are designed primarily to yield information concerning, the extent of formation damage around the borehole, reservoir permeability (degree to which the rock conducts fluid) and reservoir heterogeneity (how compartmentalised the reservoir is) [6].

Assessment of the formation damage is critical in maximisation of production-efficiency. Perforation of the well involves blasting holes in the casing within the production zone. This process leads to damage to the rock formation near the well bore, which can reduce the permeability in this region and hence reduce production-efficiency. If the extent of this damage is known, remedial action can be taken to clean up the region.

Assessment of formation damage is achieved using a process called "pressure transient analysis" [7]. In this process, a flowing well is suddenly "shut-in" (the valve above the production zone is closed and flow stops). This step causes pressure to build up due to the flow suddenly being prevented. Oil near the formation is the first to sense the shut-in as it is suddenly stopped in its tracks. Gradually, the pressure builds up throughout the reservoir as the shut-in effects extend to the reservoir boundaries. Eventually the pressure reaches the reservoir pressure that drives production.

Similarly, the procedure can be reversed if the well is opened up and allowed to flow after being shut-in, a "build-up" measurement. Again, oil near the production zone is the first to sense the disturbance and begins to flow. Eventually, oil in the far regions of the reservoir responds and also begins to flow. In the long run, such transients can be achieved during production simply by increasing or reducing the flow rate.

Measurement and analysis of the increase or decrease in well pressure during transient tests, allows the reservoir engineer to determine information about the reservoir from near the wellbore to the reservoir outer-limits.

Measurement of these pressures requires a pressure gauge to be positioned below a test

valve, as close to the production zone as possible. If the distance between the point of shut-in, (the test valve) and the formation is large, compression of the fluid column in this region by the in-flowing formation fluid can take a long time. This effect, known as wellbore storage [6], can seriously affect pressure-transient analysis and therefore must be reduced as far as possible.

Figure 1.1.2 shows three types of build-up pressure-transient tests made during the initial stages of development, the impulse, conventional and interference tests [7].
Impulse testing measures the well transient-response to a very brief flow period, typically just as the production tubing is perforated. The response to an impulse test yields information about the near wellbore condition and permeability, and indicates whether remedial stimulation of the formation is required.

A conventional test measures the build-up response of the reservoir after a lengthy flow period. During the transient test, reservoir boundaries or sealing faults in the rock formation reflect the pressure pulse back towards the well. High-resolution pressure gauges can potentially detect these reservoir limits and allow the reservoir engineer to model the formation in detail and with accuracy.

Finally, an interference test monitors the response of a well to a series of flow transients in a neighbouring well. The response yields details of the inter-well pressure communication and identifies the presence of any flow restrictions such as faults within the rock formation.

Pressure transient analysis plays an extremely important role in well testing during the initial, characterisation-phase of production. The data they produce results in a better knowledge of the reservoir for future decision-making. Measurement of the pressure during this phase of downhole pressure monitoring requires gauges with high accuracy and resolution.

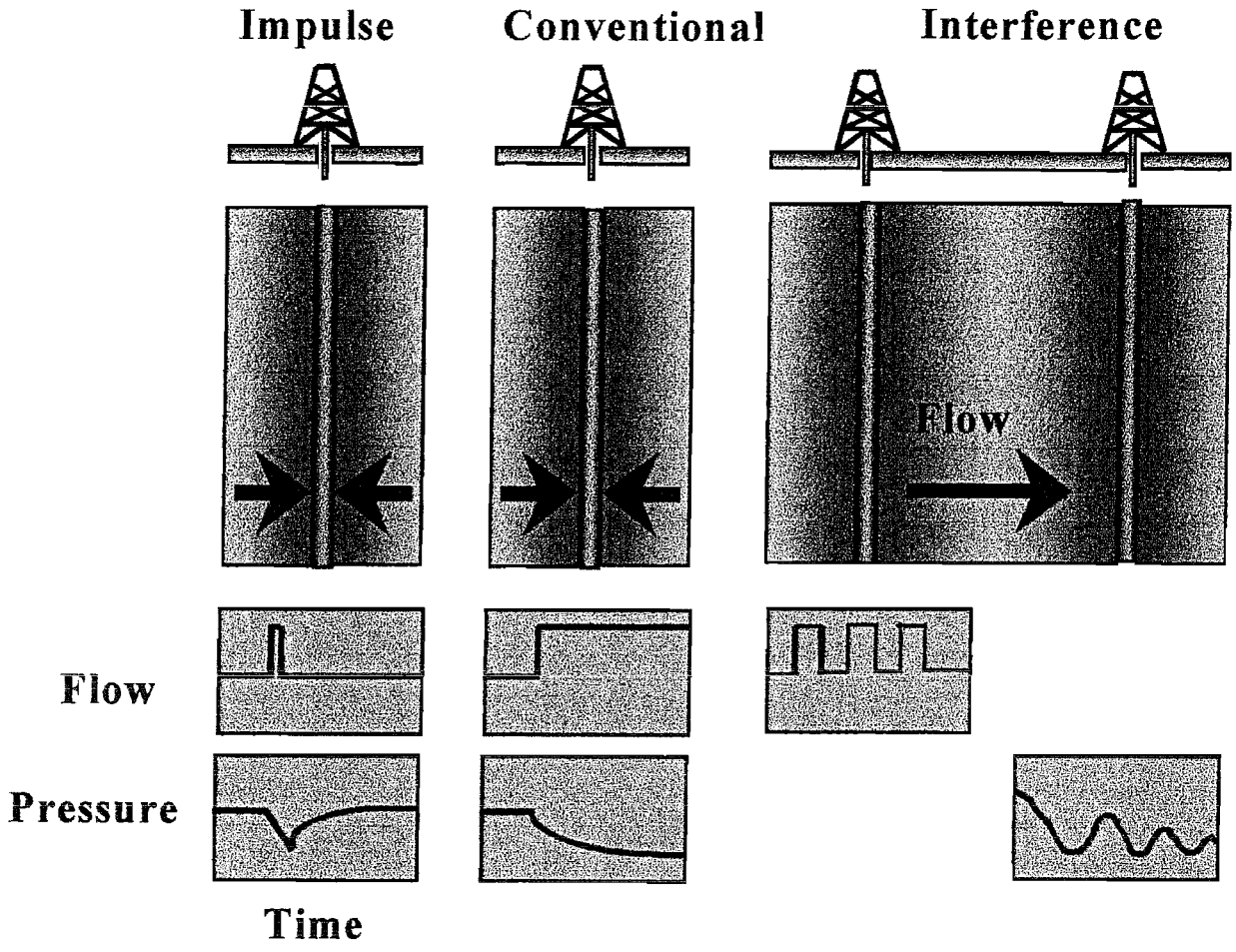

Figure 1.1.2: Types of transient well testing; impulse, conventional and interference.

Long-term, downhole pressure-testing also provides extremely important information needed to improve production and reservoir-management. For example, it is essential to operate a well with single-phase flow in order to maximise production. That is, the reservoir pressure must be maintained above the "bubblepoint pressure", the pressure below which gas begins to be released from the oil. With regular measurement of the downhole pressure, flow can be maximised whilst maintaining single-phase properties.

Also, measurement of the rate of decline in reservoir pressure during production as a function of withdrawal, enables the reservoir engineer to estimate the volume of oil initially in place [8].

During the well production lifetime, downhole pressure monitoring can provide early diagnosis of formation damage, wax deposition, leaks, failure of electrical submersible pumps etc. Stability and high reliability of the pressure gauge are essential for long-term pressure monitoring.

1.1.3 Downhole Pressure Data Retrieval.

1.1.3.1 Oil Industry Specifications.

The typical requirements of a downhole-pressure monitoring system specified by the oil industry as a standard are as follows:

- *Pressure Range* - 1 - 15,000 psi.
- *Temperature Range* - up to 250°C.
- *Accuracy* - Better than 1 psi.
- *Resolution* - 0.1 psi.
- *Stability* - Better than 1 psi per year.
- *Depth (Distance from the surface)* - up to 10 km.
- *Lifetime* - > 5 years (10 years would be preferable).

High accuracy and high resolution are essential if a gauge is to be used to measure the extreme reservoir boundaries. Furthermore, the high stability (a drift of less that 1 psi per year) is necessary for comparing downhole pressures over long periods of time.
The operational depth (up to 10km) is stated for the most highly deviated well where the wellbore may well be several kilometres from the surface instrumentation and hardware.

1.1.3.2 Conventional Pressure Gauges.

Downhole pressure testing has been in existence since the 1930's when mechanical gauges were the only available devices [9]. Most of these mechanical gauges used a Bourdon tube to convert pressure into mechanical movement. The readout of these mechanical devices was produced by a stylus that converted the pressure-induced movement into scratches on a cylinder of soft brass foil. Rotation of the cylinder via a mechanical clock produced a pressure versus time log. Mechanical gauges were robust and simple but the accuracy of such a device was limited to about 40psi.

Electronic pressure gauges, in the form of simple strain-gauges, replaced the mechanical alternative in the 1970's. The simplest of these devices is a strain-sensitive resistor mounted onto a metal membrane. As the membrane is displaced and deformed, the pressure is converted into variations in the electrical signal. The conventional strain gauge is small, fast and reliable. However, due to the physical properties of the metal membrane,

the device suffered from hysteresis. Resolution and stability were therefore poor.

The Sapphire Pressure Gauge was subsequently introduced in which the metallic substrate of the conventional strain gauge was replaced by sapphire whose single crystal structure did not suffer from hysteresis. This gauge has a high resolution, is fairly reliable and is still used as a low cost, downhole-pressure-gauge in modern developments. However, the SPG suffers from high temperature-sensitivity and has limited stability.

Another type of electronic pressure transducer is the Capacitance Gauge typically consisting of two plates, coated in conductive material and separated by a gap. Pressure-induced variation in the gap results in a variation of the gauge capacitance. Like the metallic strain gauge, they suffer from hysteresis and had a relatively poor accuracy of approximately 12 psi.

The most widely used modern pressure gauges are based on the resonant properties of quartz crystals. The natural resonant frequency of a quartz crystal can be detected by a sinusoidal variation in electrical charge on its surface as the quartz vibrates. Pressure-induced stresses in the crystal cause the sine wave's frequency to vary. Typically the pressure sensitivity of this type of gauge is low, where a change in the crystal resonant frequency of approximately 1.5Hz is caused by a 1psi pressure variation. The gauge does have a much higher cross-sensitivity to temperature, approximately 15 Hz per °C. Additional measurement of temperature is therefore required to correct for this temperature cross-sensitivity. This is achieved using either an additional quartz gauge (pressure-isolated) or a pressure-insensitive thermometer. The temperature correction process is slow and a thermal time lag is introduced which severely compromises the sensor performance, especially in pressure transient analysis.

An improvement to the quartz gauge is the Combinable Quartz Gauge in which a single quartz crystal, with two excited-vibrational-modes, is used to measure both temperature and pressure. This is the best electronic gauge that has been produced to date. There is no thermal time lag in the temperature correction as both pressure and temperature are measured by the same piece of quartz. The accuracy of these gauges can be as good as 0.025% of full scale and the stability is estimated to be as good as 1 psi per year drift [10].

1.1.3.3 Pressure Gauge Data Retrieval.

Original mechanical gauges stored the pressure measurements by mechanical inscription as described in 1.1.3.2. Data was retrieved somewhat after the test period when the gauge was pulled from the production tubing.

Electronic gauges can also use this method memory of data-storage and subsequent gauge and memory retrieval. However, this requires that the gauge has sufficient memory and battery power to last for the duration of the tests that may be several days. The individual components must survive the high-temperatures and pressures of the production environment. Furthermore, without any feedback, the reservoir engineer can only estimate when sufficient test data has been gathered from a transient measurement. Only then is the gauge and memory retrieved and subsequently analysed. It should be noted that most downhole-pressure measurements are made using memory gauges.

Real-time surface readout of the pressure during the tests is the ideal situation as it allows the reservoir engineer to monitor the gauge performance and also know when sufficient data has been acquired. Surface readout can be achieved by lowering a wireline attached to a pressure gauge into the production tubing. However, this method does not allow for closure of the test valve necessary to produce a shut-in transient.

In permanent gauge installations, it is extremely difficult to locate the gauge near to the formation as electrical connection is often made to the gauge via the annulus. Extension to the formation would require penetration of the packer. Positioning of the gauge a long way from the production zone can present a problem in transient analysis due to wellbore storage effects. In modern, deep and horizontal wells, the wellbore storage effect can be especially high resulting in distortion of the pressure-transient measurement.

1.1.3.4 Permanent Electronic Gauge Installations.

Large investments before start-up are required for most offshore developments [15]. It is therefore essential that early production is high to ensure project profitability. The necessity for downhole information increases as developments move offshore.

There is a need for an enhanced reservoir description, which requires permanently accessible downhole-data or regular data-acquisition runs. Wireline data-acquisitions cause extensive periods of non-production and require skilled service-company personnel. It is estimated that the average payback period of a permanent gauge installation is less than one

year [10].

Permanent gauge installations have been tested in many reservoirs over the past 10 to 15 years [10-14]. The problem with existing electronic gauges is that they become extremely unreliable as reservoir temperatures exceed approximately 135°C. As developments move deeper and further offshore, these temperatures can exceed 250°C.

Examples of permanent gauge installations in the early 1990's show the unreliability of electronic pressure gauges.

In a complex North Sea development [10], 40 quartz and quartz capacitance gauges were installed in two fields with downhole temperatures of 70°C and 130°C. Of these 40 installations, 23% had failed within a month of operation and 43% failed within the first two years.

The only options available on failure of a permanent gauge are to accept the loss and wastage of an investment or to pull the well and replace the gauge. The expense of the latter does not often allow this to be a realistic proposition.

1.1.4 Fibre-Optic Alternative to Downhole Sensing.

1.1.4.1 Benefits of Fibre-Optics.

For downhole data-acquisition under high-temperature, high-pressure (HTHP) conditions, optical fibres present several advantages over conventional electronic gauges:

- No electronics is required downhole.
- The signal generated at the remote transducer can be transmitted over several kilometres with little attenuation.
- Fibre-optic sensors are immune to electromagnetic interference and therefore unaffected by downhole electrical equipment.
- Optical fibre sensors offer both single point and distributed sensing capability.
- Multiplexing capability allows many downhole transducers per set of instrumentation.
- Optical fibres form the basis of the rapidly growing telecommunications industry. Advances in technology will become available for improved sensor performance.

1.1.4.2 Downhole, Optical-Fibre Sensors.

Optical fibre sensors have been developed over the last 40 years or so to measure a wide range of parameters. Of particular interest to the oil industry are: pressure, temperature, vibration, flow and acoustics. The measurement of these parameters downhole during production, on the surface during exploration and along pipelines during transport, are all of value to the oil industry.

Furthermore, technology allowing multi-point measurement of many of these parameters is emerging: the distributed-temperature sensor (DTS) [16], Brillouin distributed pressure, strain and temperature sensor [17] and hydrophone (acoustic) arrays [18].

The downhole pressure sensor is the most important sensor for downhole monitoring applications. However, it is also one of the most difficult sensors to successfully implement due to the need for pressure communication between the reservoir and the sensor itself. The (DTS) and acoustic sensors are, in principle, less of a problem as it is possible to isolate these fibres from the harsh downhole environment.

Indeed, the DTS, commercially produced and developed by York Technologies, has been successfully implemented in downhole monitoring for many years [19,20]. The multi-mode fibre cable used in the DTS can be completely encased in steel tubing and surrounded by inert gas. This component is currently available as a commercial well-logging-tool (the "Fibertube" supplied by Pruett Industries.

The first fibre-optic downhole pressure development was achieved by ALCATEL Kabel Norge in co-operation with Optoplan [21,22]. The sensor was an extrinsic device with the sensing head based on optical excitation and interrogation of a micro-machined silicon oscillator [23]. The measurement principle is based on the modification of the extrinsic Fabry-Perot interferometer (EFPI) formed by the fibre end and oscillator surface. The resonant frequency of the oscillator (approximately 100KHz) is modified as a function of temperature and pressure. Optoplan included a pressure insensitive element to the sensor head that was used to compensate and discriminate between pressure and temperature changes.

This technology, in the form of ALCATEL's Fibre Optic Well Monitoring (FOWM) system, has been installed in six production wells in the North Sea [24]. The sensor, however, is installed above the packer and is interrogated via an optical connection and armoured fibre-optic cable installed within the annulus. Other than the change from

electrical to fibre-optic connection and cable (elimination of downhole electronics), it is questionable whether the FOWM system has any advantages compared to existing quartz-gauge technology. Furthermore, after one year of operation in an 85°C gas-producing well between 1993 and 1994, this sensor showed an accuracy of approximately 3 psi compared to a calibrated wireline tool. This value suggests a drift of the order of 3 psi in 1 year at 85°C [25].

Another development was initiated by Elf Aquitaine [26]. The sensor principle was based on the optical measurement of slight pressure-induced deformations of a metallic membrane. The sensing head included a separate temperature probe for simultaneous pressure and temperature measurement. In total, the head measured approximately 25mm in diameter and 140mm in length. Again, this sensor was positioned somewhat above the packer in the production string.

Field tests of the sensor in 1997 in a 165°C well under approximately 11,000 psi (750 bar) showed an accuracy in the measurement of only ± 6psi measured at 750bar (~11,000psi) [27]. No data was supplied on the sensor stability.

A more recent downhole monitoring system has been standardised on the use of Fibre Bragg Gratings (FBG's) as the key sensing component [24]. CiDRA have developed pressure, temperature and vibration sensors based on the measurement of variations in Bragg wavelength of a perturbed FBG (discussed in greater detail in Chapter 2). The FBG sensor system presents many benefits over extrinsic fibre devices;

- All measurands can be monitored using a standard fibre Bragg grating in which the Bragg wavelength is dependent on the measurand. Interrogation of all sensors can therefore be achieved with the same instrumentation but different software.
- The FBG is an intrinsic sensor element.
- FBG's are wavelength dependent devices and can therefore be simply multiplexed and lend themselves for distributed sensing applications.
- FBG's have been extensively tested at elevated temperatures exceeding 300°C.

The CiDRA pressure sensor has been initially applied to monitoring of downhole electrical submersible pumps. Current performance of the pressure sensor device based on FBG's does not meet the oil industry required specifications for bottom-hole pressure monitoring. The FBG pressure sensor has an operational range of 0 to 5000psi, an accuracy

of approximately ± 1psi, a resolution of 1.5psi and an estimated stability of ± 5 psi per year [24]. The maximum operating temperature reported so far is 150°C.

High-resolution measurement of pressure using fibre Bragg gratings is difficult to achieve. Bragg gratings are small devices, typically only a few millimetres in length. The change in Bragg wavelength with pressure is extremely small (chapter 4) and therefore difficult to accurately measure. Pressure sensors, such as the side-hole fibre sensor described in section 1.2, are much more sensitive devices due to the high-resolution measurement of optical phase that is possible using interferometric techniques.

Furthermore, the actual sensor device, though fabricated from an intrinsic fibre sensor, is rather large (approximately 25mm in diameter). Pressure coupling to the FBG is quite complex and a significant amount of packaging is required to isolate the fibre from the production fluids. Positioning of the sensor within the reservoir is also limited as optical connection to the device, via a heavily armoured fibre-optic cable, is achieved via the annulus. This prevents the pressure sensor from being located very close to the formation, beyond the packer and therefore will experience the effects of wellbore storage.

Fibre Bragg gratings written into side-hole fibres [28] and in active fibres to form Distributed Feedback (DFB) lasers [29] are also being considered for use as pressure sensing devices in oil industry applications.

1.1.4.3 Alternative Data-Acquisition:- "The Sensor Highway"

There are many goals for permanent downhole-sensing in the oil industry including:

1. Elimination of downhole electronics.
2. Reduction of cable failures.
3. Multiple-parameter sensing capability.
4. Gauge replaceablity with low production downtime.
5. Upgradability of gauges with developing sensor technology.

In general, existing fibre-optic downhole monitoring systems have only achieved one of the potential goals, elimination of downhole electronics. The design of systems is essentially the same as that of the quartz electronic gauge but with a fibre-optic cable replacing the electrical cable.

A novel approach to downhole monitoring was proposed in 1993 [30] and was adopted

from a technique used for many years in the telecommunications industry. In this technique, cables (fibre-optic or electrical) are pumped through narrow-bore conduits using fluid drag. The method used to deploy optical fibre cables and sensors into downhole conduits is discussed in more detail in chapter 7 of this thesis.

For downhole monitoring applications, the narrow bore conduit has been in existence for many years in the form of hydraulic control lines. Such control lines are fabricated from ¼" outer diameter, stainless-steel tubing, and are installed onto the production tubing as it is lowered into the casing prior to well completion.

Fibre-optic cables and sensors can be deployed through these control lines (referred to as "Sensor Highways" or simply "highways") to remote locations within the reservoir. Figure 1.1.4 shows a schematic example of a highway installed in a vertical well.

For temperature, acoustic and other sensors, the highway can be sealed as there is no need for interaction between the well bore and the sensor. However, for downhole pressure sensing, pressure communication is required between the highway and the wellbore fluid. In its simplest form (shown in figure 1.1.4), the pressure communication port is simply an open ended highway. However, various hardware installations such as diaphragms, bellows and fluid isolation chambers can be fitted to the end of the highway.

The highway principle offers many benefits over conventional methods of downhole gauge installation;

- Sensors and cables can be deployed into the highway without interfering with normal oil production.
- Multiple sensors can be deployed into a highway to monitor several parameters.
- Sensors can be added, retrieved, replaced and upgraded.
- The highway allows in-situ calibration that helps to assure long-term accuracy of the gauges.
- There is no need for any downhole electronic or optical connections.
- Existing packers allow control line penetration that do not limit the location of the gauge even in deep, offshore wells, horizontal wells and highly deviated wells.

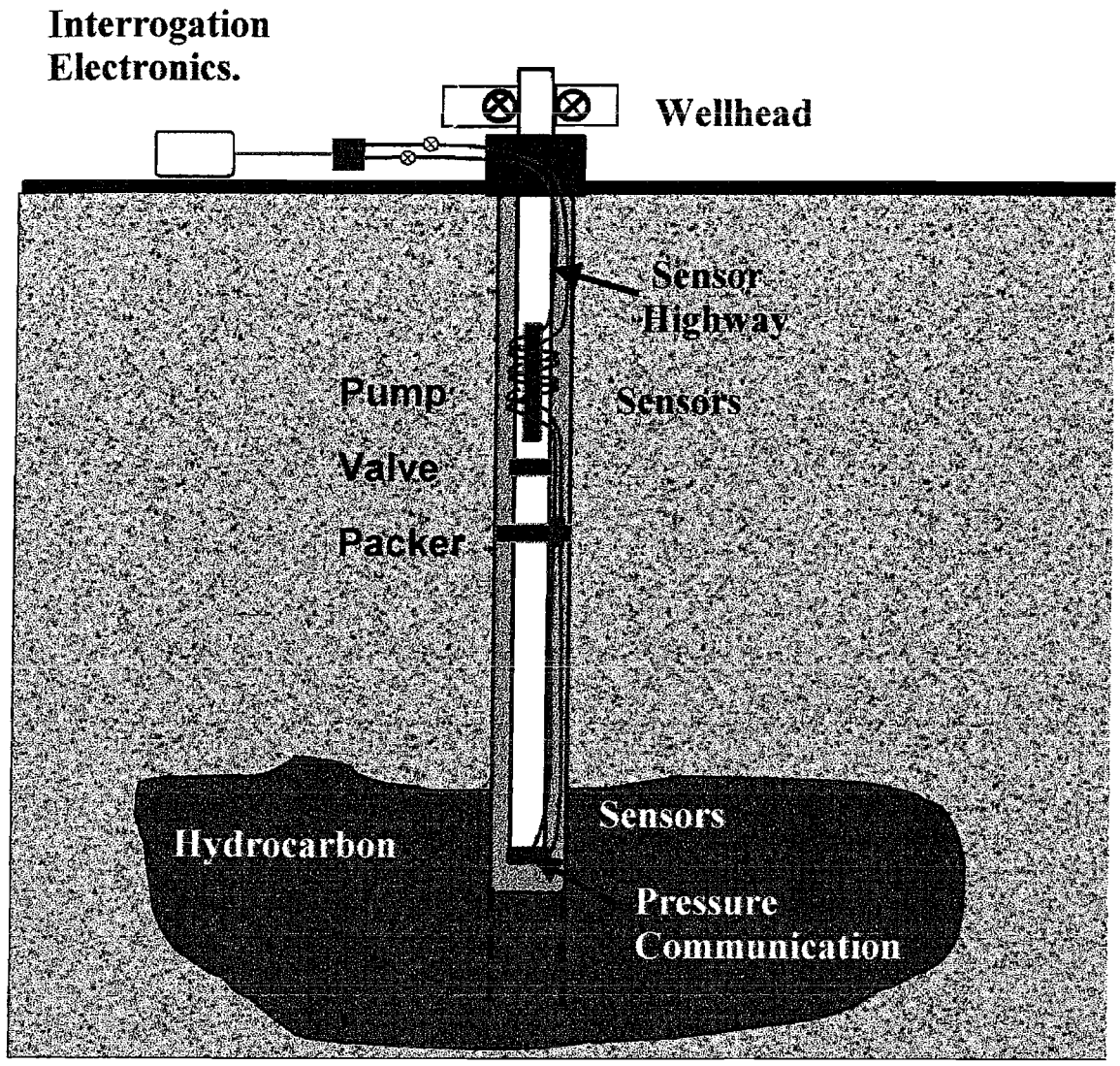

Figure 1.1.4: Schematic of a highway installed into a vertical well.

One of the main problems with the highway for downhole pressure sensing is that the dimensions of the sensor are severely restricted. The sensor must be thin and flexible enough to allow multiple cable and sensor deployments through a conduit with a bore of less than 4mm.

1.2 The Sensor Dynamics Pressure Sensor.

A polarimetric, fibre-optic, pressure sensor and interrogation technique was developed by Sensor Dynamics between 1991 and 1994, intended for use in highways for downhole monitoring.

The pressure sensor takes advantage of the pressure-induced birefringence in side-hole fibres, first reported by Xie et al [31] and since demonstrated by other authors [32, 33]. The interrogation method uses scanning, low-coherence, interferometry to remotely monitor the pressure-induced birefringence in the side-hole fibre sensor.

The sensor and instrumentation have been used throughout the course of this PhD to investigate the effects of HTHP conditions on optical fibres and sensors. The details of the sensor and instrumentation are briefly described in this section.

1.2.1 Birefringence in Optical Fibres

In a single-mode fibre, the waveguide can support two orthogonally polarised modes in the x-axis and y-axis directions. In an ideal structure, with a perfectly circular core and zero external perturbation of the core and cladding refractive index, these two modes have equal propagation constants, β, and are therefore degenerate. The degeneracy of these modes is removed if their propagation constants are made to differ (i.e. $\beta_x \neq \beta_y$). This can be achieved through the introduction of core ellipticity or asymmetric stresses across the core. The resulting birefringence, $\Delta\beta$, is given by:

$$\Delta\beta = \beta_x - \beta_y$$

Throughout the thesis, $\Delta\beta$ will be referred to as the fibre birefringence, the difference in propagation constants of light propagating in the fast and slow axes. Another parameter of interest is the beat length of a fibre. The beat length is the length of fibre after which the mode propagating in the slow axis is delayed by exactly one optical wavelength. The beat length of a fibre is therefore wavelength dependent. In this thesis the beat length is standardised to the HeNe wavelength of 633nm. As a guide, the beat length of a straight single-mode fibre is usually several metres whereas that of a Panda or Bow-Tie, polarisation-maintaining fibre can be as short as 1.5mm.

1.2.2 Birefringence in Side-Hole Fibres.

Figure 1.2.1 shows the different components of birefringence in side-hole fibres. Under the influence of hydrostatic pressure, an anisotropic, compressive stress is induced in the fibre core due to the fibre geometry. The resulting fibre birefringence is a function of pressure with the slow axis orientated as in figure 1.2.1a.

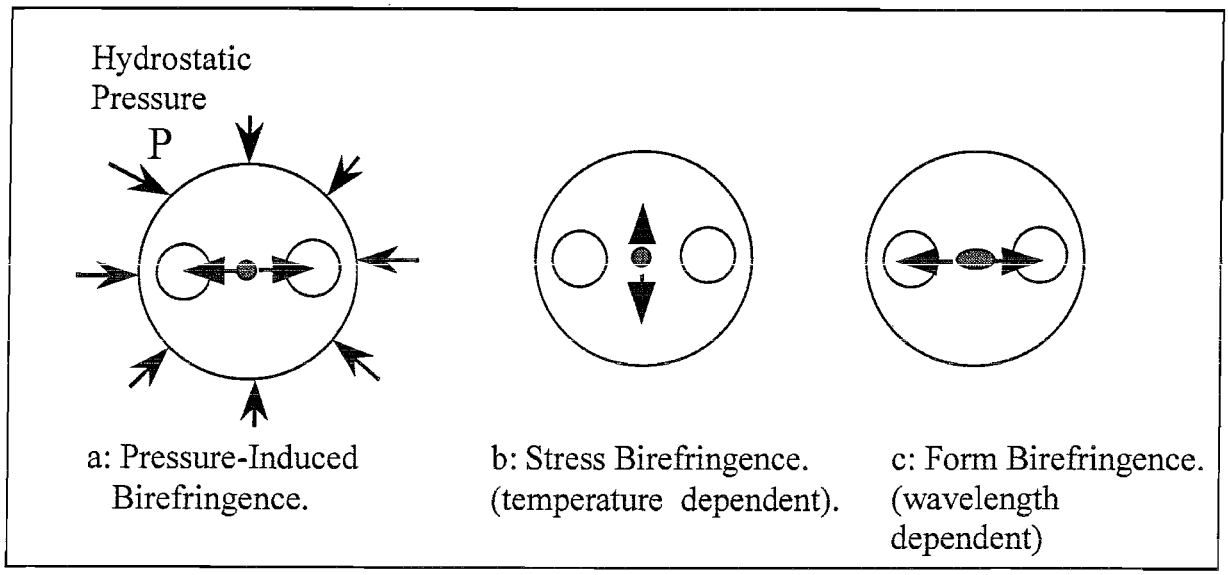

Figure 1.2.1: Showing the origins of birefringence in side-hole fibre. The arrows at the fibre core mark which polarisation sees the higher refractive index, ie. the slow axis.

Figures 1.2.1b and c show the intrinsic fibre-birefringence components. In an ideally-fabricated side-hole fibre, the cross-sectional geometry of the preform is perfectly maintained during the fibre drawing process (figure 1.2.1b). Such a fibre will have a small, inherent, stress-birefringence due to the asymmetric, cross-sectional geometry and a mismatch in the melting points of the core and cladding glasses. The magnitude of the stress-birefringence will be dependent on the relative melting points and thermal expansion coefficients of the core and cladding glasses.

Germanium-doped silica, for example, has a melting point much below that of pure silica. During the fibre drawing process, the core solidifies momentarily after the cladding (at a lower temperature). This produces tensile stress in the core as the core glass tries to contract but is prevented from doing so by the solidified cladding. The presence of the side-holes causes this stress to be anisotropic. This stress-birefringence is temperature

dependent and decreases with increasing temperature.

For tantalum-doped silica, the melting point is much closer to that of pure silica. The result is that the stress birefringence of tantalum-doped side-hole fibres is much less than that of germanium doped fibres and can be orientated in the opposite direction.

If the side-holes are positioned close to the core, there will also be an inherent waveguide or "form" birefringence due to interaction between the mode and the side-holes in one axis.

Figures 1.2.1c shows cross sections of a more realistic side-hole fibre in which the core has deformed slightly (exaggerated in this figure) and become elliptical due to the side-holes collapsing during the draw. This gives rise to form-birefringence which is due to the x- and y-polarised modes seeing slightly different average refractive indices. Due to the variation of the mode shape with wavelength, the form birefringence is wavelength dependent. To the first order, however, it is not temperature dependent.

The cross-section shown in figure 1.2.1 c is typical for a germanium-doped side-hole fibre. It is possible to reduce the side-hole collapse by pulling the fibre at high tension and relatively low temperature. It is also possible to apply a slight pressure to the inside of the holes of the preform during the pulling procedure [34] in an attempt to maintain the side-hole circularity.

For tantalum-doped, side-hole fibres it is much easier to pull the fibre without loss of the cross-sectional shape. Again, this is due to the core and cladding having similar melting points. There will inevitably be some amount of core ellipticity in tantalum-doped side-hole fibres and the orientation of the form birefringence will be determined by whether the tantalum doped glass has a slightly higher or lower melting point than that of the pure silica cladding.

1.2.3 Overview of the Polarimetric Pressure sensor

1.2.3.1 Side-hole-fibre pressure Sensor

Figure 1.2.2 is a schematic of a side-hole-fibre, polarimetric pressure sensor. The pressure sensor head comprises an input polariser, a length of side-hole fibre and a mirror. The sensor head is fusion spliced to a length of single-mode cable (the downlead) that links the sensor to the remote instrumentation.

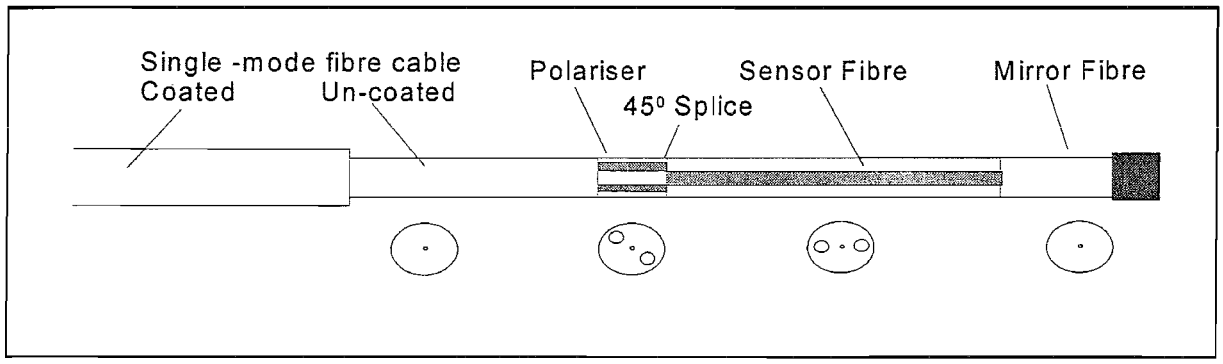

Figure 1.2.2: Schematic of a side-hole fibre, polarimetric, pressure sensor attached to a single- mode fibre cable.

Depolarised light, from the instrumentation source (an ELED), is linearly polarised by the polariser (P1), which is orientated at 45° to the birefringent axes of the side-hole fibre. The 45° alignment provides a 50% split between light entering each of the axes.

The polariser itself is an integral part of the sensor assembly and is fusion spliced to the downlead cable and the side-hole-fibre sensing-element. The polariser consists of a short length of side-hole fibre (approximately 15mm), with large side-holes positioned closely to the core. The side-holes of this fibre are filled over a length of between 5 and 10mm with gallium, a liquid metal at room temperature. The polariser works by causing a differential loss between the two polarisation-modes. The extinction coefficient is typically around 40dB although this depends on the position of the side-holes with respect to the core. Typical insertion loss for the side-hole-fibre polarisers is 1dB although this depends on the length of the gallium-filled side-hole section.

The pressure-sensitive region of the fibre is a length of side-hole fibre of chosen length. The two polarisations in the axes of the side-hole-fibre propagate at different phase velocities governed by the pressure-induced fibre birefringence.

The sensor is terminated by a mirror, which reflects the light back through the sensor and through the polariser where the two polarisation-modes interfere.

The polariser acts like a coupler in a Michelson interferometer (figure 1.2.3). The pressure-induced birefringence in the side-hole-fibre results in a path-length difference (ΔLp) between the two polarisation-modes (x and y)) emerging from the sensor. The sensor design is such that ΔLp is much greater than the coherence length of the source (an ELED), resulting in incoherent interference between the x- and y- polarised light from the

side-hole fibre.

The result is a pressure-dependent optical-path-length difference between the two polarisation modes.

Light is transmitted back to the surface instrumentation by the fibre downlead.

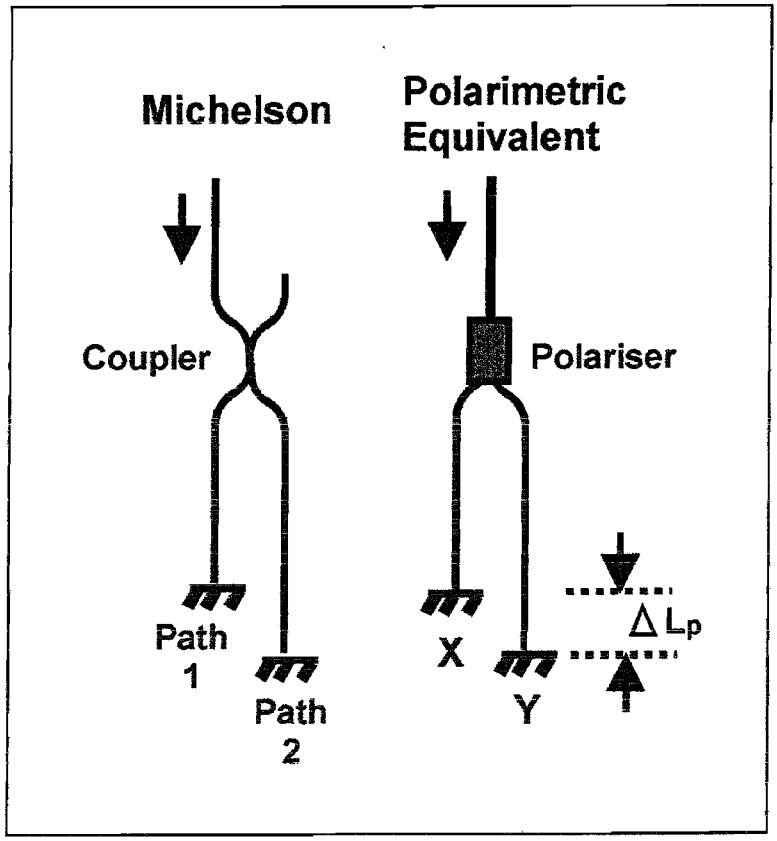

Figure 1.2.3: Role of the polariser in the polarimetric pressure sensor can be considered as a "polarisation coupler" and the interferometer can be considered as a Michelson interferometer.

1.2.3.2 Interrogation technique:- Dynamically-Matched Interferometer

Fig 1.2.4 shows a schematic of the readout interferometer that can be thought of as a dynamically matched interferometer. Light returning from the remote sensor is split into two channels, whose relative path-lengths are dynamically scanned until equal to ΔLp.

In this instrumentation, the dynamic scanning of optical-path-length is achieved by thermally scanning a length of HiBi fibre [35].

There are two separate light sources in the instrumentation; a broadband ELED centred at 1300nm and a reference source (1300nm) produced by reflection from a narrowband fibre Bragg grating.

The matched interferometer comprises an input depolariser (DP2) which ensures

polarisation-incoherent light enters the matched interferometer, an input polariser (P2), which is spliced at 45° to the birefringent axes of a length of HiBi fibre (HiBi1). Another length of HiBi fibre (HiBi2) is spliced at 90° to HiBi1.

The length of HiBi2 is chosen such that the net birefringence of HiBi1 (at ambient temperature) and HiBi2, combined, is approximately equal to the birefringence of the remote sensor under a pressure of around 6000psi. This provides a balance point for the interferometer.

HiBi1 is wrapped onto a copper cylinder whose temperature is controlled by a Peltier element. Changing the temperature of the fibre alters its birefringence and allows the differential path-length between the two polarisation-modes to be controlled. HiBi2 is wrapped around a piezo cylinder.

Another side-hole-fibre polariser (P3) is spliced at 45° to HiBi2. This can effectively be thought of as the analyser where the two polarisations interfere.

Light entering the interferometer, from the remote sensor, is polarised by P1 and 50% is launched into each of HiBi1 birefringent axes. This is achieved by the 45° splice between P1 and HiBi1. The 45° angle is not critical since errors affect the fringe visibility and not the path-length being measured.

As the path length difference of HiBi1 is thermally scanned, three separate fringe envelopes occur (figure.1.2.5). The central fringe corresponds to the x- and y-polarised light (as defined in the remote sensor) interfering, x with x and y with y.

The x- and y- polarised light will not interfere with each other unless the path-length difference in the matched interferometer is approximately equal (within the ELED coherence length) to ΔL_p.

The two side-fringe envelopes of figure 1.2.5 are referred to as the pressure-fringes and are displaced from the centre fringe by ΔLp, the pressure induced path-length difference in the remote sensor. The pressure fringes correspond to the x-and y- polarised light (as defined in the remote sensor) interfering with each other, x with y and y with x.

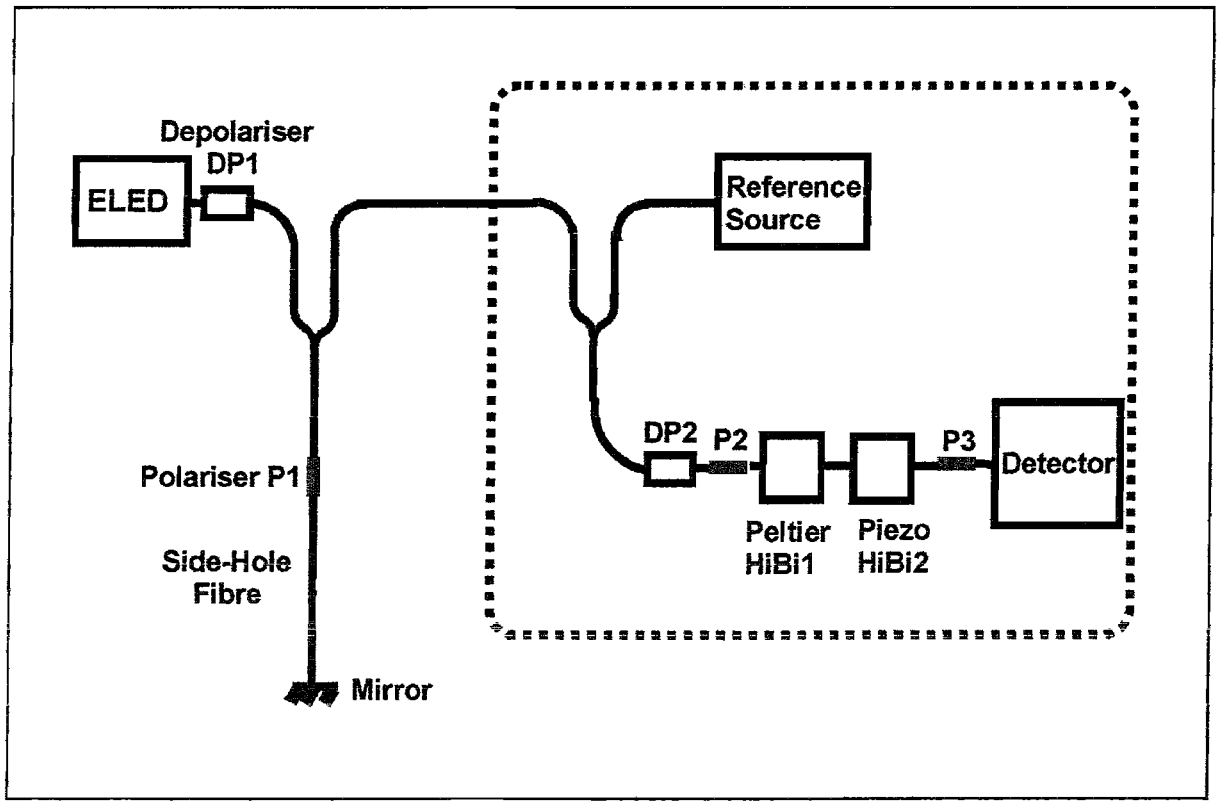

Figure 1.2.4: Schematic of the matched interferometer instrumentation used to interrogate side-hole-fibre pressure sensors.

Accurate measurement of ΔLp is made using the highly-coherent reference source that is shone through the HiBi reference arm to act as a Vernier scale. By counting the number of fringes of the reference source that occur between the central and pressure fringes, ΔLp can be measured.

An increased accuracy of measurement is achieved by measuring the phase difference between the peak of the side fringe and the corresponding reference Vernier fringe. This is achieved by the instrumentation electronics and modulation of the piezo cylinder (HiBi2) to provide a feedback element.

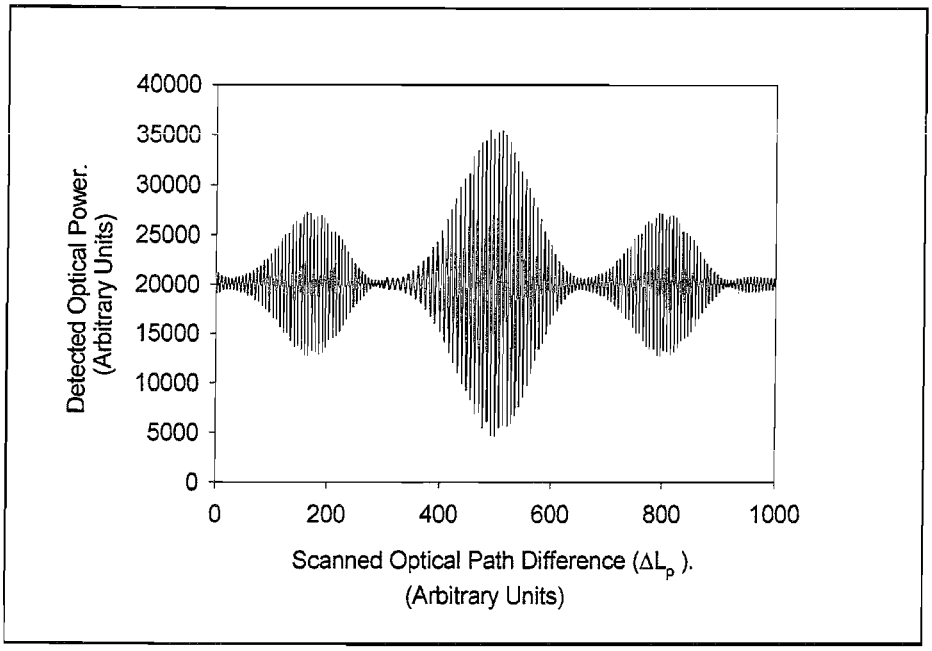

Figure 1.2.5: Typical fringe pattern from the matched interferometer instrumentation.

1.2.3.3 Calibration of Side-Hole-Fibre Pressure Sensors.

The birefringence of a side-hole-fibre pressure sensor is measured in terms of the number of reference source fringes between the central- and side-envelopes of the sensor fringe pattern. Both the intrinsic and the pressure-induced fibre birefringence contribute to this measurement.

The pressure sensitivity of the sensor is referred to as the "Scale Factor", measured in psi per fringe. The scale factor is the amount of pressure required to increase the central and side envelope separation by exactly one reference fringe. The scale factor is calibrated by applying a known pressure to the sensor and increasing the pressure until the fringe separation has increased by one reference fringe. This is repeated several times to obtain an average.

The intrinsic birefringence of the side-hole-fibre pressure sensor is referred to as the sensor "Offset", measured in psi at atmospheric pressure. The offset is given by the instrumentation reading when zero pressure is applied to a sensor with a calibrated scale factor. This value is subtracted from the reading automatically by software.

1.3 Thesis Contents and Summary.

1.3.1 Synopsis

This thesis discusses the various stages of development of an intrinsic fibre-optic pressure sensor from its conception to its final field trial before commercialisation. In general, the structure of the thesis is in a chronological order. The steps made to discover the cause of pressure sensor drift in HTHP conditions and provide a solution to this drift, are described in this thesis.

The overall project has spanned for over 10 years. The majority of the work included in this thesis has taken place within the 4 year period from 1996 to 2000. However, some experiments and results have been produced by previous researchers, prior to the start of the PhD. Such work is acknowledged throughout the thesis.

1.3.2 Effects of High-Temperature and High-Pressure on Silica, Optical-Fibre Pressure Sensors.

The results of an investigation into the damage and long-term instability of fibre sensors under HTHP conditions are presented and discussed in chapter 2. Results of this study show that exposure of side-hole-fibre pressure sensors to HTHP fluids causes a change in the zero offset of the sensor (referred to as "drift"). The offset change is observed to be "permanent", in that it remains when the sensor is removed from the HTHP fluid environment.

Measurements of the stability of the Sensor Dynamics pressure sensor in HTHP fluids were made prior to, and during the first year of this PhD. Experiments and measurements have been made by Dr. M. Fahradiroushan, Mr. J.McInnes, Dr. M. P. Varnham and myself during this period.

Early work by Dr. M. Fahradiroushan and Dr. M. P. Varnham analysed the effect that parameters such as temperature, pressure and side-hole fibre material composition had on the sensor drift.

This study was continued by Mr. J. McInnes and myself to investigate the effect that fibre geometry, fibre chemical and thermal treatments and different HTHP fluids had on the sensor stability.

Analysis of the results of this study show that the magnitude and rate of the sensor drift is dependent on the temperature and type of HTHP fluid environment alone. It is

concluded that a reaction at the surface of the fibre sensor must be responsible for the observed drifts in the fibre pressure sensor.

1.3.3 Stressy Surface Layers in Side-Hole-Fibre Pressure Sensors: Theoretical and Experimental Evaluation.

Chapter 3 introduces a finite element model (FEM) which has been used to model side-hole fibres under HTHP fluid conditions. The model was created by Dr. S. Syngellakis of the Mechanical Engineering Department at the University of Southampton.

The FEM is used to model the pressure-induced stress profiles in a side-hole fibre. Fibre birefringence is calculated from this stress profile data using the photoelastic equations and simple perturbation theory.

A relationship between the pressure sensitivity of side-hole fibre and the fibre cross-sectional geometry is reported. This relationship can be used to optimise a side-hole fibre geometry for pressure sensing purposes.

Experimental measurements of pressure sensors fabricated from various geometries of side-hole fibres are shown to agree well with the FEM predicted pressure sensitivity.

The FEM is developed to enable modification of the surface layers of side-hole fibres. The model shows that the formation of stressy surface-layers of the side-hole fibre could be responsible for the sensor drift. Furthermore, the model predicts that the "permanent" drift effects in pressure sensors could be reversed by the removal of the highly-stressy surface layers.

Experimental verification of this theory provides the basis for understanding of drifts in fibre-optic pressure sensors in HTHP fluid environments.

The FEM results of chapter 3 predict that any silica-fibre pressure sensor in HTHP fluid environments will be subject to instabilities.

1.3.4 Effects of Stressy Surface Layers on Optical Fibres and on Fibre Bragg- Grating Pressure Sensors.

Chapter 4 discusses the effect that HTHP fluids have on the optical and physical length of optical fibres and on fibre Bragg grating (FBG) Bragg-wavelengths.

A low-coherence Michelson interferometer is used to monitor the optical-path-length of single-mode fibres as a function of pressure.

Bragg wavelengths of FBG's are monitored as a function of pressure using an optical spectrum analyser. These parameters are monitored as a function of time when the fibres

and FBG's are subjected to HTHP fluids. The results of these measurements confirm the FEM prediction (chapter 3) that all silica fibre-optic pressure sensors subjected to HTHP fluids will experience long-term drifts.

The optical-path lengths of carbon-coated optical fibres as well as unprotected, silica fibres are monitored. The carbon coating is shown to be effective at reducing the effects of the HTHP environment on fibres.

The optical-path-length measurement is established as a test method of existing commercially available fibre coatings. Various carbon- and plastic-coated fibres are tested in different fluids and at different temperatures to investigate the level of protection that they offer.

A carbon / polymer coating is identified as the best available coating and is used to coat side-hole fibres for pressure sensor fabrication. Sensors fabricated from this fibre are tested at different temperatures and significant improvements in the sensor stability are shown. However, the level of improvement is insufficient and additional problems are identified in the coated sensor with increased temperature cross-sensitivity due to the polymer layer.

The coating technology is concluded to be adequate for protection of downhole cables but not for protection of downhole, optical-fibre pressure sensors.

Measurements and experiments on the optical-path-length change and sensor stability have been made by myself, Irina Grudinina and Jean Edwards of Sensor Dynamics Ltd.

1.3.5 Water Diffusion in Silica: The Cause of Pressure Sensor Drifts.

Chemical attack of the silica fibre surface by the HTHP fluid was considered a potential cause of the observed drifts in pressure sensors. However, the FEM of chapter 3 and various etching experiments in chapter 3 and 4, showed that the affected region of the silica penetrates deep into the fibre structure.

Past literature (discussed in chapter 5) shows that water can exist in silica and can also enter silica by diffusion even at relatively low temperatures.

Real-time monitoring of the attenuation in optical fibres in HTHP water is used to show the progressive build up of hydroxyl ions with time. Furthermore, a repeat of the measurement in HTHP polysiloxane oil (claimed to have low dissolved water content) is used to show that it is small quantities of water which cause drifts in optical fibre-pressure sensors. The results of these long-term loss measurements are presented in chapter 5.

The results identify water diffusion and the resulting effect of water on the silica

structure to be the root cause of drift in optical-fibre pressure sensors.

1.3.6 Solution to Fibre-Optic Pressure Sensor Drifts in HTHP Fluids.

Chapter 6 reports on a proprietary coating technique, which has been developed during the last 18 months of this PhD. The coating technique uses a liquid metal as a barrier between the silica sensor and the HTHP fluid environment.

Liquid metals such as gallium and indium are known to have high tendency to wet silica and were therefore expected to form a well-adhered interface. Furthermore, with the metal coatings in the liquid phase, unable to support shear stress, these coatings would not be expected to increase the sensor temperature dependence. This has been a major problem with metal and polymer coatings.

The uncoated, silica, pressure sensor (described in Chapter 2) is sleeved in a thin silica capillary that is subsequently filled with gallium (a liquid metal at room temperature). The packaged sensor is referred to as the SD series sensor .

The SD series sensors show extremely low drifts in HTHP fluids. Developments in the design and resulting improvements in the performance of this type of sensor are discussed throughout chapter 6.

The final sensor design, the SD 2010 sensor is shown to have excellent stability and dynamic performance, which satisfy all the pressure sensor requirements specified by the oil industry. The idea of using liquid metals as optical fibre protective coatings was developed by myself, Dr.E.L.E Kluth and Dr. M.P.Varnham of Sensor Dynamics Ltd, Prof. H.Rutt of the ORC at the University of Southampton and Mr. C.Crawley of Chevron Research and Technology.

The measurements and experiments described in chapter 6 have been made by myself and Irina Grudinina of Sensor Dynamics.

1.3.7 Field Test of the SD2010 Fibre-Optic Pressure Sensor.

The SD2010 sensor was used in a field trial in a downhole test facility in Chevron's Coalinga Steam Flood Oil Field , California.

Chapter 7 discusses the planned objectives of this field trial and the achievements made during the field trial.

The chapter also discusses the deployment technology used to install cables and sensors into hydraulic conduit ("highways") in oil wells.

Two SD2010 sensors were installed into highways during this field trial. The first ever sequential deployment of a fibre-optic pressure sensor and DTS fibre into a single highway was also achieved during the field trial.

Deployments of the sensors during the field trial were made by myself, Roy Kutlik of Chevron Research and Technology and Dr. Malcolm Varnham of Sensor Dynamics Ltd.

1.3.8 Review of Downhole Fibre-Optic Pressure Sensing in the Oil Industry.

The main conclusions are discussed in chapter 8 of this thesis.

Many institutions and companies are developing fibre-optic pressure sensors for downhole monitoring applications. Whilst most of these devices have their own mechanical and hermetic protection from the harsh downhole environment, they are all based on silica as the core material.

The effects of HTHP fluids on silica fibre sensors that have been discovered through this PhD will have an enormous effect on all downhole fibre-optic sensors and cables.

The coating technology, based on liquid-metal-filled capillaries, has provided a major improvement in the hermetic protection of optical fibres. This coating technology may have far reaching implications on other optical fibre sensors, cables and devices both in the sensing and communications fields.

The SD2010 sensor is believed to out-perform any existing, downhole pressure-sensor in the world and is currently being commercialised.

Chapter 2

Effects of High-Temperature and High-Pressure on Silica Optical Fibre Pressure Sensors.

2.1 Introduction

Chapter 1 introduced the polarimetric, fibre-optic pressure sensor developed at Sensor Dynamics between 1990 and 1993. The sensor structure was based on the use of uncoated silica fibre sections spliced together to form an intrinsic fibre sensor.

Silica was thought to be an extremely stable material, capable of survival at extremely high-temperatures. Indeed, this was originally proposed as one of the major advantages of fibre-optic sensors over electronic gauges for oil-well monitoring.

Early characterisation stages in the development of the side-hole-fibre pressure sensor (pre- 1996), identified an instability in the sensor response at elevated temperatures and pressures. The instability manifests itself as a long-term drift in the pressure sensor reading (the side-hole fibre birefringence) when the applied pressure itself is accurately maintained at a constant value. The effect of the drift is for the pressure sensor reading (the fibre birefringence) to become increasingly negative with time.

Chapter 2 focuses on characterisation of the pressure sensor drift phenomenon in high-temperature, high-pressure (HTHP) fluid environments. The HTHP test facility used to simulate downhole environments is described in detail. Details of all the sensors used in this study are provided along with a reference of the side-hole fibre, cross-sectional geometries listed and photographed in Appendix A.

Observations concerning pressure sensor drift, made prior to the commencement of this PhD (pre- 1996), are discussed. The early work established the effects of pressure, temperature, fibre material composition and fibre geometry on pressure sensor stability.

Most of the original measurements have been made by Dr.M.Fahradiroushan and Dr.M.P.Varnham. Analysis of the key results from this period are briefly discussed. Early measurements were all made using a polysiloxane, hydraulic oil as the HTHP fluid environment.

Results of experimentation during the first 12 months of this PhD are discussed in greater detail. The experiments and measurement have been made by myself,

Mr.J.McInnes and Mr.I.Hilton.

The effects that various HTHP fluids have on the fibre pressure-sensor drift and the effect of higher-temperature operation are characterised in detail.

Analysis of the various experimental results during this period of the study conclude that the drift effects in fibre pressure sensors in HTHP fluids are dependent on the fluid type, temperature and fibre diameter.

2.2 Long-Term Monitoring of Pressure Sensors in HTHP Fluid Environments.

2.2.1 The High-Temperature, High-Pressure Test Facility.

Figure 2.2.1 shows a schematic of a single HTHP test chamber used to laboratory simulate oil well high-temperature, high-pressure conditions.

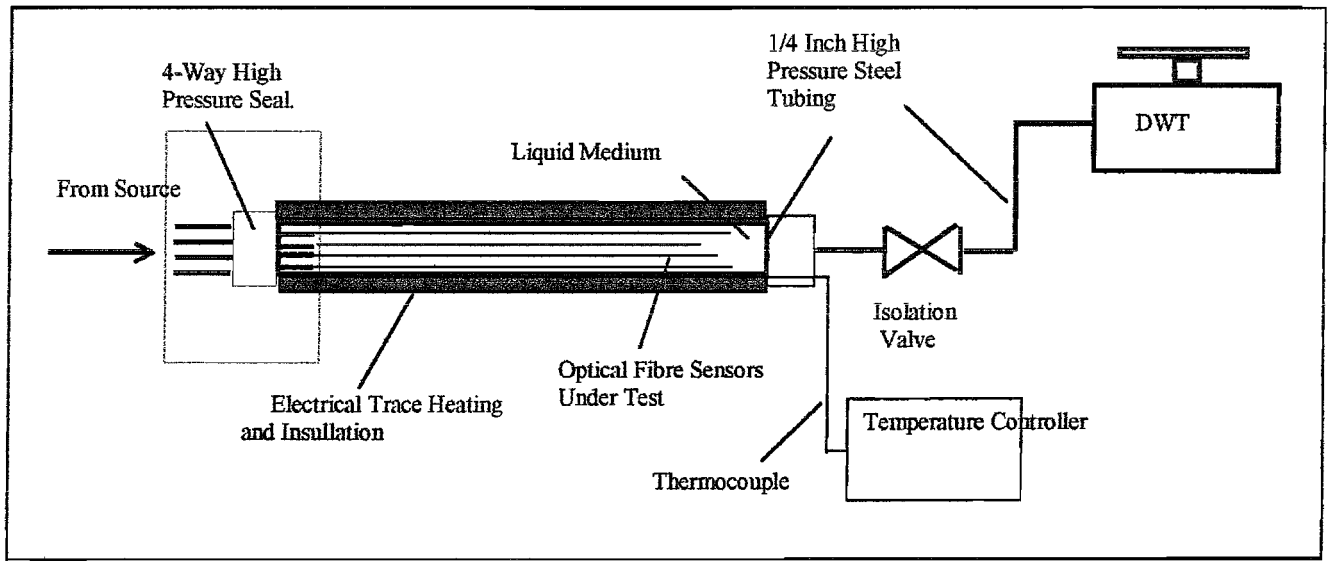

Figure 2.2.1: Schematic of a high-temperature, high-pressure test chamber used in the laboratory to simulate downhole conditions.

The total test-facility that has been developed can include up to thirteen individual HTHP chambers capable of operation at pressures up to 20,000 psi.

The HTHP chambers are fabricated from ¼ inch stainless steel tubing. A single chamber can accommodate up to 4 fibre pressure sensors at any one time. The sensor cables are epoxied into narrow-bore, steel tubing to form high-pressure seals at one end of the chamber.

Pressure is applied to the fibre sensors using a Budenbourg dead-weight-tester (DWT)

in combination with a hydraulic hand pump. Pressure can be controlled to an accuracy of approximately 0.1psi using the DWT.

The hydraulic fluid used with the two pressure sources is a Dow Corning polysiloxane oil (PSO). This fluid can be used as the high-pressure medium of the HTHP chambers. Alternatively, a different fluid may be chosen which can be isolated from the PSO by taking advantage of the differences in the two fluids' specific gravities.

The chambers can be thermally controlled between room temperature and 600°C to an accuracy of approximately 0.1°C. The temperature is controlled with respect to a single thermocouple located approximately at the centre of the chamber. Heat is applied to the chamber over a region of approximately 1.3m using high-temperature heating tape.

In order to attain a flat temperature profile across the length of the chamber , the ¼ inch tubing is sleeved in a thick, steel tube with a ¼ inch bore, to increase the thermal mass. The chamber is thermally insulated along the 1.3 metre length. Figure 2.2.2 shows a typical temperature profile of a HTHP chamber heated to 300°C. For most of the measurements made during this study, the length of fibre under test (FUT) has been less than 1metre and has been positioned centrally in the chamber. The average temperature over the length of the FUT is approximated to be uniform although not exactly flat. Slight differences between different chamber-temperature-profiles and positioning of the FUT within the chambers may account for slight discrepancies between measurements.

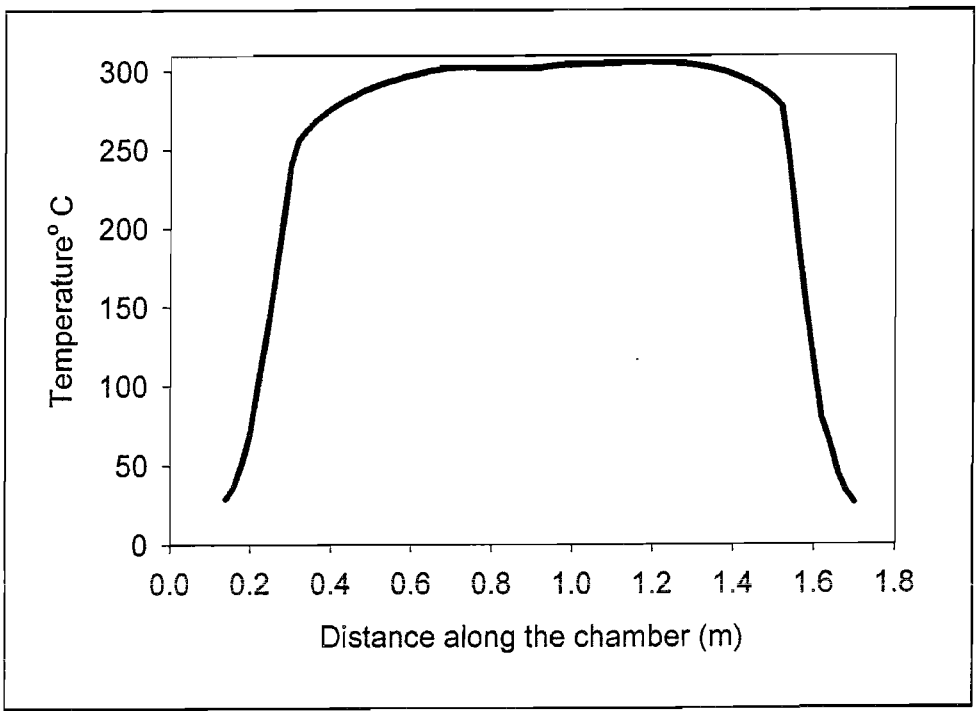

Figure 2.2.2: Typical temperature profile of a high-temperature, high-pressure test chamber operating at 300°C. The chamber length is approximately 1.5 m where the hot zone covers approximately 1.3 m.

2.2.2 Long-Term Measurement of Pressure Sensors.

The pressure-sensor instrumentation described in section 1.2 has been used throughout this study to monitor side-hole-fibre pressure sensors in HTHP fluids over extensive periods. In order to monitor the long-term stability of pressure sensors, the measurements have generally all been made at the same pressure of 4000psi (accurately controlled by the DWT) although there are some obvious exceptions (made at 6000psi) shown in the results of the following sections.

Sensors were all calibrated at ambient, laboratory temperatures before the chamber temperature was set to the required value for the experiment.

2.3 Summary of Early Pressure-Sensor Drift Results.

This section summarises the experimental results of pressure sensors in HTHP fluids prior to the commencement of this PhD. All measurements were made using a polysiloxane oil as the high pressure medium.

2.3.1 Effect of Temperature.

Long-term measurements of side-hole-fibre pressure sensors in polysiloxane oil at low temperatures (below 70°C) showed excellent stability. However, as chamber temperatures were raised, sensors began to show signs of drift. The drift rate was observed to increase disproportionately with increasing temperature.

2.3.2 Effect of Pressure.

Early measurements made on side-hole-fibre pressure sensors at elevated temperatures and various pressures showed no pressure dependence of the drift effect. Measurements were made at pressures between 2000psi and 15,000 psi.

Measurement of the pressure sensor requires a small pressure to be applied before the central and side-fringes of the interference pattern are separated. Long-term measurements at pressures below 2000psi were therefore not made.

2.3.3 Effect of Fibre Core-Composition.

Long-term stability measurements were made on pressure sensors fabricated from side-hole fibres with cores doped with germanium, phosphorus and tantalum. The results of these measurements showed no dependence of the sensor drift on the core dopant-material. This was a surprising result given that germanium is a group IV element and tantalum and phosphorus are both group V elements. Furthermore, the three doped silicas have vastly different physical and thermal properties such as melting point, thermal expansion coefficient and viscosity.

2.3.4 Effect of Fibre Composition.

Pressure sensors were fabricated from both PANDA and Bow-Tie polarisation maintaining (PM) fibre instead of side-hole fibres. Sensors fabricated from PM fibres had significantly lower pressure sensitivities but much higher offsets than side-hole fibre sensors. The PM fibre sensors also had a significant temperature cross-sensitivity due to the high intrinsic stress birefringence.

Long-term measurement of PM fibre sensors and side-hole fibre sensors under HTHP conditions showed very little difference in the sensor drifts.

2.3.5 Effect of Hydrogen

Side-hole-fibre pressure sensors were fabricated, measured and left in a high-pressure hydrogen chamber for 2 weeks. This process is commonly used to hydrogen-load fibres to enhance photosensitivity in fibre Bragg grating fabrication [36].

Of the hydrogen-loaded sensors, one was removed from the chamber and measured immediately, one was removed and heated in a furnace at 400°C for 1 hour before being measured and one was left at room temperature for several days before measuring.

The experiment was made in order to test the effects of molecular hydrogen and the effects of any temperature activated reactions between silica and hydrogen, on the birefringence of side-hole fibres.

All of the post-hydrogenation measurements, for the sensors, agreed closely with the pre- hydrogenation values. It is therefore assumed that hydrogen is not a major cause of the drift effects observed in polarimetric pressure sensors in high-temperature, high-pressure fluids.

2.4 Further Characterisation of Pressure Sensor Drift.

This section discusses the results of long-term pressure sensor measurements made in various HTHP fluids at different temperatures.

All sensors used in these measurements have been fabricated from uncoated silica side-hole fibres. Table 2.4.1 summarises the build data for each of the sensors used in these experiments. Table 2.4.1 also lists the temperature and HTHP fluid used in the experiments. In the cases where water is the HTHP fluid, several sources of water have been used throughout this study including: de-ionised, distilled and tap water (taken from domestic water supply in Winchester, UK). No differences have been noticed for measurements using water from any of these three sources. During this thesis, no discrimination is made between water taken from the different sources.

Sensor Number	Side-Hole Fibre	Sensor Length (cm)	HTHP Fluid	Chamber Temperature
001	C	20	Water	135°C
002	A	10.8	Water	155°C
003	F	25.5	Water	200°C
004	F	29.0	Water	300°C
005	A	33.1	PSO	155°C
006	A	30.0	PSO	155°C
007	F	28.0	PSO	300°C
008	F	30.0	Methanol	300°C
009	F	29.0	Propan-2-ol	300°C
010	F	26.0	Perfluorocarbon	300°C
011	D	49.9	Water	300°C
012	E	30.0	Water	300°C
013a	C	29.8	Water	300°C
013b	C	29.8	Air	195°C

Table 2.4.1: Summarising details of sensors discussed in section 2.4.

Side-hole fibres are classified with a letter from A-L. The details of these fibres are presented, along with cross sectional photographs, as Appendix A of this thesis. Most of these fibres were fabricated at the ORC at the University of Southampton.

2.4.1 Effect of Temperature.

Side-hole-fibre pressure sensors have been monitored at a range of temperatures from 135°C to 300°C in a Dow Corning polysiloxane oil. In general, sensors have been maintained at 4000psi throughout the experiment. However, 6000psi has also been used for some measurements. Previous measurements have found no pressure dependence of sensor stability.

Figure 2.4.1a shows the plots of measured pressure against time (in days), for sensors at 155°C (sensor 002), 200°C (sensor 003) and 300°C (sensor 004) in polysiloxane oil. For all the sensors, a pressure of 4000psi was applied throughout.

Figure 2.4.1b shows the plots of the same sensors but on a square-root of time horizontal axis. Some of the drift curves were noticed to obey a linear drift response with the square root of time, particularly those in water (sensors 002, 003, 011 and 012 are good examples). The drift curves were therefore occasionally plotted in this manner in order to compare sensor drift rates in psi / $(\text{time})^{1/2}$.

Observation of the curves of figures 2.4.1a and b shows that the drift rate of pressure sensors increases disproportionately with increasing temperature. Comparison of sensors 003 and 004 shows an increase in drift rate by a factor of approximately 10 when the operational temperature is increased from 200°C to 300°C.

For sensor 004, operating at 300°C, the drift reaches a maximum after approximately 4 days when the pressure reading is -2000psi and the sensor has drifted by approximately -6000psi.

After 4 days, the pressure reading began to increase again before the sensor failed after approximately 8 days. The reason for this "turn over" in drift direction was not fully understood. It was only observed during 300°C measurements although it could conceivably have occurred at lower temperatures but after longer time periods, beyond the extent of the experiments.

The drift is known to be permanent, in that the effects remain when the sensor is removed from the HTHP conditions. Putting the drift of sensor 004 into perspective, removal of the sensor from the chamber after 4 days would have produced a sensor with an offset of -6000psi. This corresponds to a side-hole fibre with a beat length of 2.4mm measured at 633nm. This is a highly birefringent fibre.

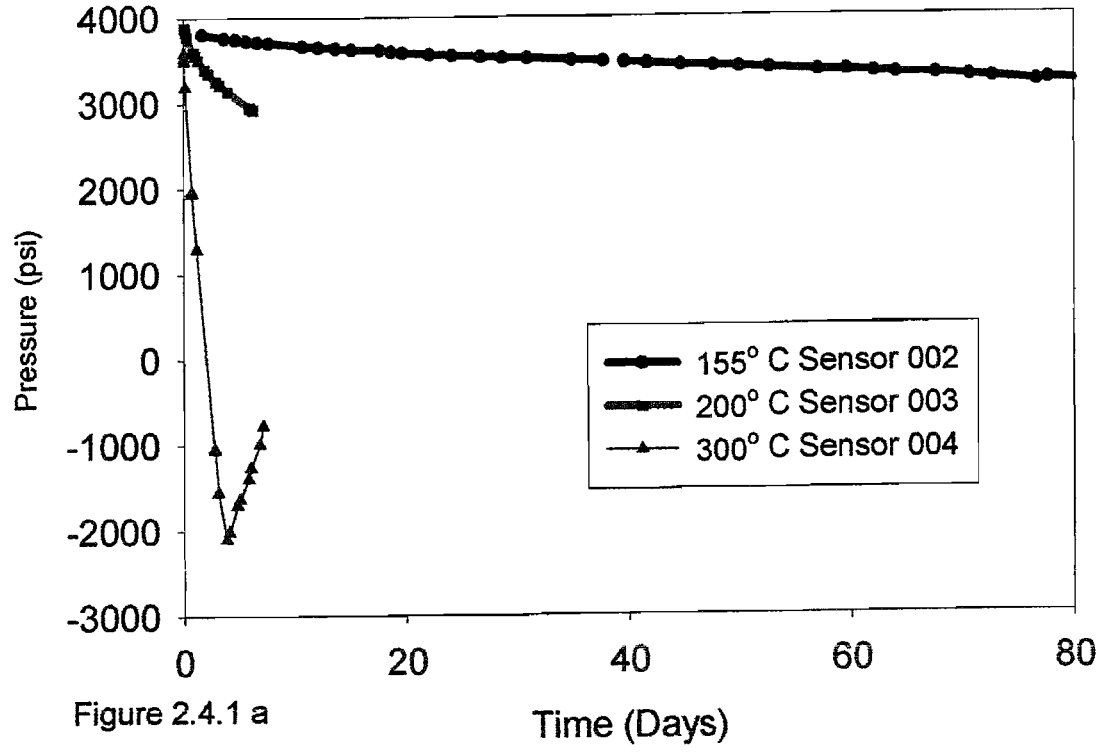

Figure 2.4.1 a

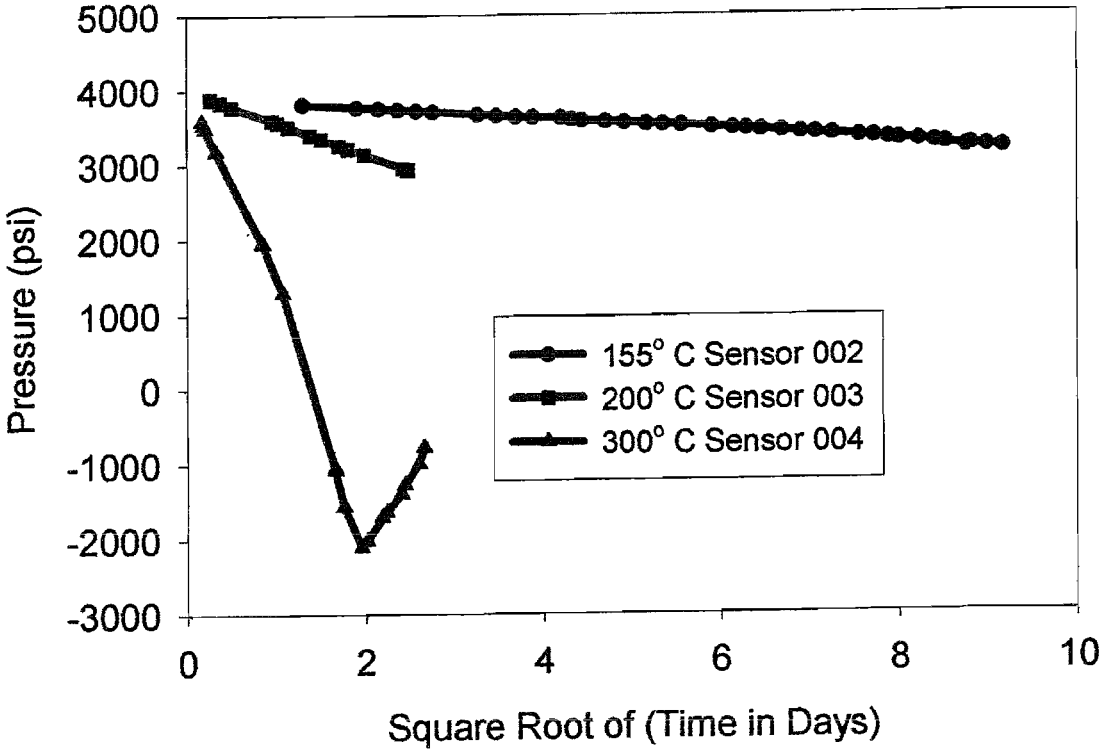

Figure 2.4.1 b

Measured pressure versus time (a) and square root of time (b) for sensors in water under 4000psi. Sensors at temperatures of 155 (sensor 002), 200 (sensor 003) and 300° C (sensor 004).

2.4.2 *Effect of Different HTHP Fluids.*

Side-hole-fibre pressure sensors were measured over extended periods at 300°C and at 4000psi in several different fluid mediums. All sensors used in the measurements in this section were fabricated from the same side-hole fibre, fibre F. Fluids used in this experiment were; water, Dow Corning polysiloxane oil (PSO), 3M Fluorinert ($(N(C_5F_{11})_3)$), methanol and propan-2-ol.

Figure 2.4.2 shows the plots of pressure reading against time for the sensors in different HTHP fluids.

All five of the sensors drifted but at different rates. Sensor 004 (in water) shows the highest drift rate while sensor 007 (in polysiloxane oil) exhibited the slowest drift.

All five sensors showed the "turn over" in drift direction but the time taken to reach this point and the magnitude of the drift at this point differs for the various fluid environments.

Table 2.4.2 summarises the observed drift results in fluids at 300°C, listing the drift magnitude and time taken to reach the "turn over" point of the drift curve.

HTHP Fluid	"Turn Over" Drift Magnitude (psi)	"Turn Over" Time (days)
Water	6000	4
Methanol	3000	14
Propan-2-ol	3500	11
Fluorinert	3200	15
Polysiloxane Oil	1200	4

Table 2.4.2 :Summary of the drift curves for sensors subjected to different fluids at 300°C and 4000psi.

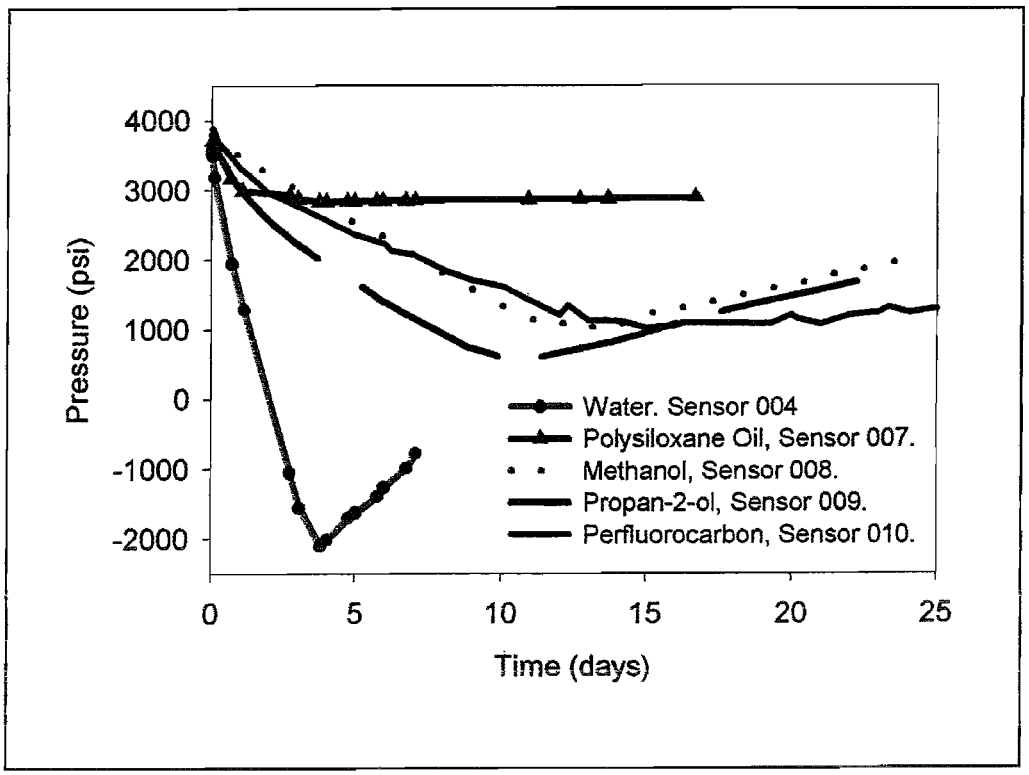

Figure 2.4.2: Measured pressure plotted against time for uncoated silica fibre pressure sensors at 300°C and under 4000psi in various liquids.

2.4.3 Effect of Water-Filled Side-Holes

A sensor was fabricated in which water was injected into the side-holes of the sensor fibre (approximately 50% filled) prior to fabricating the sensor. This sensor (sensor 005) was subsequently calibrated and monitored in polysiloxane oil at 4000psi and 155°C. A control sensor (sensor 006), fabricated with the side-holes filled with air, was also measured during the experiment. The experiment was planned to test the effect of the high-temperature fluid environment on the silica surface of the side-hole walls.

Figure 2.4.3 shows the plots of the pressure readings of the two sensors against time. The water inside the side-holes of the sensor-fibre clearly has a marked effect on the drift of sensor 005. In the first 4 days, sensor 005 drifted by approximately 2000psi compared to approximately 200psi for sensor 006. Furthermore, the curve of sensor 005 shows the "turn over" effect observed for sensors at 300°C with empty side-holes.

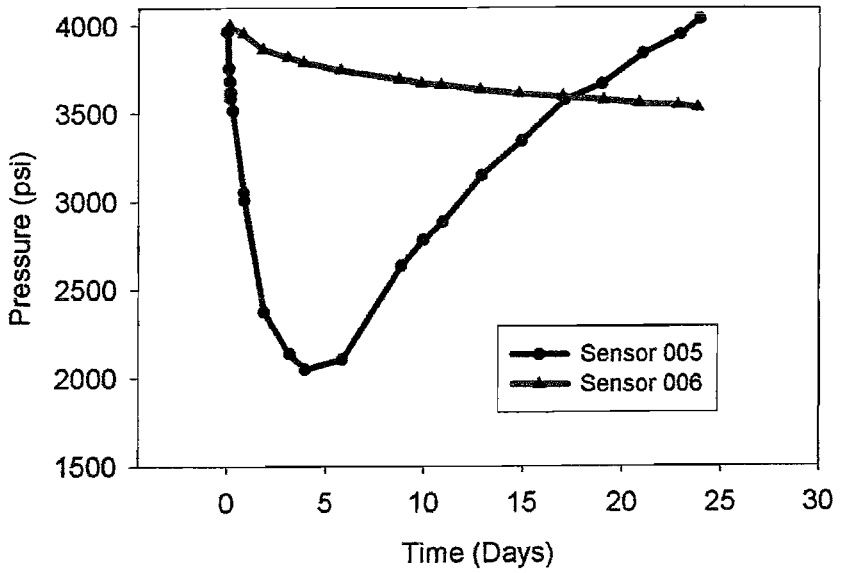

Figure 2.4.3: Measured pressure against time for sensors 005 (side-holes filled with water) and 006 (side-holes air filled) in polysiloxane oil at 155° C and under 4000psi.

2.4.4 Effect of the Side-Hole Fibre Radius.

Sensors were fabricated from fibres D (sensor 011) and E (sensor 012) with outer diameters (d) of 175μm and 130μm respectively. Both fibres were pulled from the same preform during the same pulling procedure.

The sensors were monitored at 4000psi and at 155°C. Figures 2.4.4a and 2.4.4b show plots of measured pressure against time and root-time respectively for the two sensors.

Sensor 012 (130μm diameter) clearly suffers a greater drift. Approximating the rate of drift to be linear with the square-root of time, the ratio of the drift of sensor 012 to 011 at 155°C, is approximately 1.3 to 1, close to the ratio of 1/d.

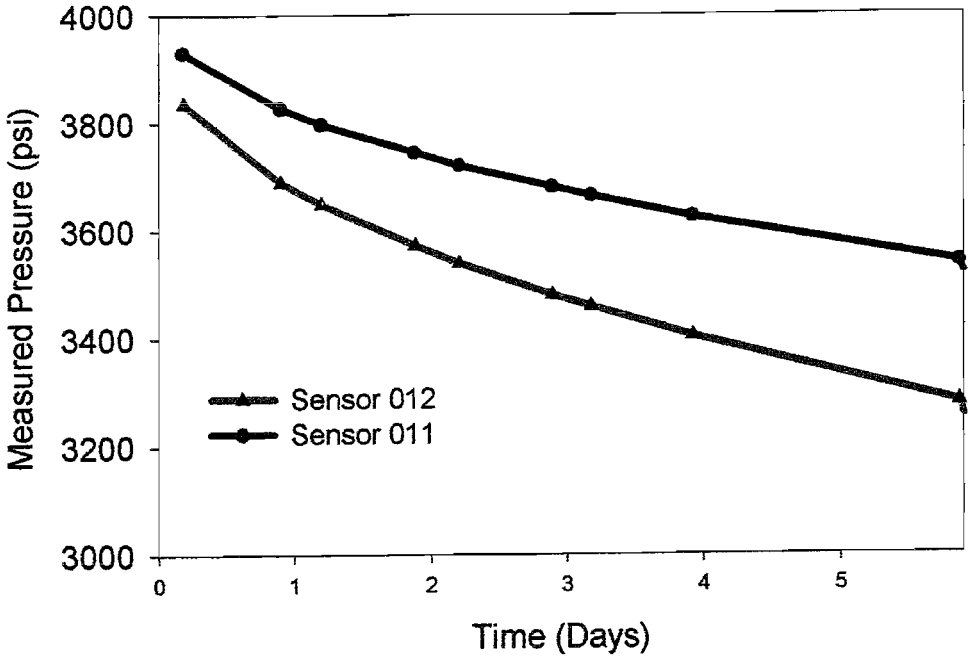

Figure 2.4.4a

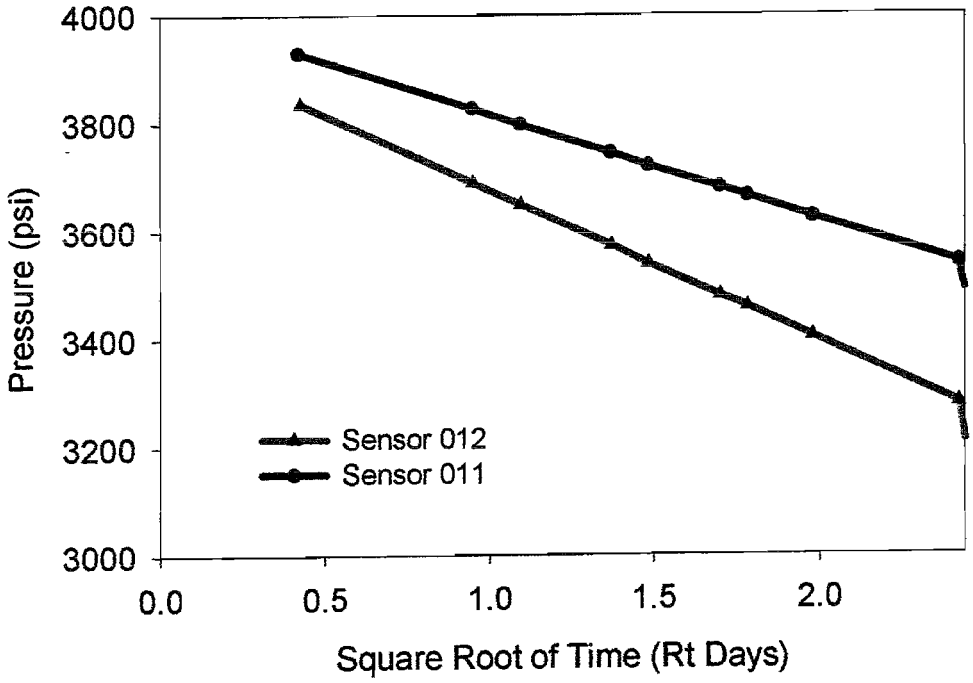

Figure 2.4.4b
Measured pressure versus Time (a) and Square root of time (b) for sensors 011 (175 um diameter fibre) and 012 (130 um diameter fibre) in water under 4000psi.

2.4.5 *Physical Effect of HTHP Water on Silica Fibres*

Samples of sensors that had been exposed to HTHP water were analysed under a scanning electron microscope (SEM) by Mrs. Ping Hua of the ORC at the University of Southampton.

Figures 2.4.5 a and b show SEM photographs of cleaved fibre end faces of a pristine side-hole fibre sample and a side-hole fibre exposed to HTHP water (4000psi) at 155°C for 14 days and at 250°C for a further 7 days .

Exposure of the silica fibre to the HTHP water appears to have modified the fibre surface layer to a depth of 1 - 2 μm. It is unclear whether this layer has any contribution to the sensor drift effect. Measurement of the fibre from cross section photographs and comparison between exposed and unexposed fibres, shows that this layer is integral to the fibre and is not a deposited layer.

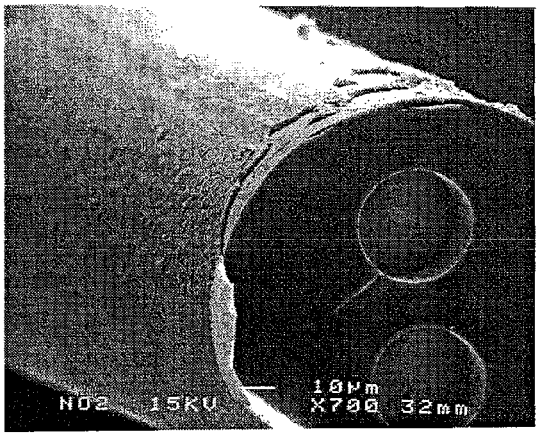

Figure 2.4.5a: SEM photograph of a side-hole fibre exposed to water at 155°C for 14 days and then at 250°C for 7 days.

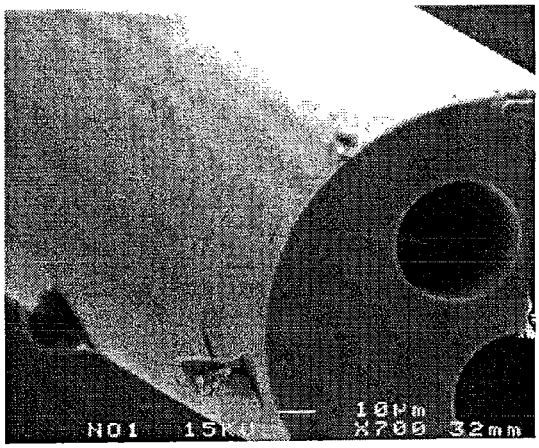

Figure 2.4.5b: SEM photograph of an untreated sample of the fibre in figure 2.4.5a.

2.4.6 Post-Treatment of Sensors Exposed to HTHP Water.

A side-hole fibre sensor was exposed to water at 4000psi and 300°C for approximately 6 days. Figure 2.4.7 shows the drift curve (pressure reading against time) for this sensor. On removal from the test chamber, the sensor had an offset pressure reading of approximately -4500 psi.

The sensor was subsequently placed into an oven at 195°C and monitored for almost 170 days. Figure 2.4.8 shows the offset pressure reading of the sensor plotted against time whilst in the oven.

The sensor offset slowly returned towards zero, reaching a value of approximately -1500 psi after 170 days after which the measurement was stopped.

The result shown by figure 2.4.7 suggests that the "permanent" effects of high-temperature, high-pressure fluids on side-hole-fibre pressure sensors can be reversed. Any surface reaction between the silica fibre and HTHP fluid is therefore a reversible one.

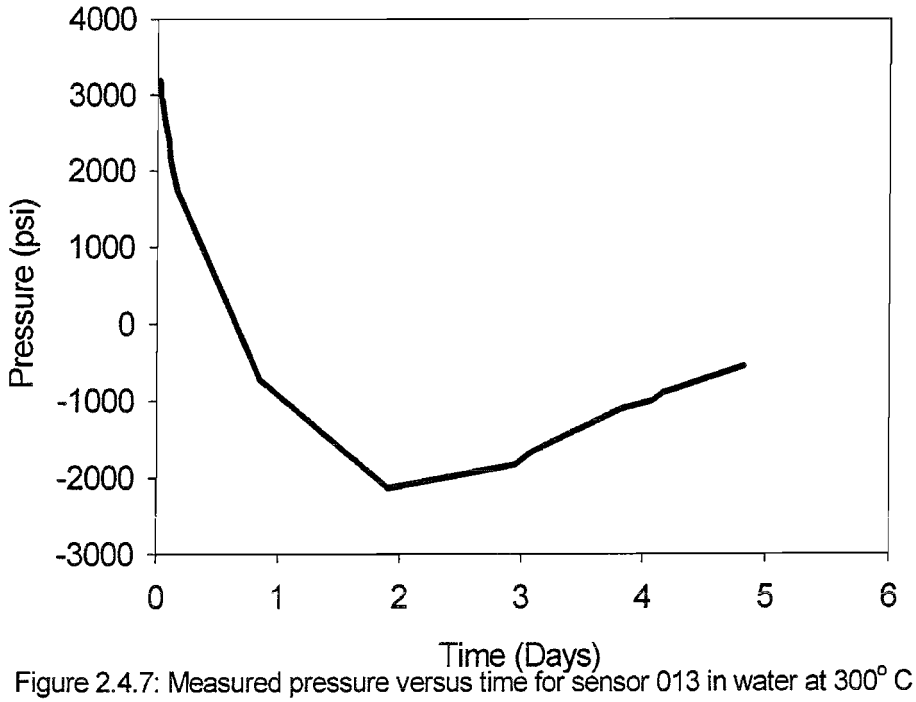

Figure 2.4.7: Measured pressure versus time for sensor 013 in water at 300° C and under 4000psi.

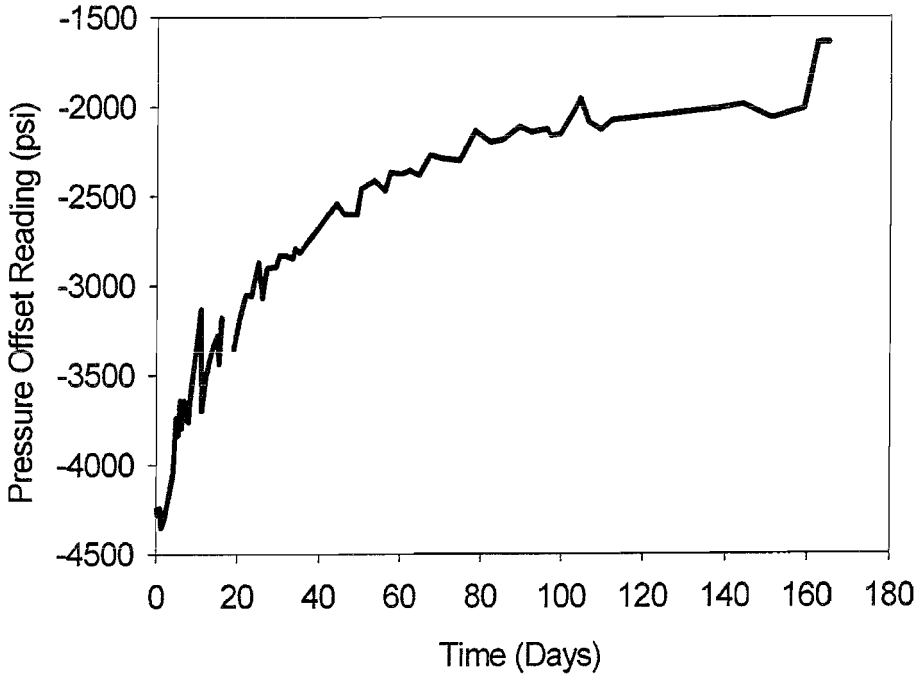

Figure 2.4.8: Pressure offset reading versus time for sensor 013b, in a dry oven at 195° C and at ambient pressure. Sensor was previously exposed to 300° C water under 4000psi for approximately 5 days (sensor 013, figure 2.4.7).

2.5 Discussion.

Results have been presented for side-hole, optical-fibre pressure sensors operating under various conditions of high-temperature and high-pressure.

All sensors show a characteristic and repeatable drift in measured pressure with time, which, in some cases, is a linear relationship with the square-root of time. The drift is such that the pressure-induced birefringence becomes increasingly negative with time.

The rate and magnitude of the drift in the pressure-sensor measurement has been shown to have no dependence on the applied pressure, the core-composition, the side-hole size and position, fibre composition or fibre inherent-birefringence. Furthermore, hydrogen-loading of the fibre does not affect the drift in any way.

Pressure-sensor drift is observed to be dependent upon the temperature, fluid medium and fibre diameter alone.

The rate and magnitude of the sensor drift increases disproportionately with increasing temperature. Furthermore, at 300°C, the drift curve shows a characteristic change in the direction after a certain time, dependent upon the high-temperature, high-pressure fluid. The "turn over" in drift direction has only been demonstrated at 300°C. At lower temperatures, the "turn over" may also occur but after a much longer time.

Sensors have been measured in a variety of different liquids, which exert their own characteristic trend on the rate of drift of the sensors. Water is shown to have the greatest effect on the pressure-sensor drift rate and this effect is accentuated when the water is injected into the side-holes of the fibre.

The drift effect is observed to begin as soon as the silica-fibre sensor is immersed in the high-temperature, high-pressure fluid.

On removal of the pressure and temperature from a sensor, the drift effects are observed to be permanent in that the fibres are transformed from low-birefringence fibres into highly-birefringent fibres due to the treatment process. These permanent effects are large enough that a sensor treated in water at 300°C can have a beat length of the order of 2.4 mm measured at 633nm after only 2 days.

The experimental results, summarised above, suggest that the cause of the pressure sensor drift is a surface effect occurring at the interface between the silica fibre and the high-temperature, high-pressure fluid.

By having the fluid - silica interface internally, (within the side-holes of the sensor fibre), the rate of drift is increased further still. The effect of having water inside the side-holes of the fibre increases the drift rate by a factor of approximately 9.

Scanning electron microscope photographs have shown the presence of thin, modified, surface-layers of silica fibres heated in water up to 250°C. The effect of these on the observed instabilities of optical fibre pressure sensors in high-temperature, high-pressure fluids has not been established.

2.6 Conclusions.

- Large drifts are observed in silica, side-hole-fibre pressure-sensors exposed to high-temperature, high-pressure fluids.
  - In water at 300°C and 4000psi, sensors drift by up to -6000psi in 2 to 4 days.
  - In polysiloxane oil at 300°C and 4000psi, sensors drift by approximately -1000psi in 2 to 4 days.
- Stresses in side-hole fibres as high as those seen in HiBi fibres are produced due to the exposure to high-temperature, high-pressure fluids.
  - Side-hole-fibres, in water at 300°C and 4000psi for only 2 days, develop a beat length of approximately 2.4mm (measured at 633nm). This can be compared to a PANDA or Bow-Tie HiBi fibre which have typical beat lengths of 1.5mm.
- The results suggest that a reaction at the interface between the silica and the high-temperature, high-pressure fluid is responsible for the observed pressure-sensor drifts.
- The surface reaction between silica and the high-temperature, high-pressure fluid can be reversed by post-treatment of the sensor at temperature in a "dry" atmosphere.

Chapter 3

Stressy Surface-Layers in Side-Hole-Fibre Pressure Sensors: Theoretical and Experimental Evaluation.

3.1 Introduction

A two-dimensional, free-strain, stress analysis of side-hole fibres under hydrostatic pressure has been made using ANSYS, a general-purpose, finite-element-modelling (FEM) package [37].

The FEM stress-analysis data has been combined with an analytical model for birefringence in fibres, based on simple perturbation theory [38].

This chapter reports on the development of the FEM, produced by Dr.S.Syngellakis of the Mechanical Engineering Department at the University of Southampton.

The pressure sensitivity of side-hole fibre birefringence is theoretically predicted using the model. A relationship between the pressure sensitivity of side-hole fibre and the fibre cross- sectional geometry is proposed. The relationship is experimentally verified using pressure sensors fabricated from various side-hole fibre geometries.

The FEM is developed to include additional surface-layers in side-hole fibres to assess the effect of surface modifications on pressure-induced birefringence.

Results of the modelling predict that stressed surface-regions, both around the side-holes and at the fibre surface, can produce the drift effects observed in pressure sensors (chapter 2).

The presence of stressy surface-layers in side-hole fibres exposed to high-temperature, high-pressure fluids, and their effect on fibre birefringence, is experimentally verified.

3.2 Modelling of the Pressure Sensitivity of Side-Hole Fibres.

3.2.1 The Finite Element Model (FEM)

The model assumes that the cross-sectional geometries are of perfect symmetry and that the fibre core, side-holes and diameter are circular. The model therefore assumes that the fibre has zero intrinsic birefringence.

Based on these assumptions, a quarter section of the fibre has been analysed in order to reduce the computing calculation requirements and to increase the available resolution of the model.

Figure 3.2.1 shows the structure of the original model with the quarter fibre-section split into two separate material regions; the core and cladding. The material properties of these two regions have been chosen so as to model a side-hole fibre with a pure-silica cladding and a core fabricated from 3% germanium-doped silica. The Young Modulus of the core and cladding (E_c and E_{cl}) have been taken to be 70.8GPa and 72GPa respectively. Values of the core and cladding Poisson Ratio (υ_c and υ_{cl}) of 0.165 and 0.173 have been used throughout [39].

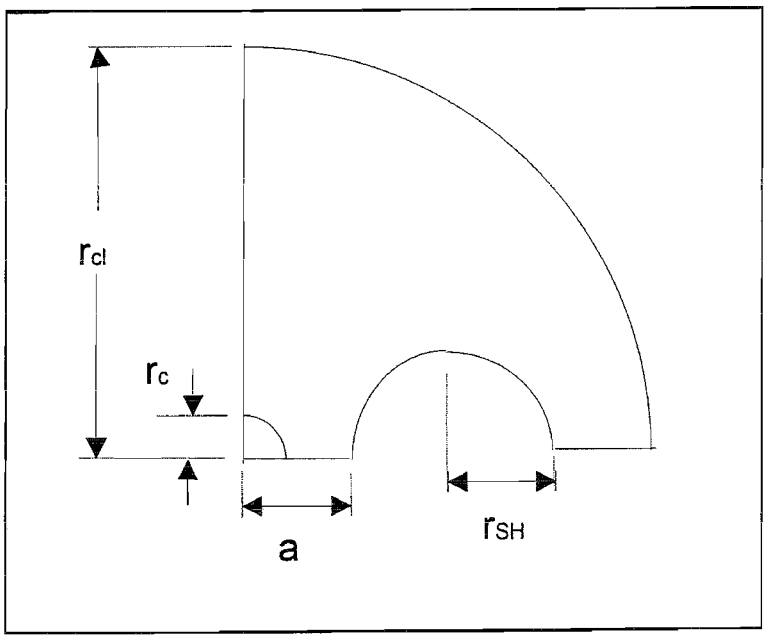

Figure 3.2.1: Quarter section of a side-hole fibre. Structure modelled using ANSYS for finite element modelling of pressure-induced birefringence in side-hole fibres.

The core- and cladding-radii (r_c and r_{cl}) are chosen to be 4μm and 62.5μm respectively in order to closely model the side-hole fibres used to make pressure sensors. The side-hole radius (r_{SH}) and the core-centre to side-hole-centre separation (a) are variables.

The mesh arrangement of the elements of the model is an automatic process in the ANSYS FEM package. The size and hence the number of the elements determines the resolution of the model but also determines the speed of the calculation.

When modelling side-hole-fibre stresses and birefringence, a high resolution is required within and close to the core as the majority of the optical power is confined within this region. The resolution becomes less important as the model extends out into the cladding

layers. An individual element size of 0.5μm has been adopted as a standard within the core region of the fibre. This element size extends to approximately 5μm at the fibre surface.

A series of models using core element sizes of 0.2, 0.5 and 1μm showed very little effect of the core element size on the modelled fibre birefringence.

The resultant output of the FEM includes the X- and Y-axial stresses for each individual element of the mesh and the centroid co-ordinates and area of each element.

The applied hydrostatic-pressure, side-hole radius (r_{SH}) and core centre to side-hole centre separation (a) have been varied throughout many trials of the FEM. This data has been used to calculate the pressure-induced birefringence of a side-hole fibre and its dependence upon the fibre cross-sectional geometry.

3.2.2 Calculation of Stress-Induced Fibre Birefringence.

The localised X- and Y-refractive index perturbations (Δn_x and Δn_y) within the fibre are related to the localised X- and Y-axial stresses (σ_x and σ_y) by the photoelastic equations (equation 3.2.1.) [40].

$$\Delta n_x = -\left[\frac{n_0^3}{2}\right]\left[q_{11}\sigma_x + q_{12}\left(\sigma_y + \sigma_z\right)\right]$$

$$\Delta n_y = -\left[\frac{n_0^3}{2}\right]\left[q_{11}\sigma_y + q_{12}\left(\sigma_x + \sigma_z\right)\right] \qquad (3.2.1)$$

where, n_0 is the unperturbed refractive index of the waveguide region and q_{11} and q_{12} are the stress-optic coefficients for silica [39].

Assuming that the stress-induced perturbation of the refractive index is small, ($\Delta n_{x,y} << n_0$), an expression may be derived to describe the modal distribution within a perturbed fibre in terms of known modes of an unperturbed weakly guiding fibre [38]. With an invariant longitudinal perturbation, the change in propagation constant may be described by equation 3.2.2.

$$\beta_{x,y} = \overline{\beta} + k\frac{\left[\int_{A_\infty}\left(n_{x,y} - n_0\right)E^2 dA\right]}{\int_{A_\infty} E^2 dA} \qquad (3.2.2)$$

where, $\beta_{x,y}$ are the perturbed propagation constants in the x- and y-polarisation directions and $\overline{\beta}$ is the unperturbed propagation constant. $n_{x,y}$ are the perturbed refractive indices in the x- and y-polarisation directions and n_0 is the unperturbed refractive index of the material. $k = 2\pi/\lambda$, where λ is the free space wavelength. A is the area of the fibre cross section and E describes the electric-field distribution. The fibre birefringence can therefore be calculated simply using the expression $\Delta\beta = \beta_x - \beta_y$ (rad/m).

For a weakly-guiding, step-index, single-mode fibre, in which the refractive index contrast is small, the field distribution can be approximated in the core by [38]:

$$E(r)_c = C\left[\frac{K_0(w)}{J_0(u)}\right]J_0\left(\frac{ur}{a}\right) \quad , \; r < a \qquad (3.2.3)$$

and in the cladding by:

$$E(r)_{cl} = DK_0\left(\frac{wr}{a}\right) \qquad , \; r > a \qquad (3.2.4)$$

Where $E(r)_c$ and $E(r)_{cl}$ are the field distributions in the core and cladding respectively. J_0 is the Bessel function of zero order, K_0 is the modified Bessel function of zero order, and a is the core radius. U and W are the eigenvalues in the core and cladding respectively, where W also determines the rate of decay of the field in the cladding. C and D are arbitrary constants used for field normalisation.

The eigenvalues, U and W, can be determined from knowledge of the fibre normalised frequency, V, and approximated to 0.1% ***(for 1.5<V<2)*** from the following relationship obtained graphically [41]:

$$W = 1.1428V - 0.9960 \qquad (3.2.5)$$

given that:

$$V^2 = W^2 + U^2 \qquad (3.2.6)$$

In calculating the fibre birefringence from FEM stress-data, the fibre has been modelled as closely as possible to a standard telecommunications fibre with an NA of 0.12, a core index of 1.462 and a cladding index of 1.457. An operating wavelength of 1300nm, used in experimental measurement of pressure sensors, is also used in the calculation.

3.2.3 *Experimental and Theoretical Side-Hole-Fibre Pressure Sensitivity.*

The FEM has been used to model the birefringence of fibre geometries G and H (Appendix A) as a function of pressure. The side-hole radii (r_{SH}) and core-centre to side-hole-centre separation (a) have been approximated from the cross-sectional photographs of the fibres.

Polarimetric pressure sensors fabricated from fibres G and H have been measured using the instrumentation described in section 1.2. The pressure sensitivity of these sensors have been converted into values of fibre-birefringence pressure-sensitivity (units: mrad / Psi.m) and are shown in table 3.1. The corresponding modelled values are also included in table 3.1.

Fibre Geometry	Core Centre to Side-Hole Centre, a(μm)	Side-Hole Radius r_{SH} (μm)	Sensitivity (mrad/psi.m)
G (Theory)	24.5	16.5	246.07
H (Theory)	30.0	9.50	44.88
G (Expt.)	≈24.5	≈16.5	244.13
H (Expt.)	≈ 30.0	≈9.50	40.75

Table 3.1: Measured and modelled fibre dimensions and sensitivities of fibres G and H.

Figure 3.2.2 shows the modelled and measured birefringence of fibres G and H as a

function of applied pressure (in psi). The measured and modelled values of fibre G are very similar, to approximately 99%. There is a larger discrepancy for fibre H however. This is assumed to be due to the non-circular fibre, holes and core, all consequences of side-hole collapse during the fibre pulling process.

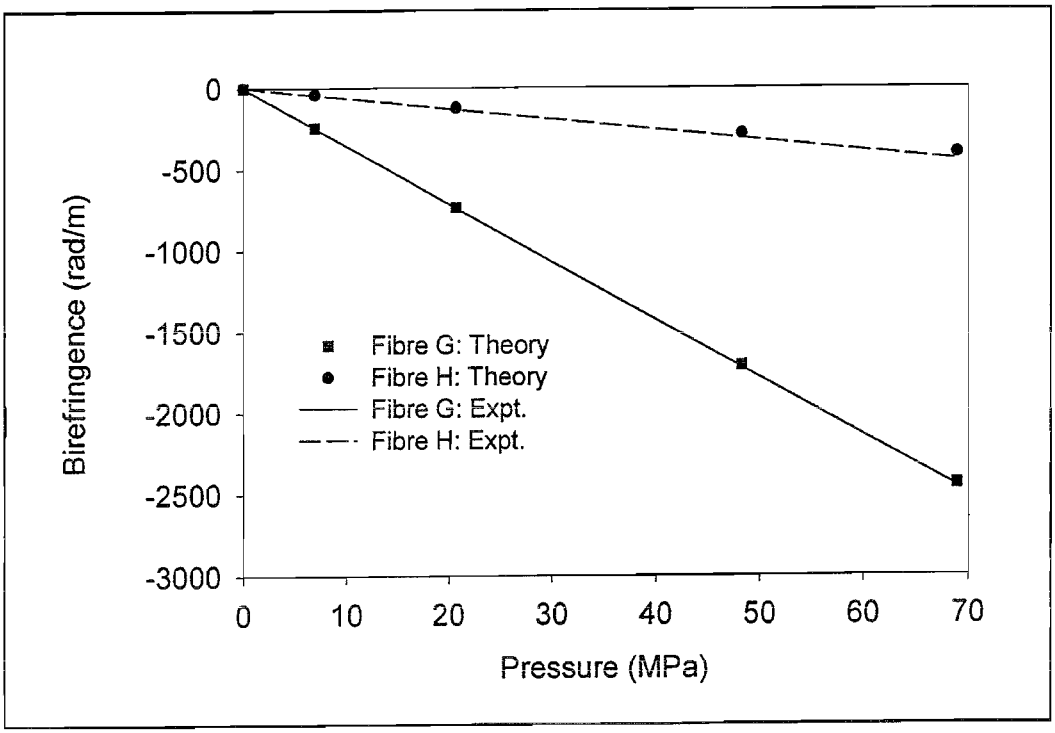

Figure 3.2.2: Experimental and modelled pressure-induced birefringence for side-hole fibres with geometries G and H.

A simple observation of figure 3.2.2 and table 3.1 shows that the fibre with large holes, positioned close to the core, has a much higher pressure sensitivity (approximately 6 times higher) than a fibre with small holes positioned further from the core.

The model has been used to investigate the relationship between the side-hole position and size and the fibre pressure-sensitivity. Side-hole fibres with the same hole position ($a - r_{SH}$), but varying hole-radius (r_{SH}), have been modelled using values of ($a - r_{SH}$) of 6, 12 and 18μm. By varying the side-hole radius and location, the angle φ between the core-centre to side-hole-centre axis and the core-centre to side-hole tangent (see figure 3.2.3 inset) is altered.

Figure 3.2.3 shows the plots of pressure-induced birefringence (4000psi applied

pressure) against φ^2 for the three different values of (a -r_{SH}). All three plots show shat the pressure sensitivity of the side-hole fibre follows a close linear relationship with φ^2 for values of φ up to 45° [42]. Angles greater than 45° were difficult to accurately model due to problems with forming a reliable mesh in the FEM. With such a fibre geometry, the side-holes are very large and form the majority of the cross-sectional area. In practice, such a fibre would be extremely fragile.

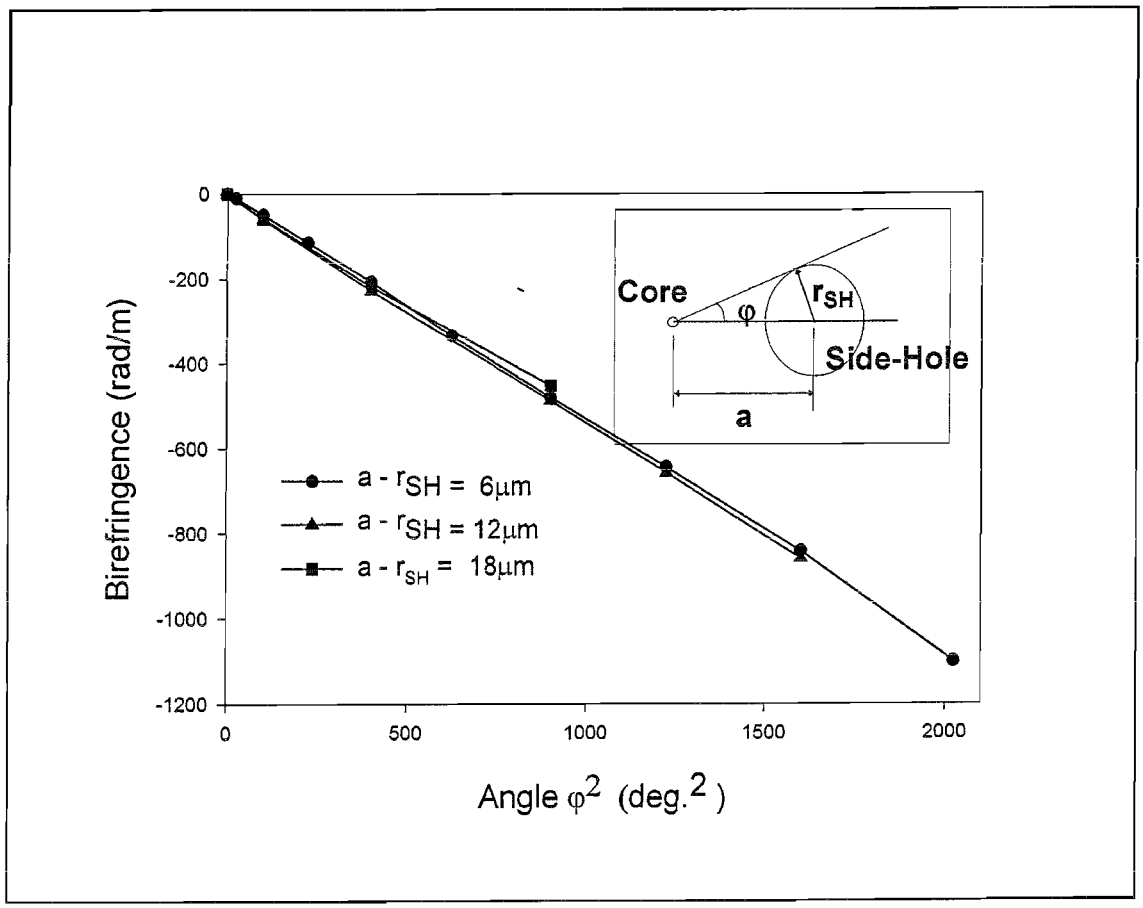

Figure 3.2.3: Modelled pressure-induced birefringence plotted against φ^2 for three fibres with core to side-hole separations of 6, 12 and 18μm. (Inset: Schematic of the fibre geometry).

3.3 Effects of Stressy-Layers in Side-Hole Fibres

3.3.1 Finite Element Modelling of Stressy Surface-layers.

3.3.1.1 Layers Around the Fibre Outer Surface.

It was thought that the observed drifts in pressure-induced birefringence described in chapter 2 could be caused by highly-stressed surface-layers in the fibre cladding.

The FEM described in section 3.2 has therefore been modified to incorporate additional surface-layers both around the fibre diameter and on the inner surface of the side-holes. Figure 3.3.1 shows the modelled, quarter-fibre section, including the outer surface layer of thickness h_1 and side-hole surface-layer of thickness h_2.

Element sizes of 0.5μm have been used in the core. The element size at the fibre surface is dependent upon the thickness (h_1 and h_2) of the two additional surface-layers.

The fibre cross-section has been dissected into five regions in which the elastic and thermoelastic properties can each be individually specified. The proposed 'stressy layers' are modelled by applying a free-strain in which the thermal expansion coefficient of either, or all of the additional surface layers are made to differ from the rest of the fibre. By simulating a temperature change in the model, a volumetric change of the surface layers is modelled as a free strain.

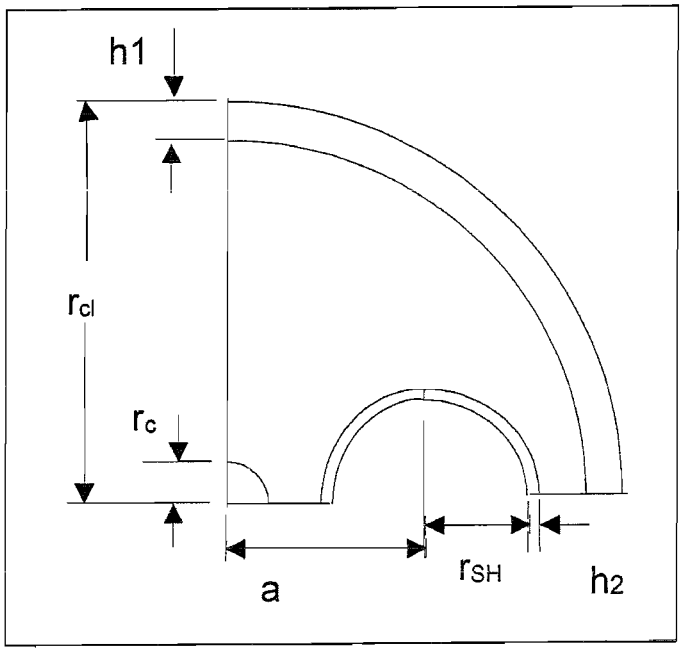

Figure 3.3.1: Schematic of the modified FEM used to model the effects of stressy surface-layers on side-hole-fibre birefringence.

In order to investigate the effects of changes in volume of the surface layers on the pressure- induced birefringence, the outer surface-layer alone has been modified.

The structure has been modelled with an applied pressure of 6000psi, varying thickness' of surface layer (h_1) and various levels of volume increase of the surface layer.

Values of the side-hole radius (r_{SH}) and core- to side-hole- centre (a) of 20μm and 30μm respectively, have been used in this model.

Figure 3.3.2 shows the relationship between birefringence and magnitude of the volume increase for different values of h_1 (3, 4, 8 and 16μm). Equivalent pressures are also provided for reference on the right-hand vertical axis of this plot.

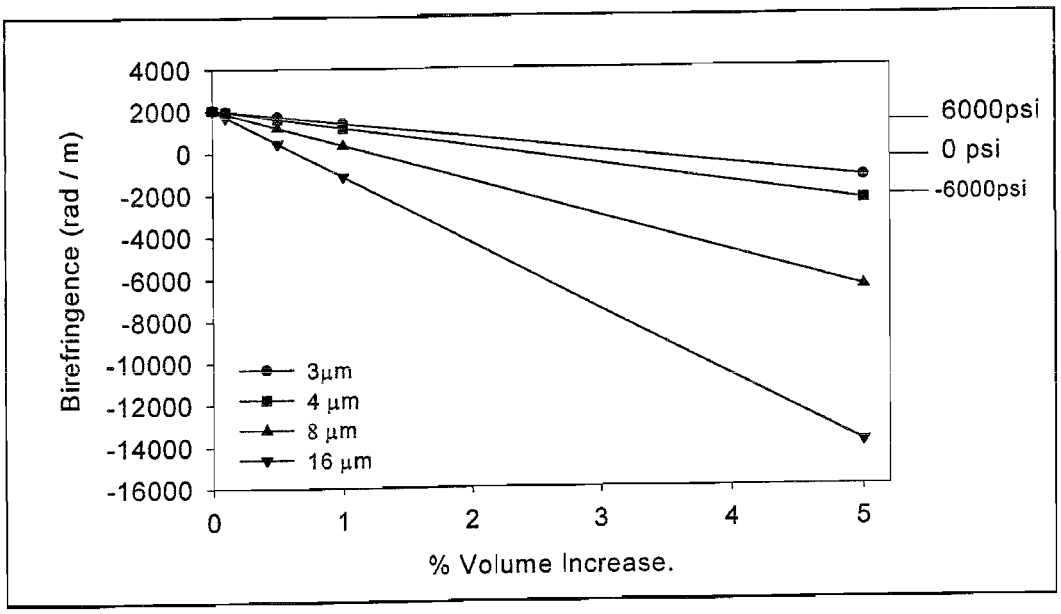

Figure 3.3.2: Modelled birefringence plotted against the percentage volume increase of a fibre surface-layer of thickness h1. Plots shown for values of h1 of 3, 4, 8 and 16μm. A pressure of 6000psi is applied to the fibre in all cases. Pressure values shown on the right hand vertical axis for reference.

The curves show, qualitatively, that an increase in volume of the surface layer causes the magnitude of the fibre birefringence to reduce through zero and continue to become more negative. The thicker the surface layer, the larger the effect of the volume increase. The FEM was modified slightly to enable the thickness of the surface layer to increase beyond the side-hole (figure 3.3.3).

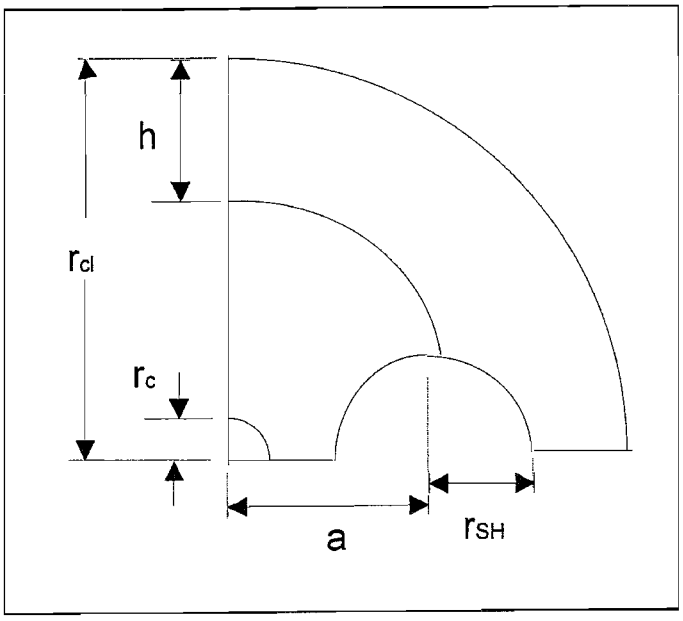

Figure 3.3.3: Modified FEM of a quarter section of side-hole fibre. Design allows the stressy surface layer to extend beyond the side-holes.

A fibre geometry, similar to that of fibre G (Appendix A), has been modelled with a side-hole radius of 16.5μm, a core-centre to side-hole-centre separation of 24.5μm and a side-hole to surface separation of approximately 21.5μm. A pressure of 4000psi has been applied in the model and the surface layer is uniformly swollen by 0.5% and 0.1 %.

Figure 3.3.4 shows the plot of birefringence against increasing thickness of the surface layer (h). Equivalent pressure values are shown on the right hand vertical axis for reference.

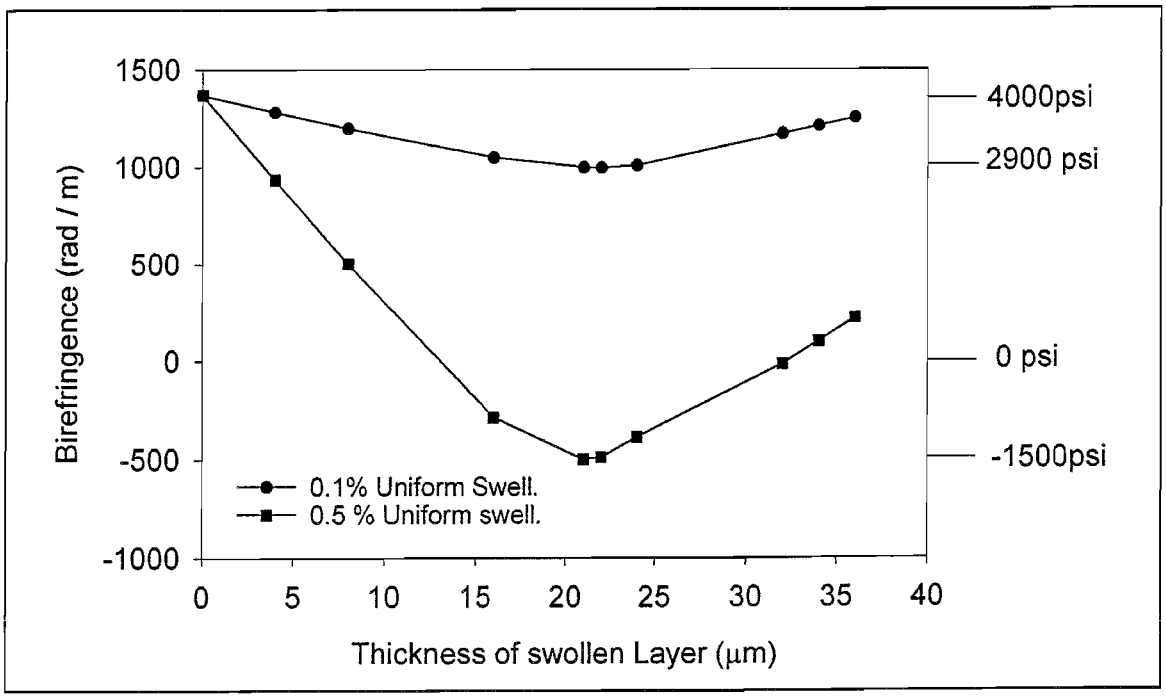

Figure 3.3.4: Modelled change in side-hole fibre-birefringence (fibre geometry G) plotted against the thickness of a uniformly-swollen layer of 0.1% and 0.5% swell. Fibre is under an applied pressure of 4000psi. Equivalent pressures are shown on the right-hand, vertical axis.

The curves for 0.1% and 0.5% swollen layers show that the pressure reading of the side-hole fibre decreases as the layer penetrates further into the fibre up to approximately 20μm. The drift curve then "turns over" and the pressure reading increases as the stressed layer penetrates further into the fibre. The exact point at which the response "turns over" was not possible to ascertain as the FEM package had difficulty in producing a reliable mesh (organisation of the finite elements) in regions where the geometry became awkward. However, the curve appears to "turn over" when the swollen layer is between 20μm and 22μm in depth. For this fibre, this coincides closely with the surface layer reaching the side-hole of the fibre.

The shape of the curve is not dependent upon the extent of volume expansion of the surface layer. The 0.5 % swell produces a maximum change in birefringence approximately 5 times greater than a layer subject to 0.1% swell. However, the point at which the curve "turns over" is the same irrespective of the volume expansion of the surface layer.

The value of 0.5% was deliberately chosen to closely model experimentally measured

drifts of side-hole fibre sensors. Pressure sensor 013 (chapter 2) was fabricated from side-hole fibre with a similar geometry to that used in the above model (fibre C, Appendix A). This sensor was measured in water at 4000psi and 300°C (results of chapter 2, figure 2.4.7). The drift curve for sensor 013 "turned over" after a drift of approximately -6000psi, similar to the modelled fibre of figure 3.3.4.

3.3.1.2 Layers Around the Fibre Side-Holes

The effect of a stressy layer being formed around the side-holes of a fibre has also been investigated. By varying the thermal properties of the two regions around the side holes, a volumetric increase has been introduced.

Figure 3.3.5 shows the relationship between birefringence and volumetric increase for a 2μm layer around the side-holes of a fibre under 6000psi. The relationship between birefringence and volume increase is also shown for a 2μm outer-surface layer for comparison.

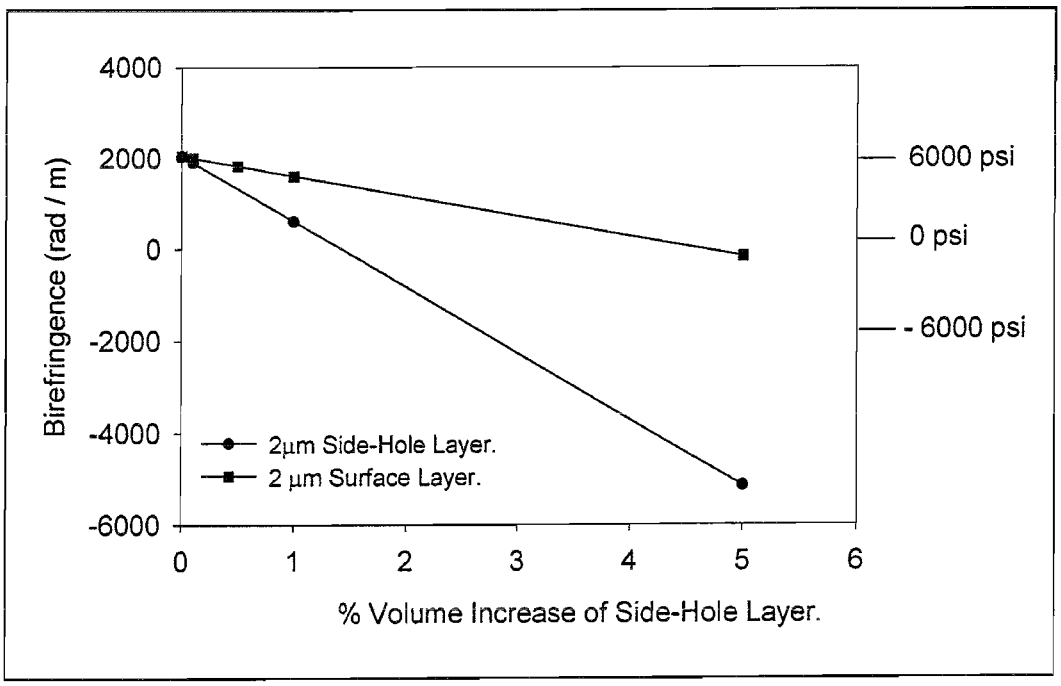

Figure 3.3.5: Modelled change in side-hole fibre birefringence plotted against the percentage volume increase of 2μm surface-layers around the fibre surface and around the side-hole. 6000psi pressure is applied to the fibre at all times. Pressure values are shown on the right vertical axis for comparison.

The formation of a stressy layer around the side-holes has more than three times the effect of that at the fibre outer-surface. The volume increase of the side-hole layer causes the birefringence to decrease towards zero and a zero crossing occurs with only a 1.5% volume increase. The corresponding value for a surface layer is approximately 4.9%.

3.3.2 Experimental Confirmation of Stressy Surface Layers.

Side-hole-fibre pressure sensors, exposed to water at 300°C and under 4000psi, were monitored over periods of 1, 1.5 and 2 days. The sensors were fabricated from fibre G and were therefore all nominally identical.

Figure 3.3.7 shows the drift curves (measured pressure against square root of time) for each of these sensors.

Sensor 014, removed after 1 day, had drifted by approximately 5700psi. Sensor 015, removed after 1.5 days, had drifted by approximately 7200psi. The drift curve of sensor 016 "turned over" after approximately 1.6 days. Sensor 016 showed a total drift of approximately 6850psi when removed after 2 days.

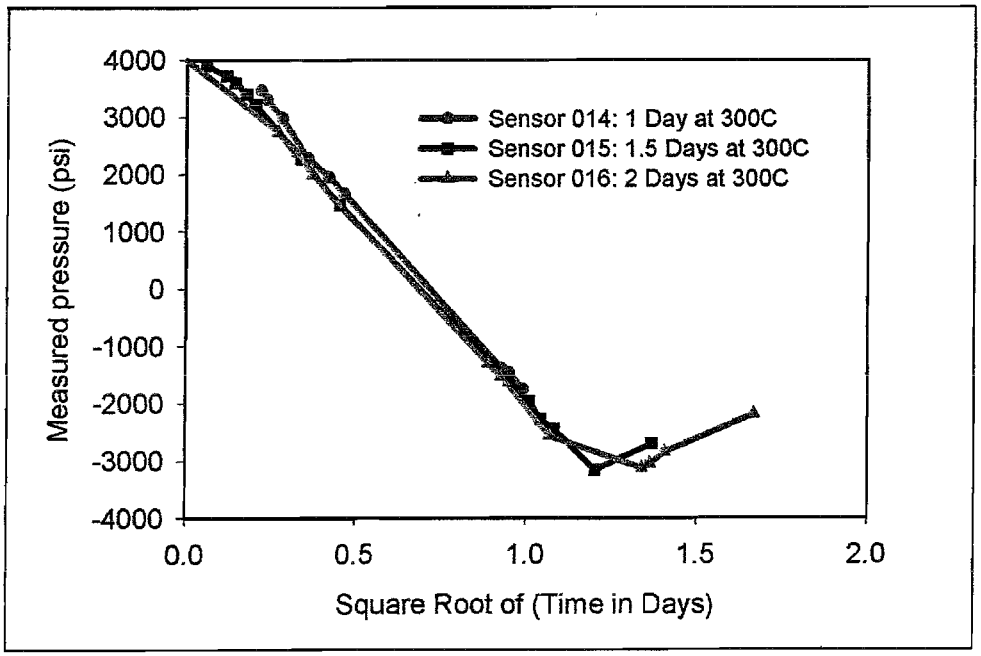

Figure 3.3.7: Measured-pressure plotted against the square-root of time of 3 nominally identical side-hole-fibre pressure sensors in water at 300°C and 4000psi.

The offset pressure readings of the three sensors, after exposure to the HTHP water, were measured at ambient temperature and pressure. The sensors were immersed in a 2:1 solution of H_2O : 48%HF and the offset pressures were monitored as the fibre cladding was

etched.

Control fibres which had been exposed to the HTHP water for 1, 1.5 and 2 days were also immersed in the etch solution and removed and measured at regular intervals. An etch rate of approximately 0.33μm per minute was estimated from these measurements.

Figure 3.3.8 shows the plots of measured offset pressure (psi) against the radial etch depth (in μm) for the three sensors.

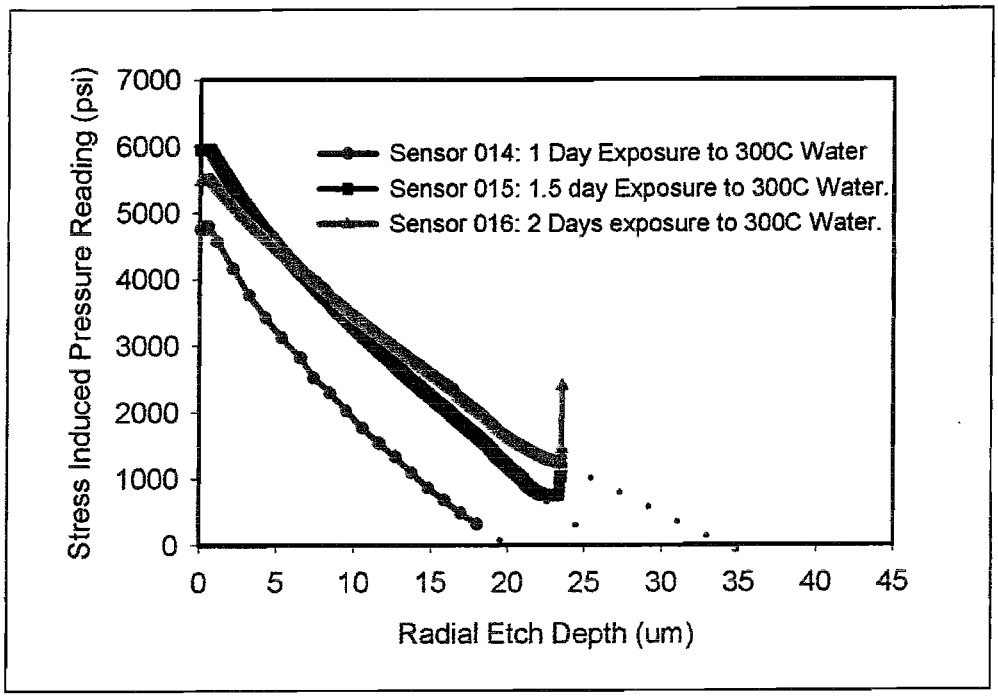

Figure 3.3.8: Measured offset-pressure plotted against radial etch-depth for sensors 014,015 and 016 etched in dilute hydrofluoric acid. All three sensors are nominally identical. Sensors were previously exposed to water at 300°C for 1 day (014), 1.5 days (015) and 2 days (016).

The offset-pressure readings all increase back towards zero as soon as the fibre is immersed in the etch solution.

The slopes of the three curves are all approximately linear. The instrumentation was not able to measure offsets close to zero due to the overlap of the interferometer fringe patterns (section 1.2.3). The etch curves have therefore been extrapolated to zero to estimate the depth of penetration of the stressy layer.

The measurement of sensor 016 (2 days) stopped well before the fibre offset had

returned to zero because the etch solution etched into the side-holes of the sensor and the polariser. Destruction of the side-hole-fibre polariser ended the measurement prematurely. Extrapolated penetration depths of approximately 20μm, 25 μm and 33μm are shown for sensors in 300°C water for 1, 1.5 and 2 days respectively.

3.4 Discussion.

A finite element model has been developed to investigate the pressure sensitivity of birefringence in side-hole fibre. The results show a linear relationship between the pressure sensitivity of a given fibre and φ^2, where φ is the angle between the side-hole-centre and core-centre axis and the core-centre to side-hole tangent. The relationship predicts that a highly-sensitive pressure sensor can be fabricated from fibre with small holes located close to the core. This has strong implications on the design of side-hole fibres compromising between the needs for high sensitivity, strength and mechanical robustness.

Experimental measurements of pressure sensors, fabricated from side-hole fibres with different cross-sectional geometries, have been shown to be in excellent agreement with the modelling predictions.

Surface layer effects in side-hole fibres have been investigated using a modification of the finite element model. Swollen layers at the fibre outer-surface and side-hole inner-surface have been used to model the effects of surface stresses on side-hole-fibre birefringence. The results of the modelling qualitatively describe the experimental drift-trends in pressure sensors reported in chapter 2.

Side-hole-fibre surface-layers, subjected to volume increases, cause changes in fibre birefringence. The birefringence changes act in a direction which directly oppose the pressure-induced birefringence.

For side-hole-fibre pressure sensors in high-temperature, high-pressure fluids, the pressure-induced fibre-birefringence becomes increasingly negative with increasing time (chapter 2).

The smallest of stressy surface-layers has an effect on the fibre birefringence. An infinitesimally small surface layer would still cause a small change in birefringence. As the thickness of the surface layer increases, the birefringence change increases in proportion.

Penetration of the layer up to and beyond the side-holes of the fibre, causes the fibre birefringence to begin to increase back towards the initial state. This is observed as a "turn

over" in the curve of birefringence versus thickness of swollen-layer. The magnitude of the fibre birefringence at the "turn over" point is determined by the amount by which the surface layer is swollen. A 0.5% volume increase produces approximately 5 times the change in birefringence of that due to a surface-layer swollen by 0.1%.

Side-hole-fibre pressure sensors, exposed to liquids at high pressure and 300°C, show such a "turn over" in the direction of the drift curve (chapter 2). In general, the amount that the sensor drifts before the "turn over" point is dependent upon the high-temperature, high-pressure fluid. In water, for a certain fibre geometry, this value was approximately -6000psi. In polysiloxane oil, the same fibre geometry drifted by approximately -1000psi before the "turn over" point was reached.

Stressy layers around the side-holes of the fibre also cause the fibre birefringence to decrease. The effect of a side-hole stressed layer is more than twice that of a layer at the outer fibre surface.

Experimental measurements of a pressure sensor with water-filled, side-holes showed such a trend in long-term drift. However, the drift rate of a sensor with water-filled side-holes was measured to be approximately 9 times higher than that of a sensor with air-filled side-holes.

The formation of stressy surface-layers in side-hole-fibre pressure sensors exposed to high-temperature, high-pressure water has been experimentally verified. Etching of the surface layers of such exposed sensors removes the stress-birefringence caused by the stressy surface- layers.

Etching measurements show that such stressed layers can penetrate as far as 35μm into the glass fibre in as little as 2 days (sensors in water at 300°C and under 4000psi). Furthermore, the results confirm that the "turn over" feature of sensor drift curves at 300°C in high-pressure fluids is caused by penetration of stressy surface-layers up to and beyond the side-holes.

A qualitative model of the pressure-sensor drift described in chapter 2 can be assumed from the results presented in chapter 3:

The drift is caused by a surface reaction between the silica fibre and the high-temperature, high-pressure fluid. The resulting modification of the silica in the surface layer creates stresses within the fibre which are anisotropic because of the side-hole-fibre geometry. The birefringence of the fibre becomes increasingly negative (with respect to

pressure-induced birefringence) due to the anisotropic stresses in the core.

As the surface reaction continues with time, the thickness of the modified layer increases, causing the birefringence change to increase accordingly. The rate and magnitude of the reaction are dependent upon the temperature and the type of high-temperature, high-pressure fluid.

As the modified layer approaches the side-holes of the pressure-sensor fibre, the change in fibre-birefringence changes in direction causing the pressure drift-curve to "turn over".

3.5 Conclusions.

- A surface reaction between high-temperature, high-pressure fluids and silica fibres creates stressy surface-layers.
- Stressy surface-layers cause the birefringence in a side-hole fibre to become increasingly negative with respect to pressure-induced birefringence (chapter 2).
- Removal of the stressy layers by etching in hydrofluoric acid, causes the birefringence to return to the original stress-free state.
- Stressy layers are shown to penetrate as far as 35μm into the silica fibre in as little as 2 days at 300°C in high-pressure water.
- Stressy layers will be formed in any silica fibre exposed to high-temperature, high-pressure fluids.
- All silica fibre pressure sensors will drift in high-temperature, high-pressure fluids.

Chapter 4.

Effects of Stressy Surface-Layers on Optical Fibres and on Fibre Bragg Grating Pressure Sensors.

4.1 Introduction

Finite Element Modelling of side-hole fibres was used (chapter 3) to demonstrate that drifts in fibre pressure-sensors in high-temperature, high-pressure (HTHP) fluids are caused by stressy surface-layers. Furthermore, using etching experiments on side-hole-fibre pressure sensors exposed to HTHP fluids, the presence of stressy surface-layers was experimentally verified.

A combination of the experimental and theoretical work concerning stressy surface-layers in fibres, predicts that any silica fibre will be effected by HTHP fluid environments. Chapter 4 discusses the effects of HTHP fluids on lengths of single-mode and multi-mode fibres and on fibre Bragg-grating (FBG) devices.

The pressure-induced change in the optical-path-length of fibres is theoretically calculated and experimentally measured using an all-fibre, Michelson interferometer. The effects of HTHP fluids on the optical-path-length of such fibres are monitored with time. Similarly, the pressure-induced changes in the Bragg wavelength of FBG's are calculated, measured and monitored with time when the devices are exposed to HTHP fluid environments.

Chapter 4 reports on the findings of this investigation and compares the effects of HTHP fluid on side-hole-fibre pressure sensors, FBG's and optical-path-lengths of optical fibre.

The optical-path-lengths of carbon-coated, single-mode fibre in HTHP fluids have also been monitored with time. The optical-path-length measurement is established as a suitable method for testing the effectiveness of coatings at protecting optical-fibre cables in HTHP fluid environments.

Results are presented for commercially-available coatings based on polymers and carbon. One particular commercially-developed coating is identified as a suitable protective coating for fibre optic cables in HTHP fluids.

Fibre pressure sensors are fabricated from side-hole fibre coated with the best,

commercially available, protective coating. The stability of such sensors in HTHP fluids is monitored and the results are presented and discussed in this chapter.

4.2 Optical-Fibre Path-Length Changes in High-Temperature, High-Pressure Fluids.

In chapter 3, the drift of a side-hole-fibre pressure sensor at 300°C and under 4000psi was qualitatively modelled using the finite element model. The model was based on a surface layer, subject to a uniform expansion of 0.5% and of thickness which increases with time.

Based on this general model, a standard optical fibre of radius 62.5μm with a 10μm surface layer subject to 0.5% uniform volume increase, would be expected to increase in physical length by approximately 0.15 %. This corresponds to an increase in length of approximately 2.3mm for a 1.5m piece of optical fibre. While this value is approximate, the FEM results predict a physical strain within this order of magnitude.

4.2.1 Theoretical Pressure Sensitivity of Optical-path-length of Fibres.

Changes in optical-path-length of a fibre under the influence of hydrostatic pressure are separated into two effects: the change in physical length of the fibre and the change in refractive index. Equation 4.2.1 describes this effect

$$\Delta L_p = k_0 L\left[n\varepsilon_z + \Delta n\right] \qquad (4.2.1)$$

where ΔL_p is the optical-path-length change, n is the unperturbed refractive index of the core, L is the fibre length, $k_0=2\pi/\lambda_0$ where λ_0 is the free-space wavelength and Δn is the change in refractive index of the core.

The refractive index change can be calculated from the photoelastic equations (3.2.1) and the axial strain calculated simply using the Hooke's law relationship:

$$\varepsilon_z = \frac{1}{E}\left(\sigma_z - \nu\left(\sigma_x + \sigma_y\right)\right) \qquad (4.2.2)$$

where E is the Young Modulus taken to be 72GPa, ν is the Poisson ratio taken to be 0.17 and $\sigma_{x,y,z}$ are the axial stresses. For the case of hydrostatic pressure, P, the stresses are uniform and equal in the x, y and z directions and are equal to -P (the negative sign indicates a compressive stress). Equation 4.2.3 describes the total effective change in the

optical-path-length of an optical fibre when subjected to a hydrostatic pressure P.

$$\Delta L_p = -PLk_0 n\left[\frac{1}{E}(1-2\nu) - \frac{n^2}{2}(q_{11}+2q_{12})\right] \qquad (4.2.3)$$

where ν is the Poisson ratio, E the Young Modulus and q_{11} and q_{12} the stress optic coefficients of silica.

Observation of equation 4.2.3 shows that there is a physical length reduction of a fibre under hydrostatic pressure (second term) combined with an increase in the core refractive index which manifests itself as an optical-path-length increase. Evaluation of equation 4.2.3 shows that for a 1.5m length of fibre, an optical-path-length change of -0.056mm per 2000psi (-0.0037%) would be expected. More generally, the pressure sensitivity of the optical-path-length of optical fibre is expected to be approximately $-18.6*10^{-9}$ m / psi.

4.2.2 Experimental Measurement of the Pressure Sensitivity of Optical-path-lengths of Fibres.

In order to measure the pressure sensitivity of changes in the optical-path-length of fibre, an interferometric technique has been adopted as shown in fig.4.2.1. The measurement technique does not monitor the absolute path length of the fibre, but its change relative to a zero pressure value.

Using a low-coherence, Michelson interferometer, lengths of fibre, in a high pressure chamber containing water and an atmospheric pressure chamber containing air (control), were monitored with time. Pressure and temperature are applied to the fibres using the facility described in section 2.2.1. Each of the fibre lengths within the chamber was approximately 1.5 m long and had a chromium mirror evaporated onto the end-face.

Each sample was connectorised with an FC/PC connector so that individual samples could be interchanged and connected to the coupler (arm B of the interferometer) for each measurement.

Drifts in the optics with ambient temperature variations were monitored using a reference fibre, which was maintained at a constant temperature. This reference fibre was measured each time a sample measurement was taken and effects of temperature fluctuations have been compensated for in the results where necessary.

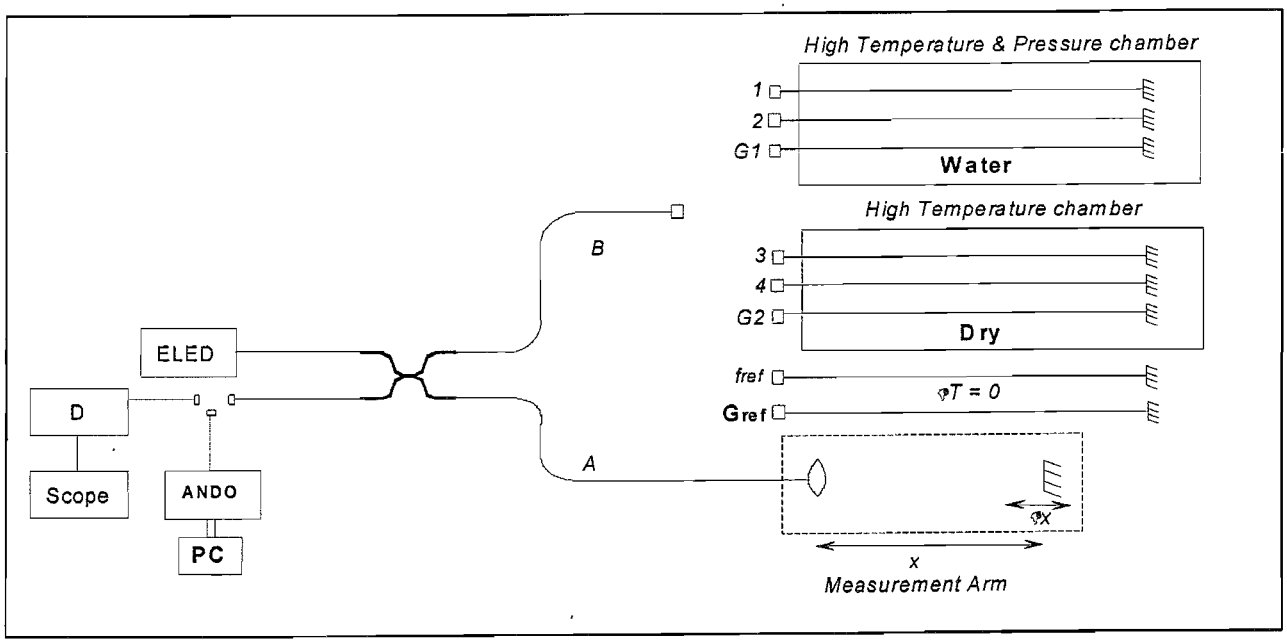

Fig.4.2.1: Schematic of the length change measurement interferometric technique.

The mirror of arm A of the interferometer is mounted on a Vernier translation stage with a resolution of 0.005 mm. The mirror to fibre-end spacing (x) is fixed as the travel of the mirror stage (approximately 25mm) is sufficient to monitor any changes in fibre lengths.

By adjusting the mirror position, arms A and B are balanced and the interference fringe is observed on the scope. Changes in optical-path-length are therefore monitored as changes in air and therefore the refractive index of the fibre (taken to be 1.46) is accounted for when converting the observed changes into percentage fibre length changes.

Whilst the Vernier resolution is 0.005mm, the actual accuracy of the measurement due to a broad interference fringe and human error in locating the fringe centre is closer to 0.02 mm.

Figure 4.2.2 is a plot of the measured (individual data points) optical-path-length change against the applied pressure in psi for a 1.5 m length of fibre. The predicted slope is given by the straight line and was calculated in the previous section to be approximately $-1.85*10^{-6}$ % per psi. An approximate value for the experimental gradient is $-2.07*10^{-6}$ % per psi. The measurement is considered to be fairly accurate, where the discrepancy with the theoretical predictions can be attributed to the errors in the measurement and errors in the estimated values of elastic modulus, core-index and photoelastic constants used in the theoretical calculation.

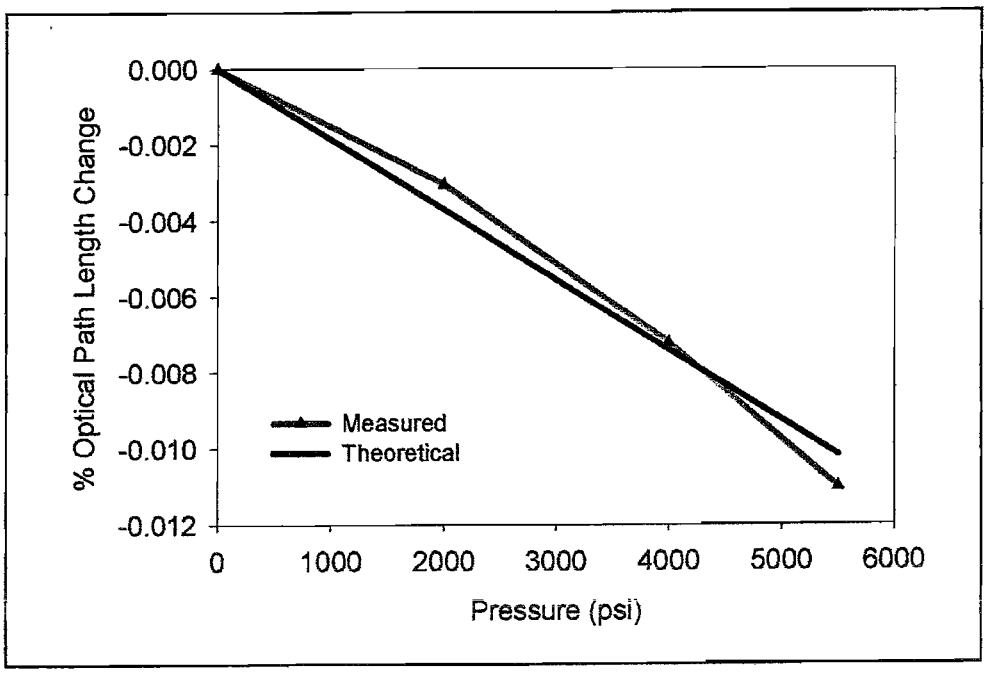

Figure 4.2.2: Measured and calculated percentage change in optical-path-length of single-mode fibres under hydrostatic pressure.

4.2.3 Optical-path-length Changes of Fibres in HTHP Fluids: Initial Findings.

The optical-path-lengths of optical fibres in high-temperature, high-pressure fluid environments have been monitored over extensive periods of time using the Michelson interferometer described in section 4.2.2.

Two separate HTHP chambers have been used in this measurement, one filled with water (referred to as the wet chamber) and maintained under 4000psi pressure, the other filled with air (referred to as the dry chamber) and at ambient pressure. Both chambers were heated to 300°C.

The two chambers each contained a length of uncoated, silica, single-mode, optical fibre and a length of carbon coated single-mode fibre procured from AT&T.

Changes in the optical-path-lengths of all fibres under test (FUT) were monitored over a period of approximately 9 days.

Figure 4.2.3 shows the results for the percentage change of optical-path-length with time of uncoated and carbon-coated, single-mode optical fibres in both the wet and dry chambers.

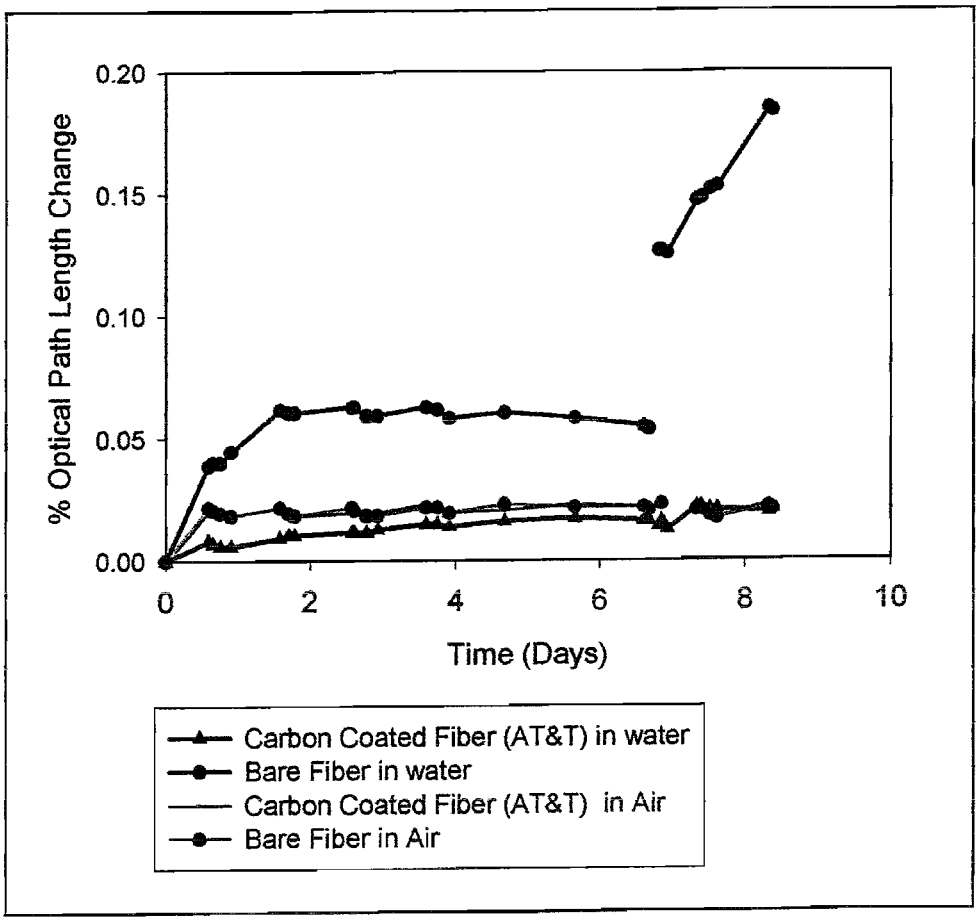

Figure 4.2.3: Measured percentage optical-path-length changes of bare silica and carbon coated silica fibres at 300°C in water under 4000psi and in air at ambient pressure.

- The curve of the uncoated, silica fibre in the wet chamber shows the optical-path-length increasing at first and reaching a maximum of approximately 0.06 % after 2 to 3 days. It should be noted that this value, when normalised to pressure, corresponds to a drift of approximately -32,000psi.
- The optical-path-length of the uncoated silica fibre in the wet chamber began to decrease slowly after 3 days, before abruptly increasing after approximately 7 days. It should be noted, that after approximately 7 days of the measurement, the chamber temperature suddenly fell to 200°C and then returned to 300°C. The resulting jump in the measured optical-path-length change due to this thermal change has not been explained but was possibly due to thermal shock effects on the stressy fibre-layers.
- The measurement was ended after approximately 9 days, when the uncoated-fibre optical-path-length had increased by approximately 0.19%.

- The curve for the carbon-coated fibre in the wet chamber shows a very small increase of approximately 0.02% in optical-path-length over the duration of the measurement. Normalised to pressure drift, this is approximately -10,000psi. However, it should also be noted that both fibres in the wet chamber showed similar changes in path length.

  It is likely that the small increase in path length for these fibres is not due to the HTHP treatment but is actually a result of stabilisation of the optical path length with temperature during the first day of the measurement.
- The carbon coating significantly reduces the effects of the HTHP fluid on the silica fibre.
- Both the uncoated and carbon-coated fibres in the dry chamber follow identical curves with very little length increase being observed after the first few hours of the measurement. The small amount of increase in the length during the first few hours of the measurement has been attributed to the temperature of the chamber stabilising.

On removing the fibre samples from the chamber, their physical lengths were measured and compared to their lengths prior to the high-temperature, high-pressure treatment.

- No change was observed for the coated fibres.
- The physical length of the uncoated fibre of the wet chamber had increased by approximately 2.5mm (±0.5 mm due to the errors of the measurement). The value of length increase is consistent with the theoretical prediction described in section 4.2.2.

4.2.4 Evaluation of Optical-Fibre Protective Coatings.

Monitoring of the optical-path-length of coated optical-fibre cables lends itself as an evaluation tool of the effectiveness of the coating at preventing drift in optical fibre pressure sensors and protecting the silica from the HTHP fluid.

Various fibre cables with commercial and experimental coatings have been assessed using the optical-path-length measurement technique previously described.

The following text and figures summarise some of the key results that have been used, in collaboration with Chevron Research and Technology Company and Spectran, to develop a suitable cable coating for downhole environments.

4.2.4.1 Commercial Carbon Coatings

Two similar AT&T coated fibres have been tested (AT&T 2 is the same fibre as figure 4.2.3) along with samples of Corning and Spectran, carbon-coated fibres. All fibre samples

were carbon coated and were initially developed to slow down the ingress of hydrogen into optical fibre cables [43].

The optical-path-lengths of the fibres were monitored at 300°C in water under 4000psi. Figure 4.2.4 plots the percentage length changes of these fibres with time.

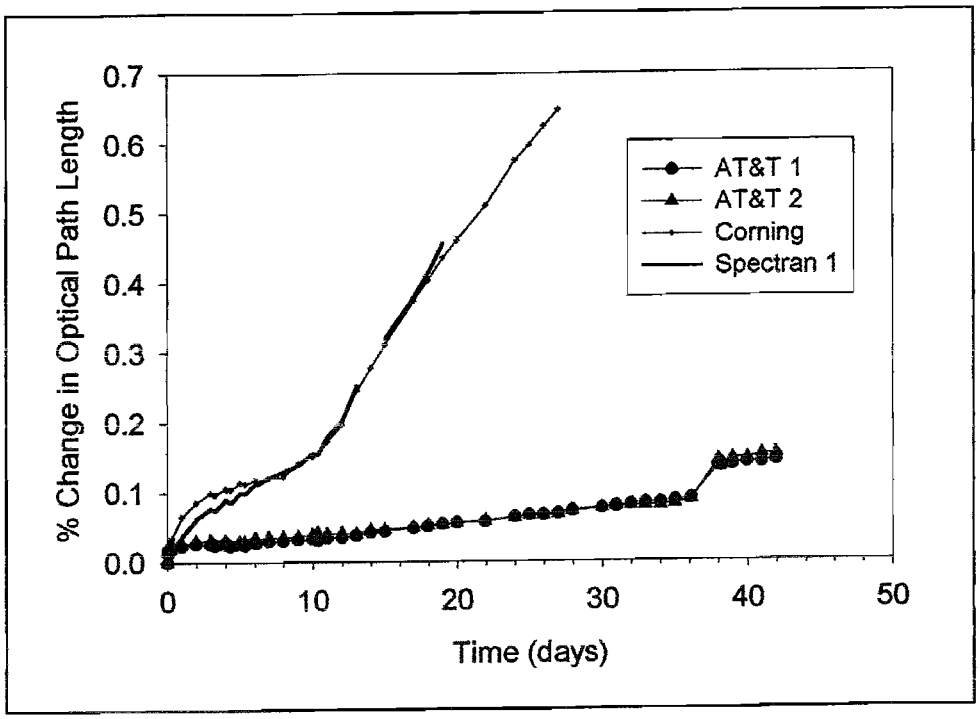

Figure 4.2.4: Measured changes in optical-path-lengths of commercial carbon coated fibres exposed to water at 300°C and 4000psi. Samples from AT&T, Corning and Spectran were tested.

- The plot shows that the two AT&T coatings are of similar quality although the long duration of the measurement indicates the presence of a small length increase that was not clear over the short-term test (9 days) shown in figure 4.2.3.
- The curves for the Corning and Spectran fibres show that the coatings are inferior to the AT&T samples.
- After approximately 12 days, both signals in the Spectran and Corning fibres began to fade and the fibres failed completely after 19 and 27 days respectively.
- On removal from the chambers after the experiment, both the Spectran and Corning coatings were observed to be severely attacked and non-uniform. The carbon coating was non-existent in several regions of the fibre and the silica underneath the coating in these regions showed signs of being etched.

The AT&T fibres also appeared to be slightly affected by the treatment but to a much lesser extent and only in very localised regions along the fibre length.

4.2.4.2 Improvement in the Coating Technology

Where the best fibre protection has been demonstrated by the AT&T carbon-coated fibre, this technology no longer exists at AT&T. Spectran continued to work on their coatings and developed improved coatings based on carbon.

A dual coating process involving carbon with a polyimide overlayer was developed. This coating is referred to as the Spectran "Chemically Resistant" coating and was originally only available on multimode optical fibres intended for downhole, distributed-temperature-sensing (DTS).

Samples of uncoated-silica, single-mode fibre (control), Spectran multi-mode fibre with an improved carbon coating, and Spectran multi-mode fibres with the chemically-resistant coating were tested in high-temperature, high-pressure water. The test started at 200°C for approximately 34 days, continued at 250°C for a further 61 days and then proceeded to 300°C for approximately 13 days. Figure 4.2.5 shows the measured optical-path-length change for the three fibres over the duration of the measurement.

- The unprotected fibre shows an increase in optical-path-length with time at 200°C, the rate of which increased at the higher temperature of 250°C. The fibre failed after approximately 13 days at 250°C.
- Both of the Spectran cables show no measureable change in optical-path-length at 200°C or 250°C outside the noise.
- At 300°C, the Spectran 2 fibre began to slowly increase in optical-path-length before failing after approximately 13 days.
- On retrieval from the high-temperature, high-pressure chamber, both Spectran cables showed signs of attack at very localised regions where the polyimide and carbon layers were removed by the HTHP water. It is at these localised regions where the water to silica contact caused failure of the fibres.
- Damage to the chemically-resistant coated fibre was much less than that of the Spectran 2 fibre.

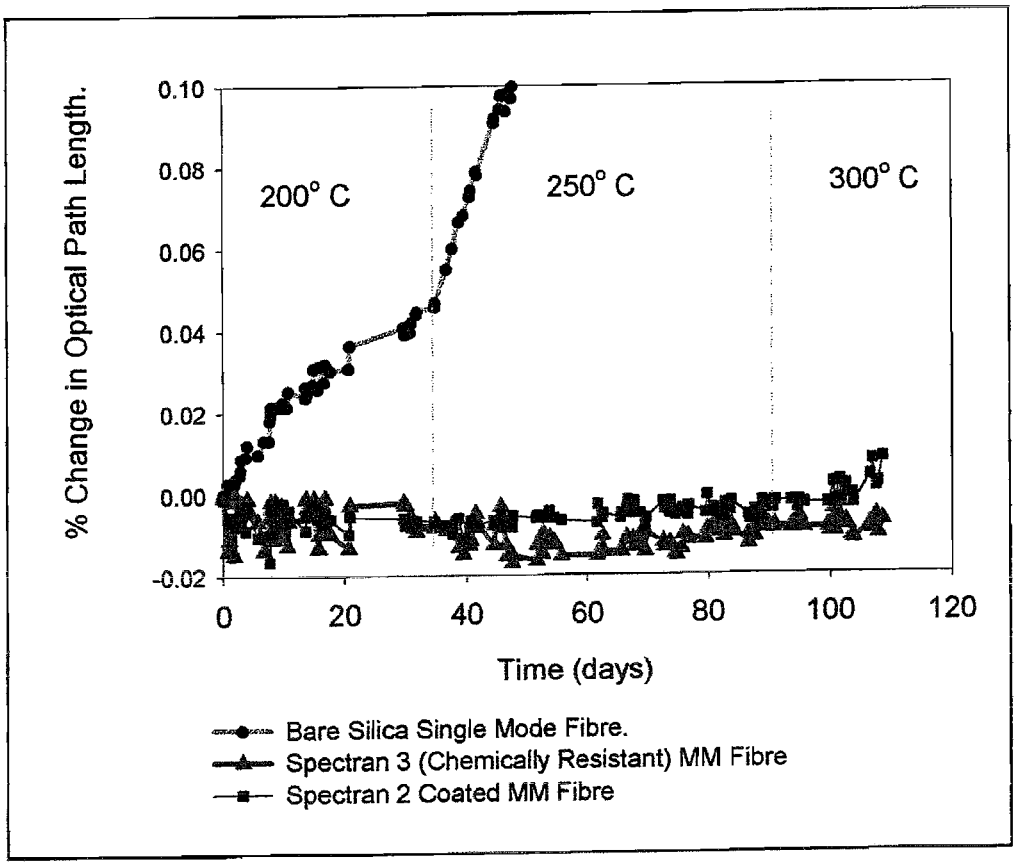

Figure 4.2.5: Measured optical-path-length change of uncoated, single-mode fibre, Spectran 2 (improved carbon-coated), multi-mode fibre and Spectran 3, multi-mode fibre with the chemically-resistant coating. Fibres were in water under 4000psi at 200°C for 34 days, 250°C for 61 days and at 300°C for 13 days.

4.2.4.3 Measurement at 200°C in a Polysiloxane Oil

The damage to the coatings in high-temperature, high-pressure water is expected to occur more rapidly as the temperature is increased. While downhole, oil-well conditions may reach 300°C, (in steam injection wells), the majority of wells will not exceed 200°C, a temperature at which the Spectran coated cables appear to show no signs of damage.

Optical-path-lengths of samples of Spectran 3 (Chemically Resistant) multi-mode fibre and uncoated, single-mode fibre were measured in polysiloxane oil at 200°C. Polysiloxane oil was used as the high-temperature, high-pressure fluid medium as this was known to be less aggressive than water to silica optical-fibres.

Figure 4.2.6 shows the measured optical-path-length changes of the fibres with time.

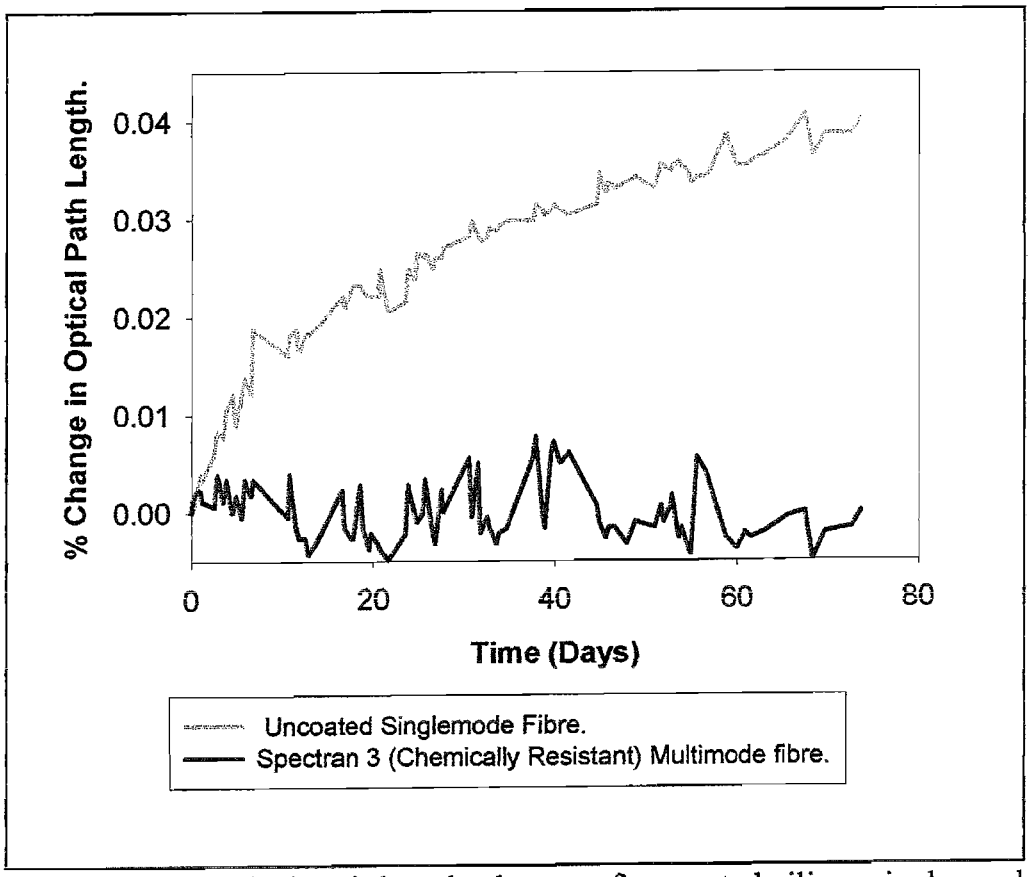

Figure 4.2.6: Measured optical-path-length change of uncoated-silica, single-mode fibre and Spectran chemically-resistant coated, multi-mode fibre. Fibres were in polysiloxane oil at 200°C and under 4000psi.

- Owing to the lower temperature and the use of polysiloxane oil rather than water, the rate of change of optical-path-length is much slower. The curves of figure 4.2.6 therefore appear more noisy than those of previous sections.
- The uncoated, single-mode fibre shows a definite change in optical-path-length with time, approximately 0.04% in over 70 days.
- The Spectran 3 cable showed no measurable change in the optical-path-length outside the noise of the long-term measurement.

4.3 Changes in Bragg Wavelength of Fibre Bragg Gratings in HTHP Fluids.

4.3.1 Theoretical Pressure Sensitivity of FBG Bragg Wavelengths.

The application of hydrostatic pressure to a FBG will cause a change in the Bragg wavelength due to two contributions: a longitudinal strain which changes the period of the index modulation and a change in the average refractive index via the photoelastic effect. The total effective change in Bragg wavelength can be described by:

$$\Delta\lambda_B = -P\lambda_B\left(\frac{1}{E}(1-2\nu)-\frac{n^2}{2}(q_{11}+2q_{12})\right) \qquad (4.3.1)$$

where λ_B is the unperturbed Bragg wavelength, E is the Young modulus of silica, taken to be 72GPa, ν is the Poisson ration taken to be 0.17, n is the unperturbed refractive-index of the core taken to be 1.462 and q_{11} and q_{12} are the stress-optic coefficients for silica evaluated from the strain-optic coefficients [40] to be 4.056×10^{-13} and 2.827×10^{-12} respectively.

Evaluation of equation 4.3.1 for a λ_B = 1525nm, predicts a pressure sensitivity of approximately -2.8×10^{-2} pm / psi.

The Bragg grating has a low sensitivity to pressure and changes in the Bragg wavelength of approximately 0.03pm per psi therefore make high-resolution pressure measurements extremely difficult.

4.3.2 Experimental Measurement of the Pressure Sensitivity of FBG Bragg Wavelengths.

A fibre Bragg grating with Bragg wavelength of approximately 1524.5nm was spliced to a fibre-optic, high-pressure seal and placed into a high-temperature, high-pressure chamber. The reflection spectrum of the grating was monitored using an ANDO optical spectrum analyser. The Bragg wavelength was approximated from this spectrum. Pressure was applied to the chamber using a dead-weight-tester as described in chapter 2.

Figure 4.3.1 show the results of the change in Bragg wavelength of the fibre Bragg grating with applied pressure, in psi. The individual points on the plot are the experimentally measured values which show an approximate pressure sensitivity of the grating of $-2.2*10^{-2}$ pm / psi. This can be compared to the predicted sensitivity, plotted as

solid line in figure 4.3.1, of approximately $-2.8*10^{-2}$ pm / psi.

The discrepancy between the theoretical and measured result can be attributed to the estimated values for the elastic properties and photoelastic constants used in the theoretical prediction.

The low sensitivity of Bragg gratings to pressure and the inaccurate wavelength measurement-technique used in this experiment, (using an optical spectrum analyser), are also expected to introduce errors.

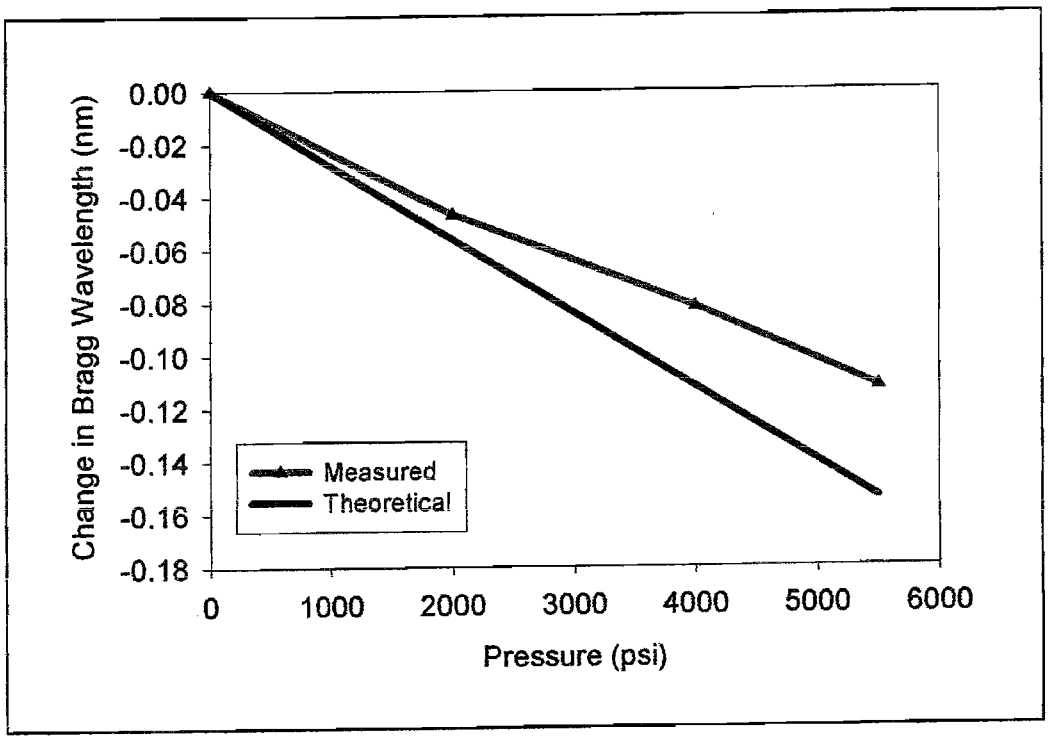

Figure 4.3.1: Measured and theoretical change of the Bragg wavelength of a Fibre Bragg Grating with hydrostatic pressure.

4.3.3 Bragg Wavelength Changes of FBG's in HTHP Fluids.

Two nominally identical fibre Bragg gratings with Bragg wavelengths of 1524.5nm and 1524.9nm were placed in high-temperature, high-pressure chambers. The chamber containing the 1524.5nm device was water-filled and pressurised to 4000psi and is referred to as the wet chamber. The other chamber was air-filled, at ambient pressure and hence referred to as the dry chamber.

Both chambers were heated to 300°C and the Bragg wavelengths of the two gratings were monitored over a 9 day period.

This experiment was carried out in conjunction with optical-path-length measurements discussed in section 4.2.3.

Figure 4.3.2 shows the responses of the Bragg wavelengths of the two gratings in water and air at 300°C with time.

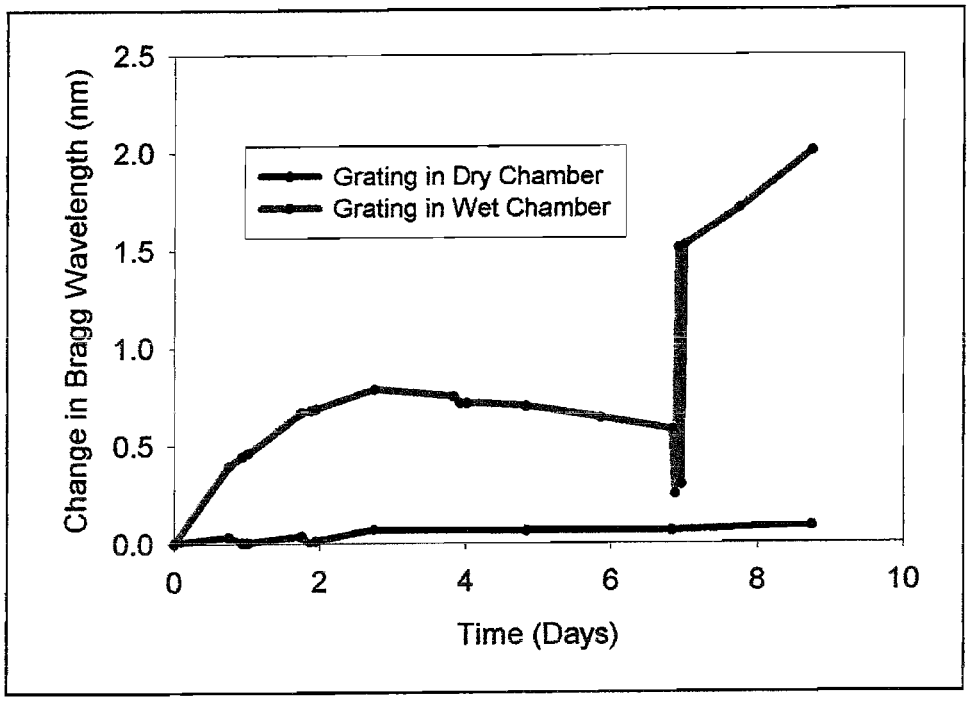

Figure 4.3.2: Shows the change in Bragg wavelength of Fibre Bragg Gratings at 300°C in air (dry chamber) and water (wet chamber under 4000psi) with time.

- The grating in the dry chamber remained relatively unchanged over the 9 day trial (to within the experimental accuracy). The total change in Bragg wavelength for the grating in the dry chamber was approximately 0.08 nm, corresponding to a drift in pressure of approximately 2800psi. However, it is unclear as to whether this change in wavelength was due to the HTHP environment or to experimental errors.
- After 2 days, the Bragg wavelength of the grating in the wet chamber increased to reach a maximum of approximately 0.7nm. Normalised to pressure, this corresponds to a drift of approximately -32,000psi. The Bragg wavelength then began to slowly decrease.
- After approximately 7 days, the wet chamber temperature abruptly fell to 200°C and was returned immediately to 300°C. During this thermal cycle, the grating Bragg

wavelength took an abrupt jump by over 1 nm. This effect, as observed with lengths of uncoated silica fibre (section 4.2.3), is not explained.

- The Bragg wavelength of the grating in the wet chamber increased by approximately 2nm in total during the 9 day measurement.

4.3.4 Stressy Layers in FBG's Exposed to HTHP Fluids.

The exposure of fibre Bragg gratings to 300°C water at 4000psi for approximately 9 days, produced an increase in the Bragg wavelength of the grating of approximately 2.0 nm from 1524.5nm to 1526.4 nm. As with the observed drifts in birefringence of side-hole-fibre pressure sensors, the cause of such Bragg wavelength increases has been attributed to the build up of stressy layers in the fibre cladding. In order to identify the presence of such layers, the two gratings used in high-temperature measurements were etched in a dilute, hydrofluoric acid, etch solution and their wavelengths were monitored with time.

An etch solution of 2:1 H_2O : 48%HF was used to etch the fibre gratings at an etch rate of approximately 0.33μm per minute. Control silica fibre samples, also exposed to 300°C water at pressure, were included in the etching experiment. Samples were removed and their diameters were measured regularly during the etch to accurately determine the etch rate.

Figure 4.3.3 shows how the Bragg wavelengths of the two gratings changed as the fibre radius was etched.

- The wavelength of the grating treated in high-temperature water was observed to reduce almost linearly as the fibre was etched from 1526.4 nm to approximately 1525.0nm. At this stage the fibre failed at a measured diameter of 45μm indicating a radial etch depth of approximately 40μm.
- The original Bragg wavelength of the grating prior to the high-temperature water treatment was 1524.5 nm and the dashed line of figure 4.3.3 is an extrapolation of the etch curve back to this Bragg wavelength.
- The etch result suggests that the stress producing layer had penetrated at least 40μm into the silica fibre after 9 days in water at 300°C. The actual value, estimated from the extrapolation, is probably closer to 60μm.

- The control grating, heated at 300°C in air for 9 days, showed no noticeable change in Bragg wavelength during the etch down to a diameter of 45nm as expected [44].

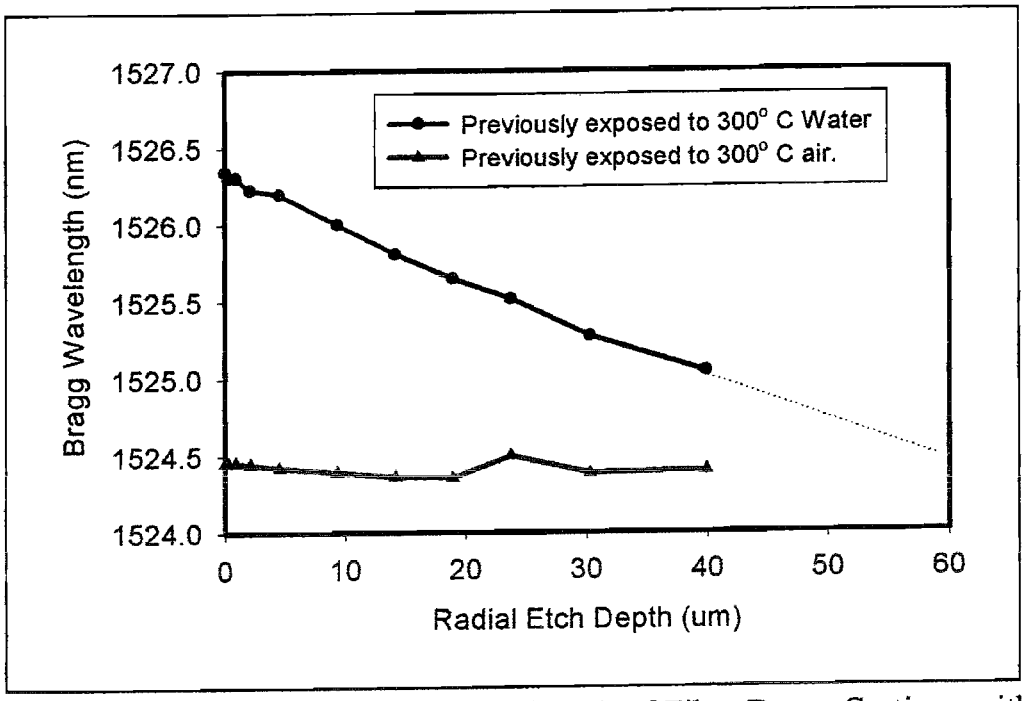

Figure 4.3.3: Shows the change in Bragg wavelength of Fibre Bragg Gratings with radial etch depth from the fibre surface. Gratings were previously exposed to 300°C water under 4000psi and 300°C air for approximately 9 days

4.4 Coated Side-Hole-Fibre Pressure Sensors.

The improved coating formula developed by Spectran shows great potential for cable protection in downhole environments and is used on multi-mode fibres commercially in downhole, distributed-temperature monitoring.

To assess the effectiveness of the coating at reducing optical fibre pressure sensor drifts (chapter 2) in high-temperature, high-pressure water, a side-hole fibre, coated with carbon and polyimide, was pulled by Spectran. A cross section photograph of this fibre (fibre L), stripped of the coating, is shown in appendix A.

4.4.1 Fabrication of Coated, Optical-Fibre Pressure Sensors.

Figure 4.4.1 is a schematic representation of a sensor fabricated from Spectran carbon / polyimide coated side-hole fibre. The sensor has the same general structure as the uncoated sensor shown in figure 1.2.2. However, in order to splice to Spectran coated fibre, the fusion splicer requires that approximately 8mm of polyimide be stripped in the region close to the splice. Polyimide stripping was achieved using hot, concentrate

sulphuric acid, or a butane gas flame.

The splicer also strips approximately 0.5mm of the carbon layer in a "pre-fuse" cleansing arc prior to splicing two fibres together.

The polariser fibre itself cannot be fabricated from Spectran coated fibre. As discussed in chapter 1, the side-hole fibre, pressure-sensor polariser is in the form of a side-hole fibre with gallium injected up the side-holes. The fabrication process of the polarisers requires visual observation of gallium movement through the fibre. This process would not be possible with carbon coated fibre.

The sensor therefore has three unprotected splices (shown by the vertical lines in figure 4.4.1) and a 1cm long, bare-silica fibre-polariser. These regions are unprotected during the high-temperature, high-pressure tests.

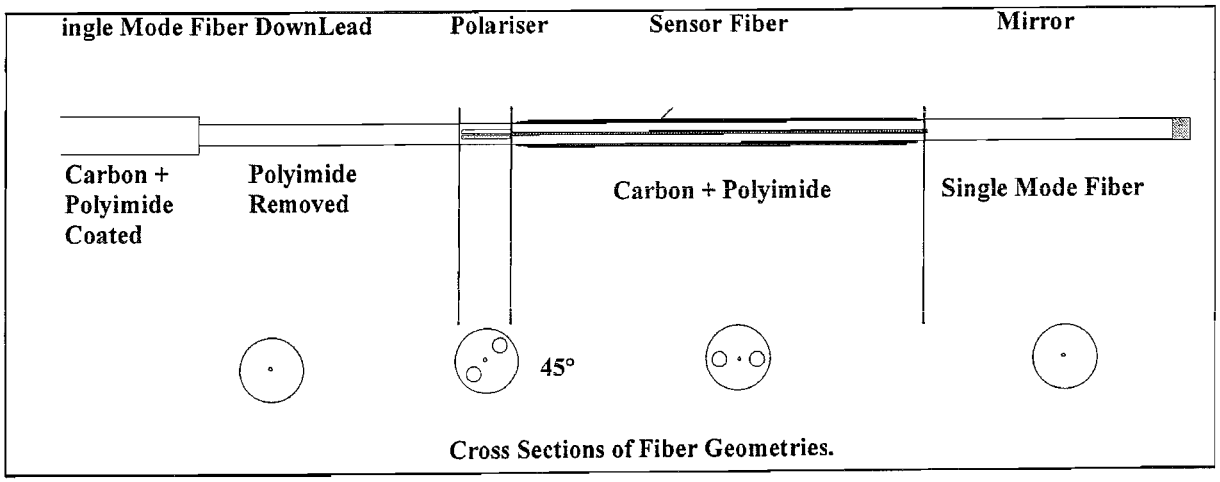

Figure 4.4.1 Schematic representation of a Spectran coated side-hole-fibre pressure sensor.

Mirrors also present a problem in operating at high-temperature and high-pressure. In general, mirrors are fabricated by evaporating chromium or electroless-plating silver onto fibre cleaved end-faces. The unprotected fibre and mirror are exposed to the high-temperature, high-pressure fluid environment.

4.4.2 Stability of Coated, Optical-Fibre Pressure Sensors in HTHP Fluids.

Carbon / polyimide-coated, side-hole-fibre pressure sensors were measured at high-temperature and high-pressure to evaluate their long-term stability. Sensors were monitored at 155°C and at 250°C in polysiloxane oil. In each experiment, conventional, uncoated-silica, fibre-pressure-sensors were also measured for comparison. A chamber pressure of 4000psi has been accurately maintained throughout all the measurements.

At 155°C, a Spectran coated sensor was also tested with the polyimide layer removed. Polyimide was stripped using hot, concentrated sulphuric acid.

4.4.2.1 Polysiloxane Oil at 155°C.

Figure 4.4.2 shows results of Spectran-coated sensors and bare-silica sensors in polysiloxane oil plotted over time. Note that there were two separate experiment chambers in operation, which were started approximately 9 days apart. This accounts for the varying time scales shown on the plot. Figure 4.4.3 is a plot for the same Spectran-coated sensors but on a finer pressure scale to improve the clarity.

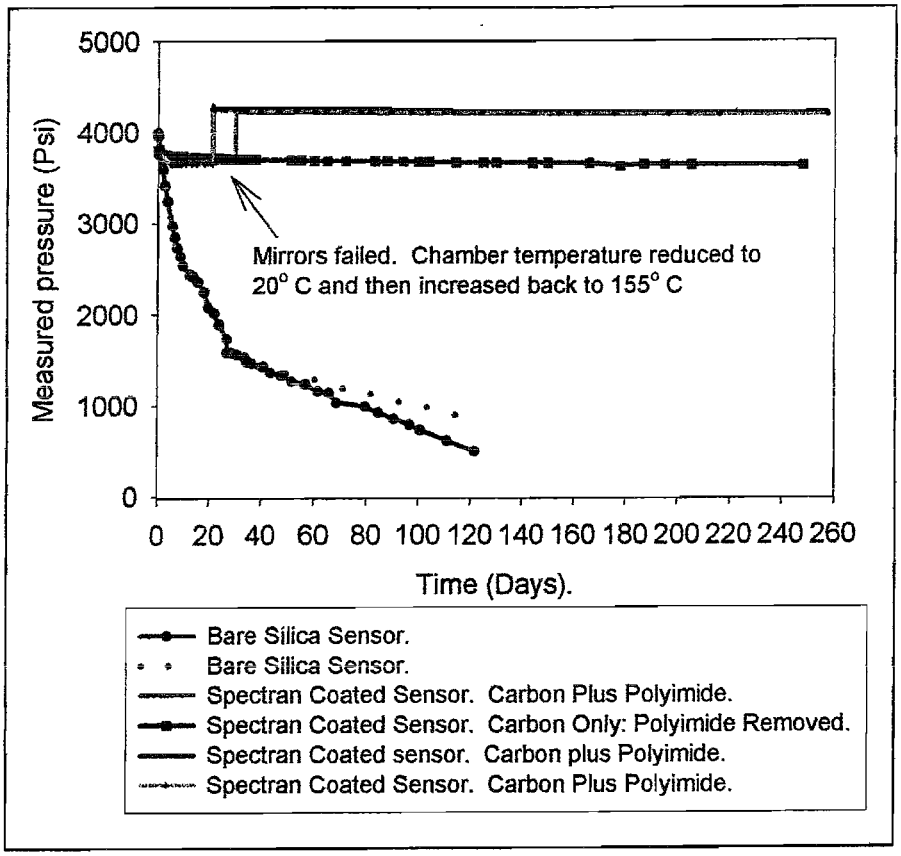

Figure 4.4.2: Measured pressure against time for Spectran coated side-hole-fibre pressure sensors and uncoated silica side-hole-fibre pressure sensors in polysiloxane oil at 155°C and 4000psi.

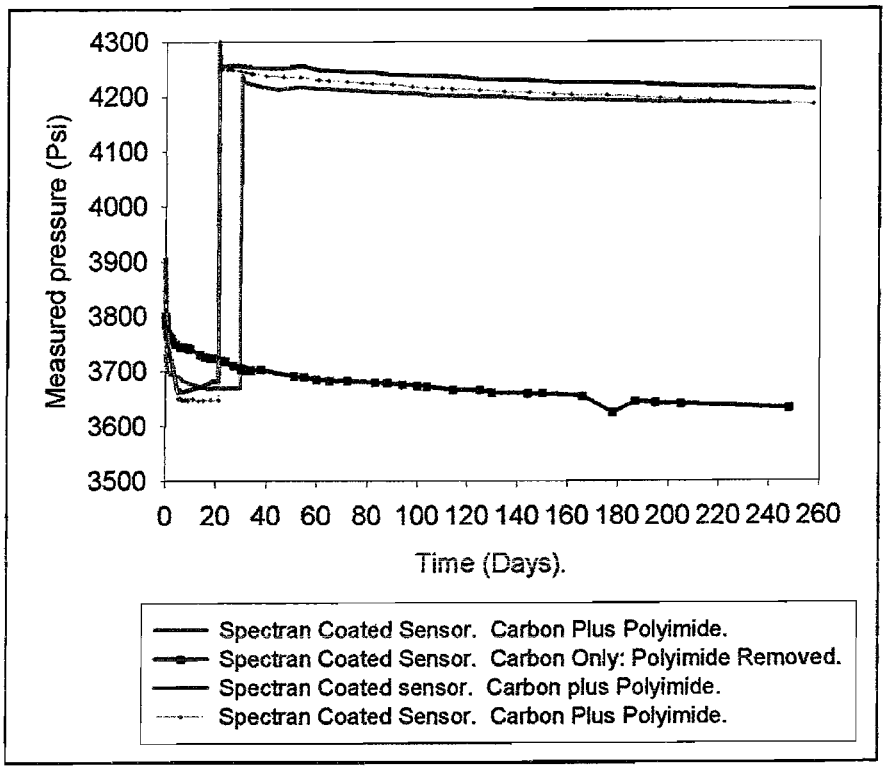

Figure 4.4.3: Measured-pressure against time for Spectran-coated, side-hole-fibre pressure sensors and uncoated-silica, side-hole-fibre pressure sensors in polysiloxane oil at 155°C and 4000psi.

- Spectran-coated sensors show a higher temperature sensitivity than uncoated sensors. For uncoated sensors, the temperature sensitivity is approximately -0.2 psi/°C compared to more than -1.5 psi/°C for Spectran-coated sensors.
- The mirrors failed on all sensors after approximately 20 and 29 days for the two chambers respectively. Sensors were returned to ambient temperature, removed from the chamber and new mirrors were added before continuing the measurements. On returning the temperature to 155°C, all the carbon/polyimide sensors show a consistent change in their offset by approximately +600psi.
- The carbon-only coated sensor did not show any significant effects due to thermal cycling.
- All the coated sensors show an initial drift over the first 5 days of approximately -200psi after which the response becomes much more stable.
- The initial drift can be removed by re-calibration after 5 days. Ignoring the initial drift

and the offset jump due to thermal cycling, the Spectran-coated sensors show a stabilised, long-term drift of approximately 7 psi per month. This is an improvement in the sensor stability by a factor of approximately 200 times over uncoated silica sensors.

- The carbon-only sensor shows a slightly higher long-term drift than the carbon-plus-polyimide-coated sensors. It is unclear whether this is due to the polyimide providing additional protection to the coating or whether the carbon layer was damaged during the polyimide-stripping process.

4.4.2.2 Polysiloxane Oil at 250°C.

Figure 4.4.4 shows a plot of measured pressure against time for sensors made from Spectran carbon / polyimide-coated, side-hole-fibre and unprotected, silica, side-hole fibre in polysiloxane oil at 250°C and 4000psi.

- The initial drifts observed for coated sensors at 155°C (figure 4.4.2) is also seen at 250°C. However, the magnitude of the drift is much larger at 250°C (approximately 500psi at 250°C compared to 200psi at 155°C) and takes place over a shorter period of time (2 days at 250°C compared to 5 days at 155°C).
- Once the sensor has undergone the initial large change, it shows a slow, positive drift, which has not been previously observed for any other sensor. The averaged drift rate over the last 40 days or so of the measurement is approximately +6 psi per day.
- The positive drift of the Spectran-coated sensors is assumed to be due to effects on the polyimide layer.
- The averaged drift rate for the uncoated sensor is approximately -65 psi per day.

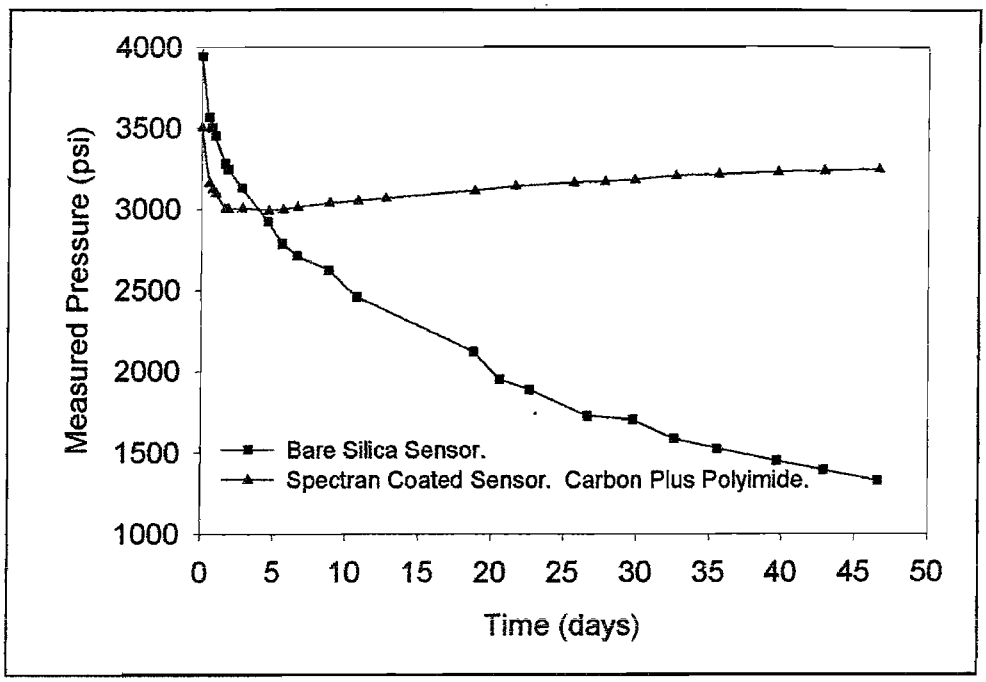

Figure 4.4.4: Spectran-coated, side-hole-fibre pressure sensor and an uncoated-silica, side-hole-fibre pressure sensor in polysiloxane oil at 250°C and under 4000psi. Measured-pressure plotted against time.

4.5 Discussion.

4.5.1 Stressy Surface-Layers in Fibre Pressure-Sensors.

Finite Element Modelling of the effects of surface layers on side-hole-fibre pressure sensors (chapter 3) predicted that silica fibres should experience volumetric changes when subjected to high-temperature, high-pressure fluids.

Using a Michelson interferometer, the optical-path-lengths of silica fibres are shown to increase by up to 0.2% in only 9 days in water at 300°C and under 4000psi.

The optical-path-length change due to the silica expansion is composed of two opposing effects due to a decrease in the refractive index of the core and an increase in physical length of the fibre.

A similar effect is expected for Fibre Bragg Gratings. The Bragg wavelength is dependent upon the core refractive index and the pitch of the refractive index modulation, both of which are sensitive to strain.

Fibre Bragg Gratings showed an increase in Bragg wavelength of almost 2nm in 9 days when exposed to 300°C water under 4000psi.

When normalised to pressure, the optical-path-length increase in fibres, and Bragg-wavelength increase in gratings, both correspond to a drift of approximately -32,000psi in 2 days at 300°C in water. Side-hole-fibre pressure sensors under the same conditions exhibit drifts of approximately -6000psi in the same time scale. This observation is summarised in figure 4.5.1, comparing the pressure-normalised drifts of the three types of pressure sensor.

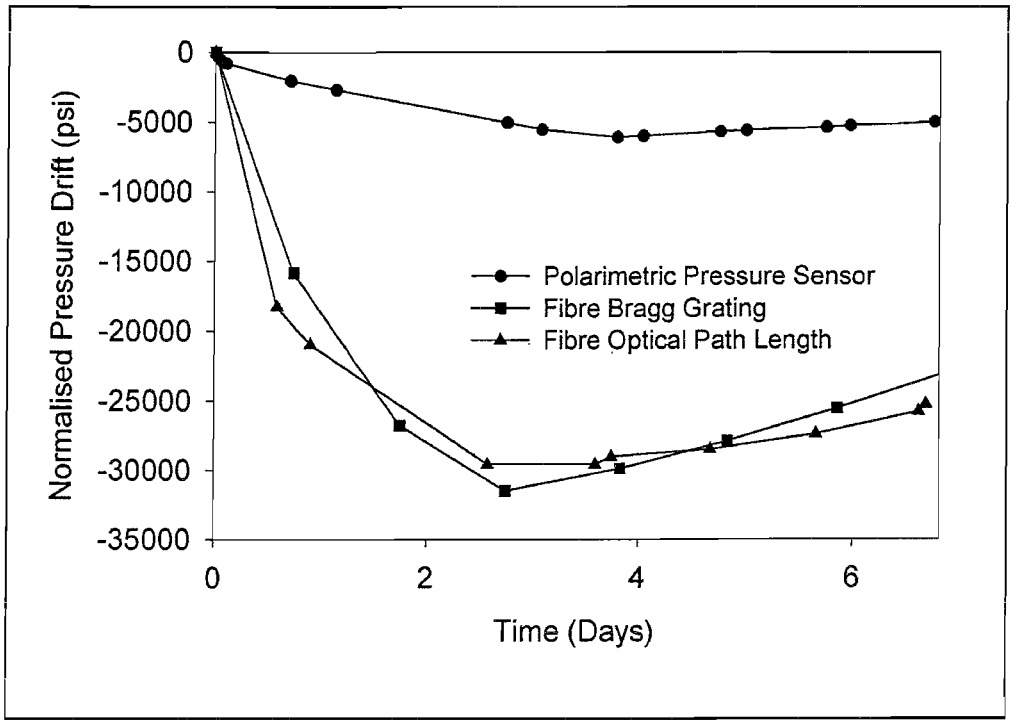

Figure 4.5.1: Changes in birefringence of a polarimetric pressure-sensor, Bragg wavelength of a fibre Bragg grating and optical-path-length of a length of fibre, all normalised to pressure. All measurements made on fibres in water at 300°C and under 4000psi.

Stressy surface-layers have been identified as the cause of the changes in Bragg wavelength of fibre Bragg gratings exposed to high-temperature, high-pressure water. A Bragg grating, exposed to 300°C water for 9 days, showed almost a 2nm increase in Bragg wavelength. Subsequent etching of the surface of this device in hydrofluoric acid caused the Bragg wavelength to reduce back towards its original, stress-free value. Approximately 40μm of the cladding radius was removed before the fibre failed. The stress-free Bragg wavelength was not reached after the etching, which suggests that the "surface layer " penetrated much further than 40μm into the fibre cladding. Extrapolation of the etch line predicts that the stressy layer had penetrated almost 60μm into the fibre.

Stressy layers are expected to occur in any silica fibre device when exposed to high-temperature, high-pressure fluids.

4.5.2 Coatings to Protect Fibre Cables

Carbon coatings were originally designed to prevent the ingress of hydrogen into sub-sea and submarine cables. Whilst hydrogen is not assumed to be a cause of pressure-sensor drift in HTHP fluids,(section 2.3.5), carbon coatings are shown to significantly reduce the effect of high- temperature, high-pressure fluids on optical fibres.

The optical path-length of many commercially-coated optical fibres have been monitored over time when immersed in high-temperature, high-pressure fluids. The results show significant reduction in the change in optical-path-length in comparison with uncoated, silica fibres. The results also show a diversity between the quality of these coatings and their efficacy at protecting fibre-optic cables.

A Spectran, carbon and polyimide, dual-coating process (the chemically-resistant coating) has been identified as being the best available coating for fibre protection in downhole conditions. This coating is now in commercial use for protecting multi-mode, distributed, fibre-sensor cables in oil wells.

Whilst the chemically-resistant coating is effective at protecting cables in oils or at relatively low temperatures (less than 200°C), it cannot protect the fibre from water at temperatures above 200°C. Under these conditions, the coating is damaged at very localised positions along the fibre, which results in eventual fibre failure.

4.5.3 Coatings to Protect Fibre Pressure Sensors

Carbon coatings have been shown to successfully protect fibre cables from attack in high-temperature, high-pressure oils. However, the high-resolution, side-hole-fibre pressure sensor is far more sensitive to the effects of high-temperature fluids. The best commercially- available, "hermetic" coating (the Spectran chemically-resistant coating) is shown to be inadequate at preventing drift in side-hole-fibre pressure sensors in polysiloxane oil at high-temperature and high-pressure.

Spectran chemically-resistant coating was put onto side-hole fibre during the pulling process. This carbon plus polyimide coating can be used to partially protect the sensor assembly at 155°C in oil. However:

- Splice regions remain unprotected and leave structural integrity as a long-term problem.
- Stability improvement is inadequate, (-7 psi per month at 155°C in polysiloxane oil). 1psi per year is a realistically acceptable stability for the oil industry.

- The polyimide layer of the coating makes the sensor unpredictably sensitive to temperature.

4.6 Conclusions.

- Stressy layers, formed in silica optical-fibres exposed to high-temperature, high-pressure fluids, affect other pressure-sensitive devices.
  - Optical fibre lengths increase with time in high-temperature, high-pressure fluids.

    In water at 300°C and 4000psi, optical-path-lengths of uncoated, silica fibres increase by up to 0.2% in 9 days.
  - Fibre Bragg-grating wavelengths increase with time in high-temperature, high-pressure fluids.

    In water at 300°C and 4000psi, Bragg wavelength increases of up to 2nm in 9 days are observed.
  - Normalised to pressure, the effect of high-temperature, high-pressure fluids on Bragg gratings and optical cables is more than 5 times greater than on polarimetric fibre-pressure-sensors.

    In water at 300°C and 4000psi, side-hole-fibre pressure sensors drift by approximately -6000psi in 2 to 4 days. For fibre optical-path-lengths and Bragg wavelengths, the drift is approximately -32,000psi under the same conditions.
- Carbon-coatings can be used to protect optical-fibre cables in high-temperature, high-pressure fluids.
- Carbon-coatings do not provide sufficient protection for optical-fibre pressure sensors:
  - Splice regions are left unprotected.
  - Carbon-coated sensors still drift unacceptably (-7psi per month at 155°C and 4000psi in polysiloxane oil).

Chapter 5

Water Diffusion in Silica:

The Cause of Fibre-Optic Pressure Sensor Drift.

5.1 Introduction

Throughout this thesis, results have been presented which show the instabilities of silica optical-fibres in high-temperature, high-pressure fluid environments.

Finite Element Modelling (chapter 3) was used to show that the instabilities may be caused by the build-up of highly-stressed layers within the silica fibre.

Side-hole-fibre pressure sensors with surface layers, subjected to a uniform volume increase over the layer thickness, were modelled. The results demonstrated that a uniformly swollen surface layer, propagating into the fibre structure with increasing time, could qualitatively describe the observed drifts in fibre-optic pressure sensors.

Etching experiments (chapters 3 and 4) showed that such layers do exist and are capable of penetrating more than 40μm (more probably up to 60μm) into the glass after only 8 days in water at 300°C and under 4000psi. Whilst the presence of the "stressy" layers has been proven through etching experiments, their cause has not been defined.

Chapter 5 focuses on the diffusion of water into silica glass and the effects that the process may have on the glass material-properties. This area of materials science has been intensively studied over the past 40 years. A brief summary of the relevant literature is presented in this chapter.

A novel method of measuring the diffusion of water into optical fibres is developed. The method provides real-time measurement of the build-up of water during exposure of fibres to high-temperature, high-pressure fluids.

Experimental results are presented which prove that water has the capability of diffusing large distances into silica glass at high-temperature and high-pressure.

Water is also shown to be the diffusing species when fibres are exposed to high-temperature, high-pressure polysiloxane oil.

The expected water diffusion profiles, calculated from values of the diffusion coefficient reported by other authors, are compared to the measured results of this study.

Discrepancies are found between the measured water diffusion of this study, and previously reported water- diffusion measurements.

The results of this chapter have been treated qualitatively as this is not considered to be an area of expertise. However, the findings of this chapter, and the method developed to measure water diffusion into optical fibres can provide significant research opportunities in this area of material science.

5.2 Water Diffusion in Glass

It has been known for many years that water, in the form of hydroxyl, can exist in fused silica glass. Early experiments involving the out-gassing of glasses, heated to high-temperatures, showed that water formed the majority of the evolved gases [45]. Similarly, during evacuation, glass vacuum-enclosures evolved water [46] and the process continued indefinitely indicating that the evolved vapour was not surface-adsorbed water but was due to the out-diffusion from the glass interior.

Commercial and synthetic silicate glasses can contain between 0 and 0.03% (by weight) "water" in the form of hydroxyl ions [47]. However, the network of the glass, even at room temperature, is not considered too rigid to expand while accepting absorbed water. Many authors have reported the successful steam hydration of silicate glasses melts and observed that the hydroxyl solubility was proportional to the square root of the partial pressure of water. This relation suggests that for every water molecule entering the glass, two hydroxyl ions are formed by the following reaction [48-50]:

$$\equiv \text{Si-O-Si} \equiv + H_2O_{(g)} \rightarrow \equiv \text{Si-OH} + \text{Si-OH} \equiv \qquad \text{-5.1-}$$

The diffusion of water into silica glass at high temperatures (600°C to 1200°C) was studied by Moulson and Roberts [51] and their results supported the above reaction mechanism. They described the diffusion process as the motion of hydroxyl groups, formed from the dissociation of water molecules absorbed to the silica surface, through the silica network. This process, however, would require the breaking of Si-O bonds (needing extremely large activation energies) to allow the hydroxyl ions to propagate through the glass.

An alternative mechanism was suggested by Doremus [50] who proposed that molecular- water diffuses interstitially through silica until it finds a favourable site to react

with the lattice to form an immobile hydroxyl-pair. This was subsequently supported through the use of O^{18} tracer diffusion measurements [54, 55]. O^{18} tracer experiments [55] show $[O^{18}]/[H]$ (the concentration ratio of O^{18} to hydrogen) to be approximately 0.5 at short treatment times indicating that molecular water is the dominant species. This value increases with time, indicating reaction 5.1 is occurring.

Diffusion is a temperature-dependent process where the empirical equation of diffusion is given by:

$$D = D_0 T \exp\left(\frac{Q}{RT}\right) \qquad \text{-5.2-}$$

where D is the diffusion coefficient, D_0 is a constant, Q is the activation energy for diffusion (constant with temperature), R is the gas constant and T is the absolute temperature.

The activation energy, Q (in Kcal/mole) for molecular diffusion in glass (for gases) was shown to be proportional to the square of the molecular diameter of the diffusing species [56, 62] according to the relationship:

$$Q \sim 4.8\,(d - 1.1)^2 \qquad \text{-5.3-}$$

where d is the diameter of the diffusing species in angstroms. Approximating the molecular diameter of water to be 3.3 angstrom, this suggests a value for the activation energy of water diffusion to be approximately 23 Kcal/mole, which compares favourably with reported values of 18Kcal/mole [51].

Several studies of the diffusion of water into silica glass have been made at various temperatures [55-61] to calculate the diffusion coefficient (D) of water in glass. It has been noticed [56] that direct extrapolation of the diffusion coefficient and solubility of water in glass from high temperatures (greater than 500 °C) cannot be made to calculate low temperature values. Studies have shown [61] that there may be two mechanisms that occur during water diffusion into silica glass at low temperatures and high temperatures.

For this investigation, the interest lies in the low temperature regime in which it is expected that the surface concentration of hydroxyl does not reach equilibrium immediately but may take several days to saturate.

Relevant values for the diffusion coefficient of water in silica (D_{H2O}), at the temperatures of interest in this study, are shown in table 5.2.1, with reference to three sources.

Temperature	Diffusion Coefficient	Reference.
155°C	$5.0 * 10^{-14}$ cm^2 / s	[55]
200°C	$1.0 * 10^{-13}$ cm^2 / s	[55]
200°C	$1.0 * 10^{-13}$ cm^2 / s	[56]
250°C	$2.1 * 10^{-13}$ cm^2 / s	[56]
300°C	$5.0 * 10^{-13}$ cm^2 / s	[56]
350°C	$1.5 * 10^{-12}$ cm^2 / s	[56]
192°C	$1.0 * 10^{-13}$ cm^2 / s	[57]
350°C	$2.5 * 10^{-11}$ cm^2 / s	[57]

Table 5.2.1: Reported values for the diffusion coefficient of "water" in silica glass.

Whilst the diffusion coefficient is determined by temperature, studies have also identified a dependency on the thermal history (fictive temperature) of the glass [62], the applied stress and hydrostatic pressure [63] and the concentration of OH in the glass [64, 65].

With increasing OH concentration, the viscosity, density and refractive index of silica glass all decrease whereas its thermal expansion coefficient increases [66].

5.3 Measurement of Water Diffusion in Fibres

Many of the measurements of water diffusion into glass have been made using Infrared spectroscopic techniques [56-59]. A process involving the consecutive etching, weighing and surface IR-spectrum measurement, enabled researchers to measure OH profiles through glass samples.

This measurement technique is time consuming and hydroxyl content cannot be measured real-time. Furthermore, the measurement must be made using bulk samples and therefore cannot be used on optical fibres.

In the visible range of the spectrum, hydroxyl ions affect the optical properties of silica due to the fundamental OH absorption band at 2.72μm and the corresponding overtones at approximately 0.95μm, 1.25μm and 1.38μm.

The OH absorption band at 1385nm is approximately 21.5 times greater than the peak at 1250nm and 39 times greater than the OH absorption peak at 945nm [67 - 69].

The diffusion of water or hydroxyl into optical fibres in high-temperature, high-pressure fluids has been investigated. The loss spectra of fibres were monitored over a period of time to look for real-time increases in loss at or around the wavelengths corresponding to

OH absorption bands at 1385nm and 1250nm.

Figure 5.3.1 shows the loss-measurement, experimental set-up used. Lengths of optical fibre (fibres-under-test) were spliced to a high-pressure seal and installed into high-temperature, high-pressure chambers (described in chapter 2). Measurements were made in the reflection mode and each fibre therefore had a mirror spliced to its end. The effective lengths of fibre at high temperature were approximately 1.2m.

Loss spectra for the fibres were measured using a monochromator and lock-in detection set-up. The wavelength of the source was scanned between 1100nm and 1500nm with incremental steps of 1.5nm, limited by the resolution of the monochromator.

The detected-power versus wavelength was monitored for each fibre-under-test before exposure to the high-temperature, high-pressure fluid. The process was repeated regularly during the high-temperature, high-pressure testing.

The loss spectrum of a fibre under test at any given time was calculated with respect to the loss spectrum of the fibre prior to high-temperature, high-pressure exposure.

A reference fibre, not exposed to the high-temperature, high-pressure environment, was also monitored to look for changes in the test set up over time.

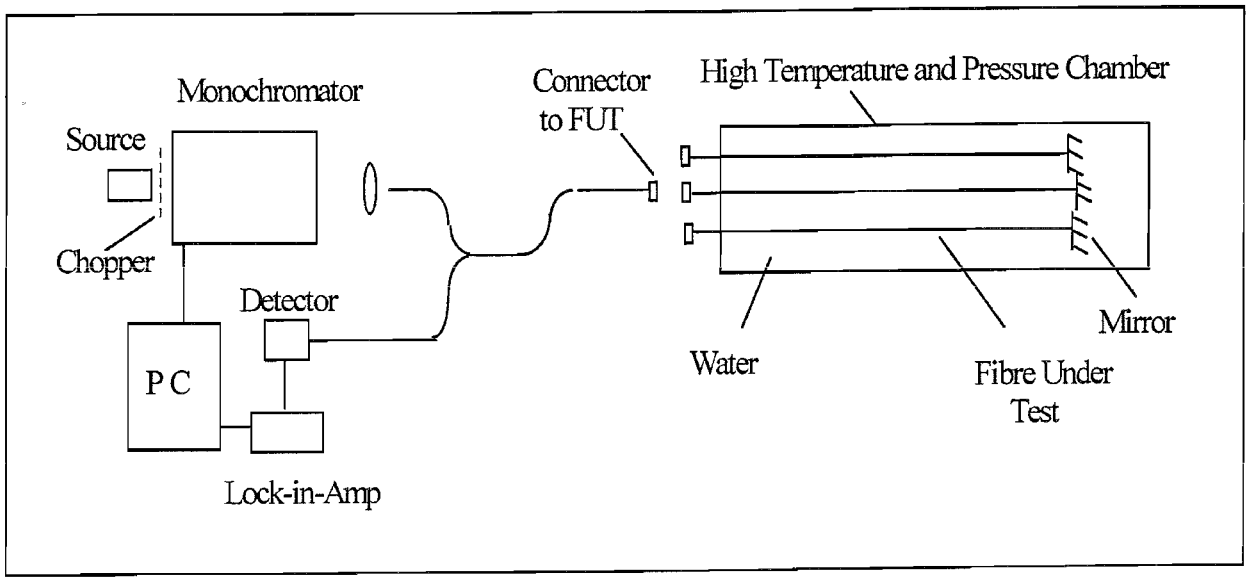

Figure 5.3.1: Schematic of the loss measurement set up used to measure the ingress of "water" into optical fibres from high-temperature, high-pressure water.

5.3.1 High-Temperature, High-Pressure Water.

The loss spectra of fibres immersed in water at 300°C and 4000psi were monitored over several days. The two fibres used in this measurement were:

-1- 130μm uncoated, eccentric-cored fibre. The core-to-fibre-surface spacing for this fibre was approximately 30μm.

-2- 125μm uncoated side-hole fibre. The core-to-side-hole spacing for this fibre was approximately 6μm and the side-hole to fibre-surface spacing was approximately 22μm. The core-to-surface spacing for this fibre was effectively 28μm at its minimum.

Figures 5.3.2 shows the absorption spectra of the eccentric-cored fibre at different times during the experiment and figure 5.3.3 shows the absorption spectra for the side-hole fibre. These figures are shown at the end of the chapter.

The signal levels in this experiment were poor due to the use of poor quality mirrors on the fibres under test. A 16 point moving average has therefore been applied to the data of figures 5.3.2 and 5.3.3 in order to improve the clarity of the curves.

General observations of these loss spectra are summarised:

- Initial measurements of the spectra (during the first 36 hours) were made over the range 1200nm to 1400nm. However, as the loss around 1385nm began to increase after approximately 22 hours for both fibres, the scan was extended to 1500nm.
- Both fibres show very similar loss characteristics with increasing time. However, the levels of OH entering the core of the eccentric cored fibre appear to be slightly higher than that of the side-hole fibre at any given time. This is almost certainly due to the different geometries of the two fibres under test.
- Both figures 5.3.2 and 5.3.3 show the loss peak at 1385 associated with OH absorption loss begins to occur at very similar times, around 22hours, for both fibres. This shows that water is able to diffuse up to 30μm in one day at 300°C.

- The first detection of the less-sensitive OH absorption peak around 1250nm is seen after approximately 32 hours and this peak also increases and becomes broader with increasing time.
- With increasing time, the loss due to the 1250nm and 1385nm OH absorption bands becomes excessive and eventually, for the eccentric cored fibre, no light was detected over the entire spectrum. The measurement was terminated at this point.

5.3.2 High-Temperature, High-Pressure Polysiloxane Oil.

The optical-fibre loss measurement described in 5.3.1 was modified to use a polysiloxane oil as the high-temperature, high-pressure test fluid instead of water. Furthermore, eccentric- cored fibres with different core eccentricities were fabricated for this experiment. Fibres were measured in polysiloxane oil at 300°C and under 4000psi.

The fibres used in this experiment were:

-1- Eccentric-cored fibre with approximate core-to-surface separation of 15μm. EC1

-2- Eccentric-cored fibre with approximate core-to-surface separation of 25μm. EC2

-3- Eccentric-cored fibre with approximate core-to-surface separation of 35μm. EC3

-4- A single-mode fibre with a core-to-surface separation of approximately 62.5μm. EC4

-5- An AT&T carbon-coated single-mode fibre.

The mirrors used on fibres in this experiment were improved and hence higher signal to noise was achieved for the system.

Figures 5.3.4, 5.3.5, 5.3.6,5.3.7 and 5.3.8 (at the end of this chapter) show the loss spectra at different times for EC1, EC2, EC3, EC4 and the AT&T coated fibres respectively. The inset curves of the figures show how the losses increased with time at 1385nm, 1350nm and 1250nm.

General observations of these loss spectra are summarised:

- The plots of the loss spectra of all four fibres show the build up of hydroxyl with time, shown by the increasing losses due to the 1385nm and the 1250nm OH absorption bands.
- The loss is seen first by EC1 in under 10 hours and last by EC4 after approximately 20 days.
- In all four fibres, the loss at both 1385nm and 1250nm increases with time.

- For EC1, EC2 and EC3, the loss appears to saturate after a certain amount of time. This occurs firstly in EC1, then EC2 and finally EC3. For EC4, saturation had not occurred after approximately 33 days when the experiment was stopped.
- The AT&T carbon-coated fibre showed no measurable increase in spectral loss over the duration of the experiment. Figure 5.3.8 shows three spectra after 2 hours, 394 hours and 790 hours. The spectra overlay each other and show no increase in loss due to hydroxyl.

After approximately 33 days, the oil in the chamber was replaced with fresh polysiloxane oil to test whether the loss saturation of EC 1, 2 and 3 was due to changes in the oil (exhaustion of the dissolved water source). No change in the loss spectra of these three fibres was observed over several days.

5.4 Water Diffusion in Cylinders.

Assuming that the quantity of water entering the silica fibres is small compared to the total amount of water (ie. that the diffusion source is replenished and constant), the concentration at any radial point, at any time, can be expressed as: [69]

$$C(r,t) = C_0\left[1-\frac{2}{a}\sum_{n=1}^{\infty}\frac{\exp\left(-D\alpha_n^2 t\right)J_0\left(r\alpha_n\right)}{\alpha_n J_1\left(a\alpha_n\right)}\right] \qquad \text{-5.4-}$$

where α_n are the positive roots of :

$$J_o\left(a\alpha_n\right) = 0$$

C_0 is the saturation- or surface- concentration, a is the radius of the cylinder and J_0 and J_1 are the Bessel functions of order zero and one respectively.

The assumption made, that the diffusion source is replenished, is assumed to be accurate for both cases where the high-temperature, high-pressure fluid is water or polysiloxane oil.

Using the value for D^{300} from reference [56], shown in table 5.2.1, the diffusion profile has been calculated for a cylinder of radius 62.5μm at 300°C. These results are shown in figure 5.4.1 The concentration at any given point within the fibre, relative to the surface concentration, is plotted at various times.

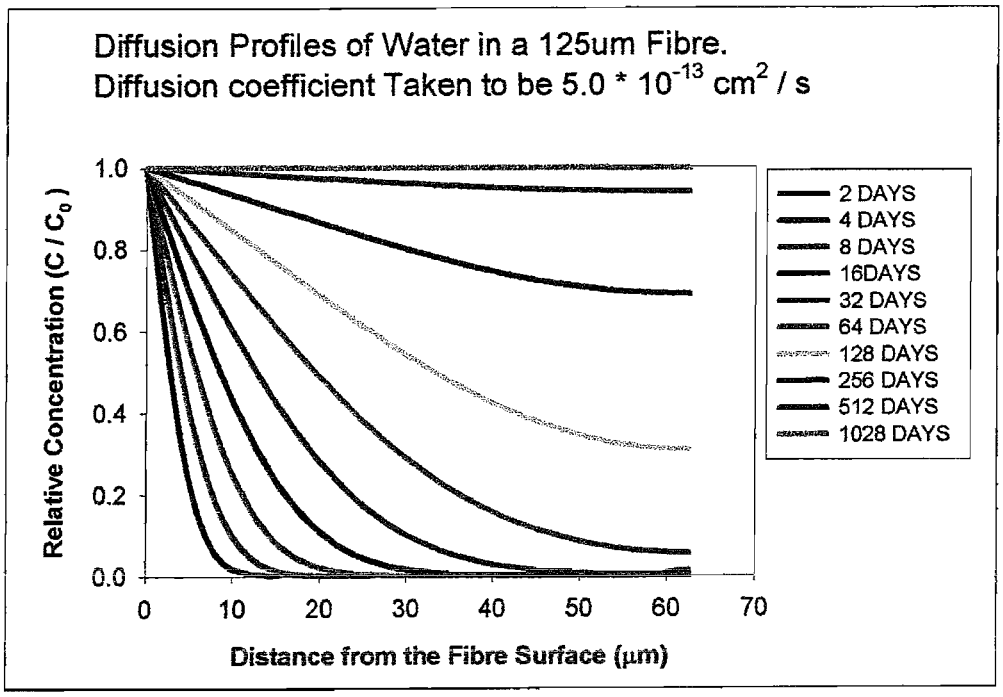

Figure 5.4.1: Calculated water diffusion profiles at 300°C at various times. Calculated using equation 5.4 and a diffusion coefficient of 5.0 10^{-13}cm^2/sec [56].

The expected time to reach complete saturation of the fibre, (ie. the water concentration within the fibre becomes uniform over the whole cross-section), is predicted to be in excess of 1000 days from this model.

At approximately 15μm into the fibre, the water concentration will be close to saturation after more than 250 days. At 25μm to 35μm, the time taken before the water concentration is close to saturation will exceed 500days.

From the results of water-diffusion measurements in fibres at 300°C in polysiloxane oil, (section 5.3.2), saturation levels of water were achieved in much shorter time scales than the model predicts. For a core positioned 15μm from the fibre surface, saturation was achieved between 10 and 15 days. At 25μm from the fibre surface, the saturation level of water was reached between 16 and 24 days. At 35μm, the water concentration was approaching saturation after 24 days.

It is assumed that water diffusion is the root cause of drifts in fibre pressure sensors and the effects on fibre Bragg gratings in high-temperature, high-pressure fluids. Experiments

fibre-Bragg gratings to high-temperature, high-pressure water and subsequent etching of the fibre surfaces to remove stressy layers. Results of these experiments showed:

- For fibre Bragg gratings exposed to 300°C water (4000psi) for approximately 8 days (chapter 4), stressy layers were identified more than 40μm into the fibre. Extrapolation of the etch curve showed that penetration of the stressy layer was closer to 60μm into the fibre.
- For side-hole-fibre pressure sensors exposed to 300°C water (4000psi) for 1, 1.5 and 2 days (chapter 3), stressy layers were identified with penetration depths of approximately 20, 25 and 33μm respectively.

Comparison of these values with the predicted 300°C diffusion profiles of figure 5.4.1 shows that the maximum penetration of water at 2 days will be less than 15μm. After 8 days, the maximum penetration depth will be less than 30μm. For these values, the concentration of water at 15μm and 30μm, will be extremely small. The actual diffusion depths of an appreciable amount of water, capable of producing highly stressed regions of the silica, are estimated to be 5μm and 10μm for 2 days and 8 days respectively. These values are based on a concentration, relative to the surface concentration, of 0.3.

Whilst the comparisons between the measurement and calculation are only qualitative, they suggest that there is a large discrepancy between the modelled water diffusion at 300°C, and the actual water diffusion, the effects of which have been demonstrated throughout this thesis.

5.5 Discussion.

5.5.1 Water Ingress into Optical Fibres.

A real-time, spectral-loss, measurement technique has been used to identify the process of "water" diffusion into silica optical fibres in high-temperature, high-pressure fluids.

Increases in optical-fibre spectral-loss-peaks at 1250nm and 1385nm show the build-up of OH in silica optical fibres immersed in water under high-temperature and high-pressure.

Increases in optical-fibre spectral-loss-peaks at 1250nm and 1385nm show the build-up of OH in silica optical fibres immersed in polysiloxane oil under high-temperature and high pressure. The OH loss is attributed to dissolved water in the polysiloxane oil.

The effect of immersing fibres in water is much greater than in polysiloxane oil. After only 6 days in water at 300°C and under 4000psi, between 1200nm and 1500nm, almost all the light was absorbed in 1.2m of eccentric-cored fibre (30μm core-to-surface separation).

In polysiloxane oil at 300°C, an eccentric-cored fibre with a 25μm core-to-surface separation showed a loss of less than 2dB at 1250nm after approximately 6 days. This demonstrates at least an order of magnitude reduction in OH entering the fibre from oil compared to water.

The OH loss of fibres in polysiloxane oil reaches saturation after long-term exposure. This is not due to exhaustion of the dissolved water in the polysiloxane oil as no further loss is observed with the introduction of fresh oil into the chamber.

A carbon-coated fibre, immersed in polysiloxane oil at 300°C, showed no increase in hydroxyl loss in over 33 days of exposure.

In all the measurements of this chapter, the core of the fibre was treated as a point waveguide and hence the profile of the mode within the fibre core has been ignored. The results of spectral loss measurements on optical fibres have therefore not been quantified as part of this study. However, the feasibility of this technique has been demonstrated for future materials investigations into the dynamics of water diffusion in glasses.

Using fibres with cores located at varying distance from the fibre surface, the profile of the "water" diffusion with time can effectively be measured. The measurement is not limited to silica glasses alone and is also not limited to hydroxyl measurement.

5.5.2 Impact on optical Fibre Sensors.

Key observations of silica-fibre pressure sensors in high-temperature, high-pressure fluids are summarised as bullet points. Literature findings and measurement results of water diffusion in silica are also summarised as corresponding bullet points to associate the effect of water diffusion as the major cause of drift in optical fibre pressure sensors in high-temperature, high-pressure fluids.

Results discussed in chapter 2 showed that the birefringence in side-hole fibres under hydrostatic pressure drifts with time in high-temperature fluids:

1. The rate of drift is disproportionately increased with increasing temperature.
2. The rate of drift is unaffected by increases in pressure
3. The rate of drift is approximately 6 times higher in water than in polysiloxane oil at a given temperature.
4. At 300°C and 4000psi, the rapid drift in the fibre birefringence occurs until 1.5 to 2 days (the "turn over" point) at which time the drift direction changes. The turn over point occurs at the same time in water and in polysiloxane oil.
5. Carbon coatings, applied to side-hole-fibre pressure sensors, (Chapter 4) significantly reduce the effects of drift.

Literature concerning water diffusion in silica suggests that water molecules diffuse through silica interstitially until they react with the silica network to form hydroxyl groups. A combination of these findings and measurements of hydroxyl loss in optical fibres suggests:

1. The rate of diffusion is disproportionately increased with increasing temperature.
2. There is very little pressure dependence of the diffusion coefficient of water in silica.
3. The amount of hydroxyl entering silica fibres, immersed in water, is an order of magnitude higher than for silica fibres in polysiloxane oil.
4. The hydroxyl loss measurement of side-hole fibres in water at 300°C shows that hydroxyl is present in the core of the fibre after 1.5 to 2 days at 300°C and will definitely have reached the side-holes at a somewhat earlier time.
5. Using carbon coatings on silica fibres, the amount of hydroxyl entering the fibre was reduced below the measurement threshold.

5.5.3 Comparison with Modelled Water Diffusion Profiles.

Many authors, working in the field of materials science, have studied water diffusion into glasses under various treatment conditions. In general, the diffusion measurements have been made using saturated-steam environments. Also, the measurement methods have used bulk glass samples and have not monitored the real-time diffusion.

Reported values of the diffusion coefficient of water into silica glass have been combined with the predicted, analytical model for diffusion in cylindrical structures.

Comparison between the predicted diffusion profiles, the measured (real-time) water-diffusion in optical fibres, and the effects of high-temperature, high-pressure fluids on fibre-optic pressure sensors, shows a large discrepancy between other researchers' work and the results of this study.

The discrepancy may be due to several reasons:

- In this study, the fluid medium has always been in the liquid state whereas most other diffusion measurements have used steam-hydration techniques.
- There may be a significant difference between the diffusion process in bulk glasses and fibre-optic glasses due to:
  - Differences in glass fabrication techniques for bulk and fibre-optic glasses.
  - Differences in the surfaces of bulk and fibre-optic glasses.

There is scope for a great deal of materials-science research into the diffusion process of water (and other molecules) into silica optical fibres.

5.6 Conclusions.

- Real-time monitoring of molecular-water diffusion into silica optical-fibres has been demonstrated.
- The measurement method is a novel way of measuring water diffusion into glass.
- Loss associated with water is also demonstrated for optical-fibres in polysiloxane oil.
- Small amounts of molecular-water, dissolved in the polysiloxane oil, are identified as the cause of drift in pressure sensors in HTHP polysiloxane oil.
- Carbon-coatings reduce the amount of water that diffuses into the glass and the rate of the diffusion beyond the measurement threshold.
- Discrepancies are shown between the measured water diffusion in this study and other

published data on diffusion coefficients of water in glass.

- Published data suggests that the maximum penetration-depth of water into silica at 300°C is approximately 15μm. Etching experiments on side-hole-fibre pressure sensors in chapter 3, suggest the penetration depth is considerably larger, at least 33μm.
- Published data of water diffusion at 300°C, suggests that the expected time for a saturation level to be reached at 15μm penetration, will be greater than 250 days. Measurements of water diffusion from 300°C polysiloxane oil into eccentric-core fibres, showed a saturation level at 15μm achieved between 10 and 15 days.

- Future research into water diffusion in optical fibres and the effect on the silica structure is possible using the measurement method demonstrated in this chapter.

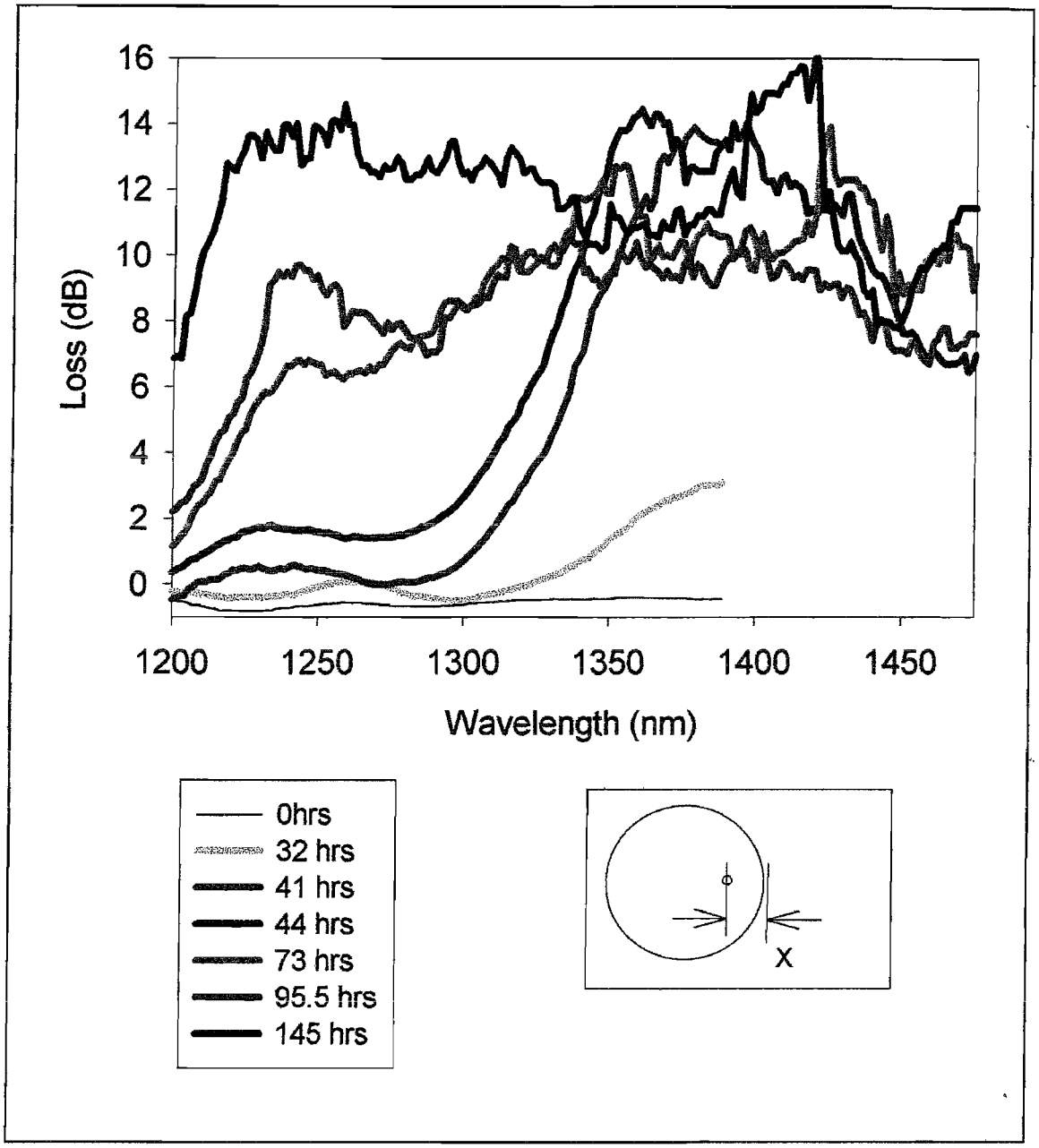

Figure 5.3.2: Plots of the loss spectra at various times for an eccentric cored fibre (x~ 30μm) in water at 300°C and 4000psi. Due to poor signal to noise of the measurements, all of the loss spectra plotted in figure 5.3.2 are 16 point moving averages of the raw data.

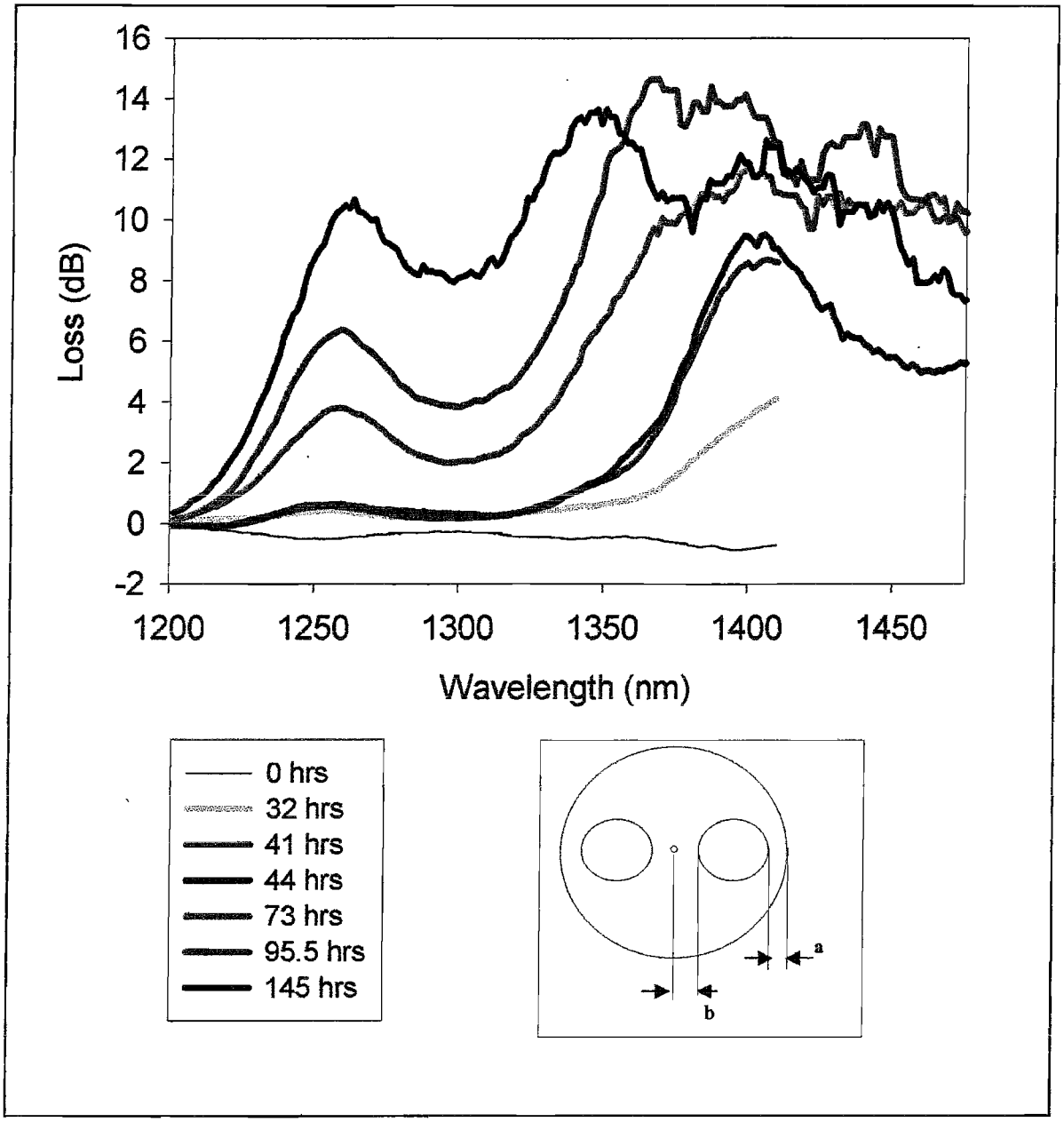

Figure 5.3.3: Plots of the loss spectra at various times for a side-hole fibre (a ~ 20μm, b~ 6μm) in water at 300°C and 4000psi. Due to poor signal to noise of the measurements, all of the loss spectra plotted in figure 5.3.3 are 16 point moving averages of the raw data.

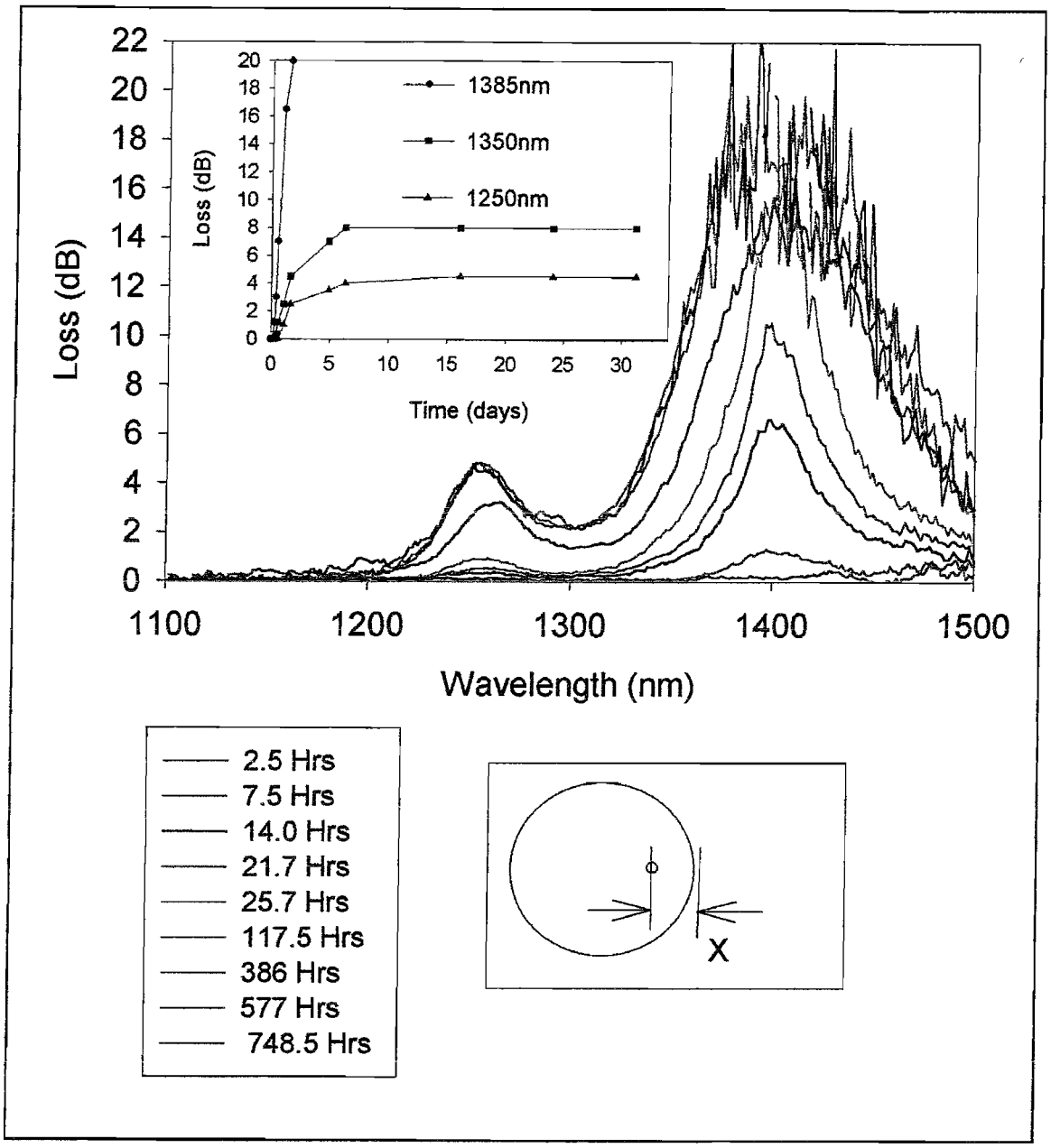

Figure 5.3.4: Plots of the loss spectra at various times for an eccentric cored fibre (x ~ 15μm) in polysiloxane oil at 300°C and 4000psi. The inset curves show the increase in loss with time at 1385, 1350 and 1250nm wavelength.

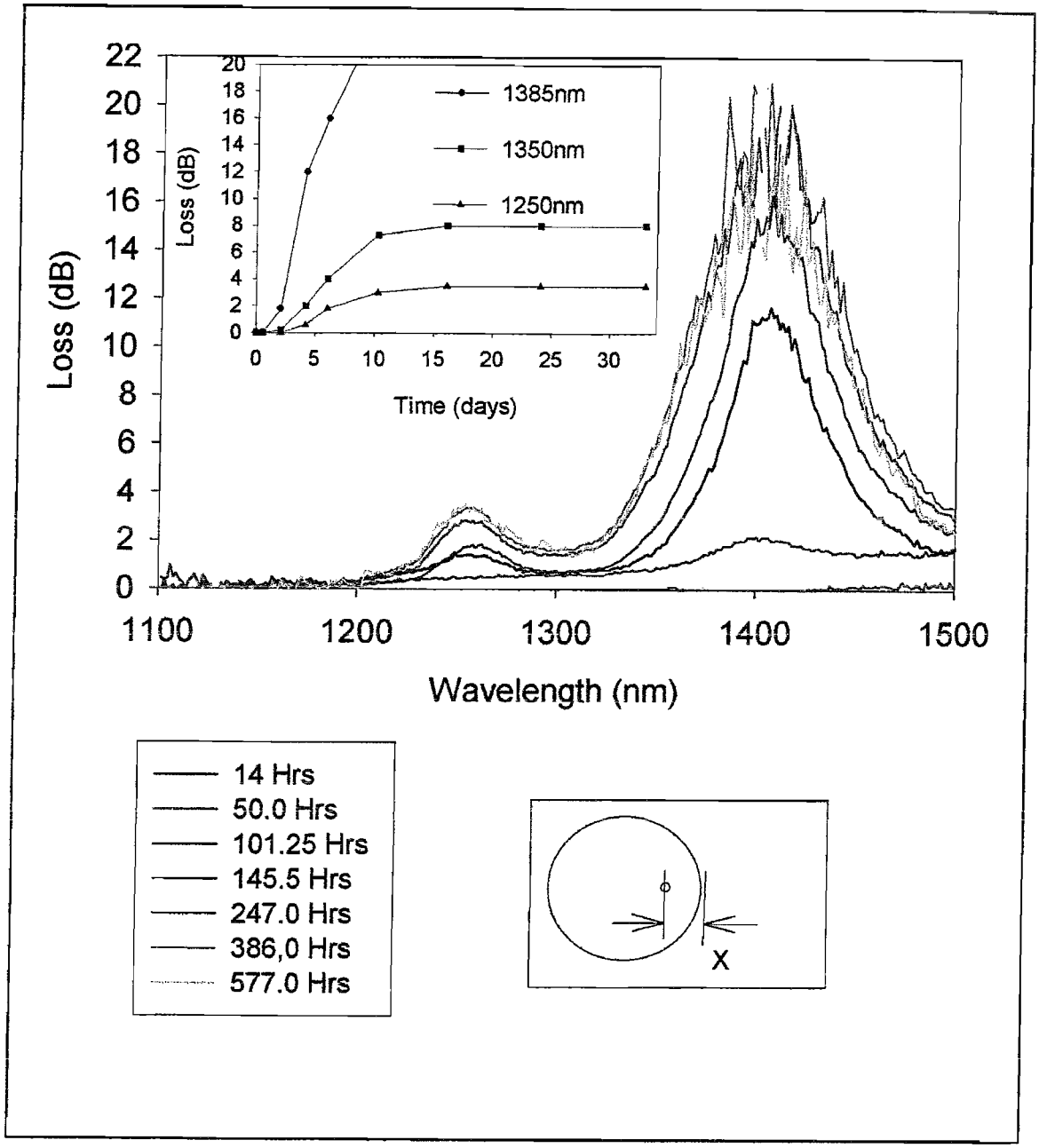

Figure 5.3.5: Plots of the loss spectra at various times for an eccentric cored fibre (x ~ 25μm) in polysiloxane oil at 300°C and 4000psi. The inset curves show the increase in loss with time at 1385, 1350 and 1250nm wavelength.

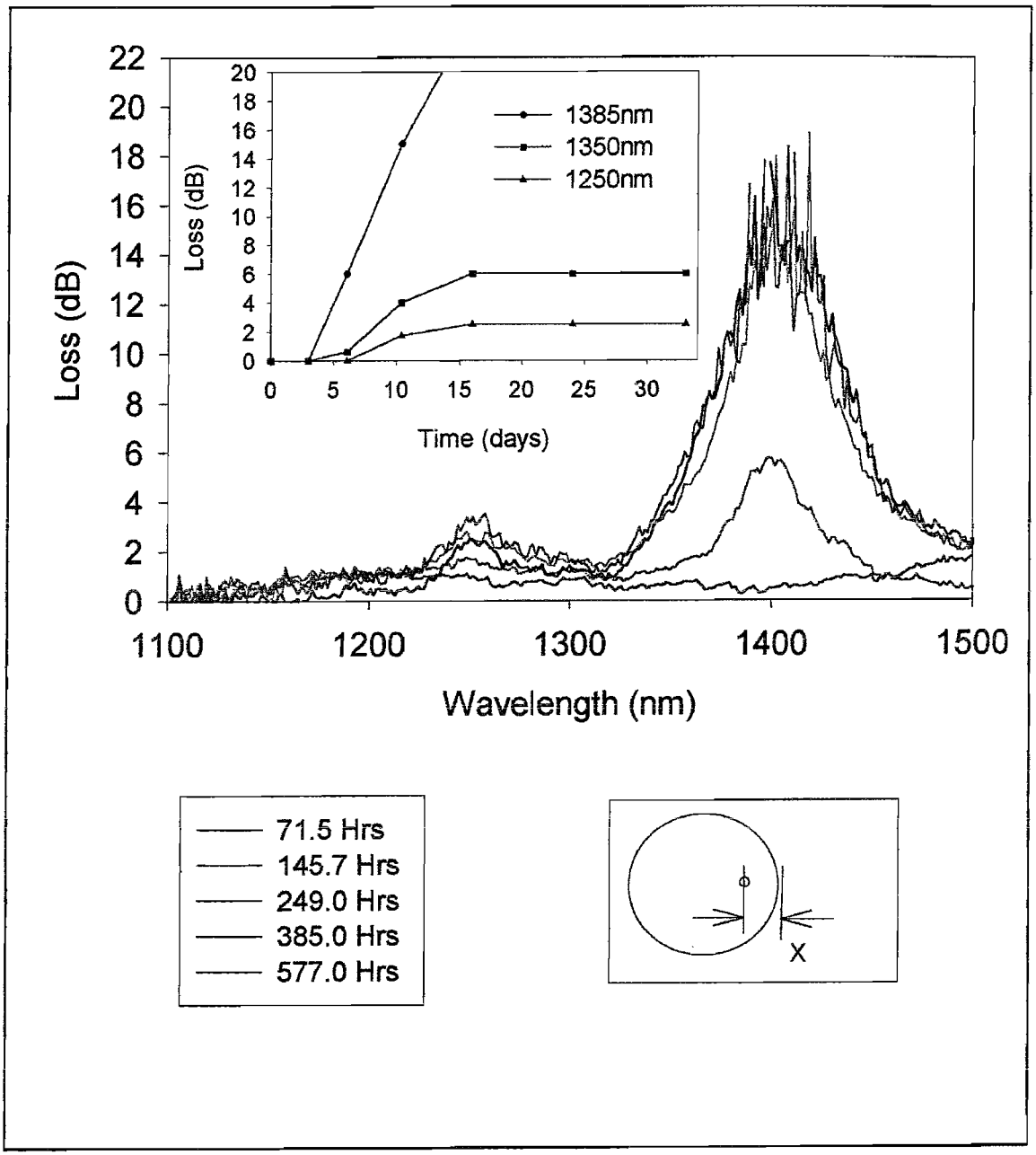

Figure 5.3.6: Plots of the loss spectra at various times for an eccentric cored fibre (x ~ 35μm) in polysiloxane oil at 300°C and 4000psi. The inset curves show the increase in loss with time at 1385, 1350 and 1250nm wavelength.

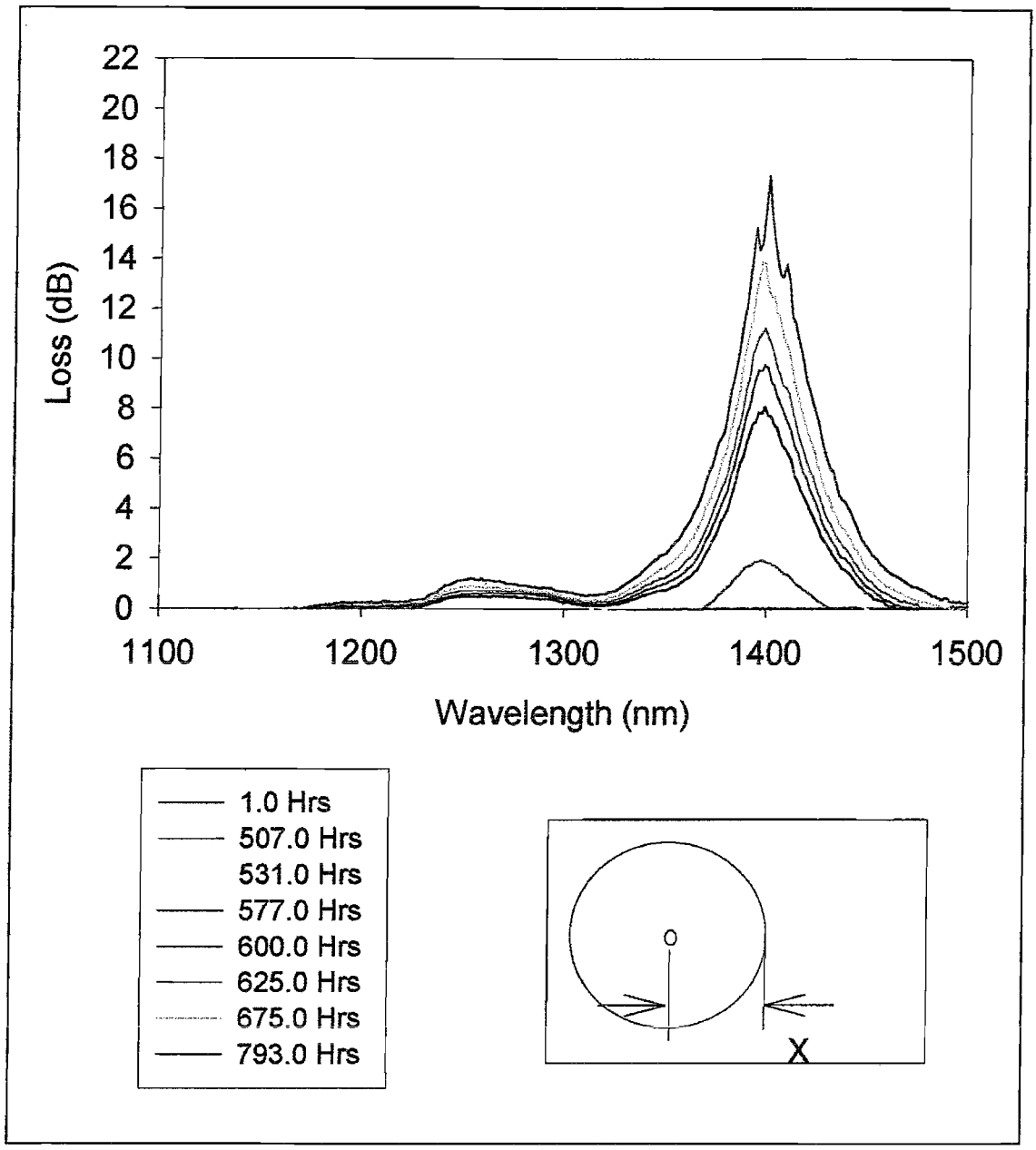

Figure 5.3.7: Plots of the loss spectra at various times for a single-mode fibre (x ~ 62.5μm) in polysiloxane oil at 300°C and 4000psi. The inset curves show the increase in loss with time at 1385, 1350 and 1250nm wavelengths.

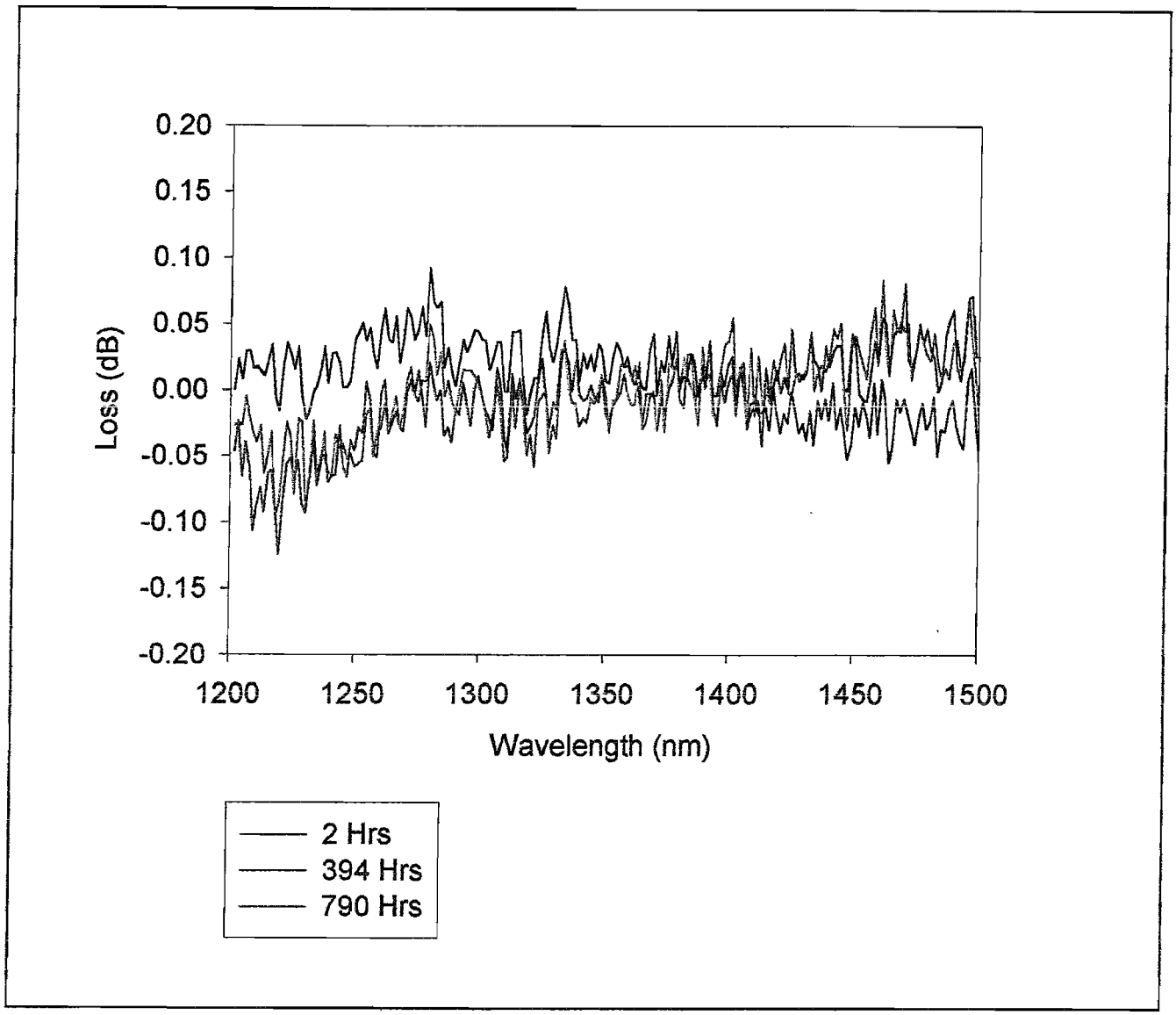

Figure 5.3.8: Plots of the loss spectra at various different times for a carbon coated fibre (x ~ 62.5μm) in polysiloxane oil at 300°C and under 4000psi. The three curves overlay each other within the noise of the spectroscopic measurement. No change in loss is observed throughout the experiment at 1250 or 1385nm.

Chapter 6

Solution of Fibre-Optic Pressure Sensor Drift In High-Temperature, High-Pressure Fluids.

6.1 Introduction

Chapter 6 discusses the development and evolution of an "hermetic package" for protecting fibres and sensors in high-temperature, high-pressure fluids [70].

The novel, hermetic-protection, discussed in the chapter, is based on the use of liquid metals as barriers between high-temperature, high-pressure fluids and silica optical fibres and sensors. Such liquid metals can include Gallium, indium and alloys of gallium and indium although gallium is the only liquid metal, used to protect sensors, which is discussed in this thesis.

Gallium is a liquid near room temperature, having a melting point of 29.77°C (dependent upon purity), is highly reflective and non-toxic. It is also claimed to be chemically un-reactive and has a high tendency to wet glass [71].

Liquid metals, applied to optical fibres as coatings, do not change the sensor temperature coefficient (liquids do not sustain shear stress). The difficulty with liquid-metal coatings, however, is maintaining the coating integrity during handling and deployment.

A solution to this problem was extensively explored and successfully implemented during the course of this PhD. Details of this coating method and its evolution are discussed throughout this chapter.

The pressure sensors utilising the packaging technique are referred to as SD sensors where a four digit number, following SD, corresponds to modifications or changes in the packaging design and differences in side-hole-fibre used to fabricate the pressure sensors. These differences are outlined in table 6.6.1 at the end of this chapter.

Two general designs of the sensor package are reported in this chapter: the SD1 series and the SD2 series. SD2 series sensors have an additional, PTFE sleeve around the package for improved mechanical protection and are discussed in greater detail in section 6.5. The remainder of the packaging of SD1 and SD2 series sensors is identical.

6.2 Liquid-Metal Hermetic Packaging.

The hermetic-packaging technique developed during this PhD incorporates a liquid-metal fibre coating and glass capillary container.

All measurements presented in this chapter have been made using the side-hole-fibre pressure-sensor design described in chapter 2, combined with the liquid metal and capillary packaging technique. However, the packaging technique is expected to be equally suitable at protecting other fibre-optic pressure sensors such as fibre Bragg gratings and Fabry-Perot air gap sensors. It may also be used as cable protection and protection of distributed fibre-optic sensing devices.

The SD1 series sensor design is shown schematically in figure 6.2.1. The general side-hole-fibre pressure sensor, previously described in chapter 2, consists of a downlead single-mode cable spliced to a side-hole fibre polariser which is spliced at 45° to a length of side-hole fibre, which is terminated by a single-mode fibre mirror spliced to the sensor end.

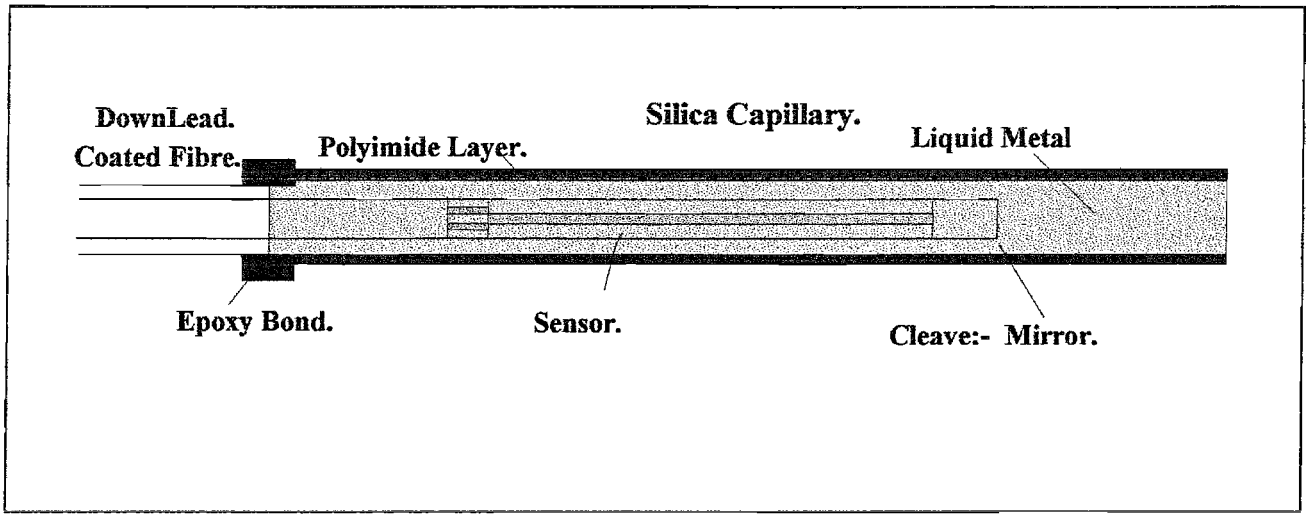

Figure 6.2.1: Schematic of the SD1 series Fibre-Optic pressure Sensor design.

The sensor itself can be made from bare silica side-hole fibre or a thinly coated side-hole fibre, for example carbon coated. Packaged sensors fabricated from side-hole fibre with germanium doped cores, are referred to as SD1000 sensors. Packaged sensors, fabricated using a side-hole fibre with a thin carbon layer, are referred to as SD1100 sensors. Packaged sensors, fabricated using a side-hole fibre with a tantalum-doped core, are referred to as SD1200 sensors. All SD1000 sensors have been fabricated from fibre I (appendix A) and all SD1200 sensors have been fabricated from fibre K (appendix A).

After fabrication, the sensor is sleeved in a silica capillary. For early SD sensors, this

process was done by hand after carefully cleaning the silica fibre sensor and cleaving the fibre end-face. This process involved handling of the uncoated, silica-fibre sensor, which inevitably led to occasional sensor breakage and almost certainly contaminated the silica surface to some extent.

For later SD sensors, such as those discussed in sections 6.4 and 6.5, the process of sleeving the sensor in the silica capillary was modified to remove any physical handling of the sensor after the final cleaning and degreasing procedure. The improved method uses a "pull through" fibre. The "pull through" fibre is an 80μm, UV-acrylate-coated silica which does not have a core. This fibre is hand fed into the capillary and spliced to the end of the sensor. The capillary sleeve is then moved over the sensor to the point where the single-mode section of the sensor (the mirror fibre) is exposed. The single-mode fibre is cleaved and the capillary is then moved back over the sensor.

This method of sleeving the sensor produces a slightly different design to that shown in figure 6.2.1 since the capillary bore is too small to fit over the coated downlead cable section. Spectran chemically-resistant, single-mode cable is therefore used as the downlead cable for sensors sleeved in this manner. The cable has an outer diameter of approximately 180μm, which fits inside the bore of the capillary sleeve.

For experimental purposes the capillary sleeve is of sufficient length to completely cover the pressure-sensor fibre, polariser and mirror-fibre, with an additional 30cm, (not established as an optimum), included at either side of the sensor.

The capillary itself has a bore of approximately 230μm (± 10%), an outside diameter of approximately 320μm and is coated with a thin, protective layer of polyimide. The polyimide coating provides no hermeticity at all and is merely there as mechanical protection. Figure 6.2.2 shows a photograph of the cross section of this capillary.

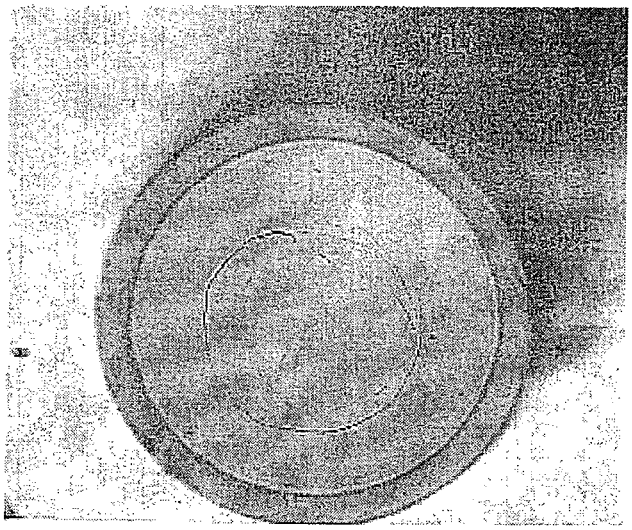

Figure 6.2.2 Cross-section of the silica capillary used to package sensors. The polyimide layer is not shown in this photograph.

The capillary used throughout this PhD is commercially available and normally used in high- pressure liquid chromatography. The dimensions and coating of this capillary have therefore not been optimised. Ideally, the capillary would have an hermetic coating on the outside such as the Spectran Chemically Resistant coating discussed in chapter 4.

After sleeving the sensor in the capillary, liquid metal (gallium) is injected into the capillary to completely fill the annulus surrounding the sensor. The capillary is bonded to the coated downlead -fibre using an epoxy or polyimide-resin.

This sensor package design provides complete protection to the whole sensor, including all splice regions and mirror.

In the original, unprotected sensor design, the mirror was formed by either evaporation or electroless-deposition, of chromium or silver, to the cleaved end-face of a length of single-mode fibre. This type of mirror was a constant source of failure of pressure sensors in harsh environments.

In the SD sensor design, the mirror is formed by the interface between the cleaved-fibre end- face and the gallium. The reflectivity of this type of mirror is as high as the best silver-coated mirror achieved by electroless deposition. Furthermore, the mirrors are more consistent and do not require chemical preparation and time consuming procedures.

In the SD1000 sensor design, the mirror end of the capillary is left open to communicate pressure to the sensor.

6.3 SD1-Sensor Stability in High-Temperature Fluids.

SD1000, SD1100 and SD1200 sensors have been monitored at elevated temperatures and pressures in both water and polysiloxane oil environments. Spectran-coated fibre-sensors (discussed in chapter 4) and uncoated-silica fibre-sensors, described in chapter 2, have also been measured for comparison.

The SD1000 sensors were fabricated from uncoated, germanium-doped, silica side-hole fibre prior to being packaged. SD1100 sensors were fabricated from Spectran chemically-resistant side-hole fibre (also germanium-doped) with the polyimide layer removed using hot, concentrated sulphuric acid.

SD1200 sensors were fabricated from uncoated, tantalum-doped, silica side-hole fibres prior to being packaged. Side-hole fibres with tantalum-doped cores have very low intrinsic birefringence (section 1.2). Sensors fabricated from such fibres therefore have extremely low offset values.

All sensors were monitored using the matched interferometer instrumentation described in chapter 1. Pressure and temperature control have been achieved using the high-temperature, high-pressure test chambers and facility described in chapter 2.

6.3.1 Polysiloxane Oil at 155°C.

Figure 6.3.1 shows plots for an SD1000 sensor, an SD1100 sensor, a Spectran chemically - resistant-coated sensor and an unprotected-silica fibre-pressure-sensor, monitored over time at 155°C and 4000psi in polysiloxane oil. Figure 6.3.2 shows the SD1000 sensor, the SD1100 sensor and the Spectran coated sensor on a finer pressure scale for clarity.

- The time-zero offsets of the curves of figures 6.3.1 and 6.3.2 show that the SD1 sensors have very similar temperature sensitivities to uncoated silica sensors.
- The slight difference in the offsets of the SD1100 and SD1000 stability curves is due to different temperature cross-sensitivities of the two pressure-sensor fibres.
- The capillary / gallium mirrors performed well throughout the experiment and continue to do so after approximately 13 months. This performance had not previously been attained at 155°C for any other type of mirror.
- Both the SD1000 and the SD1100 sensors show an initial change over the first 5 to 10 days of approximately 50 psi after which they both become more stable.
- The initial drifts of the SD1000 and SD1100 sensors over the first 5 or 10 days can

effectively be eliminated by re-calibration when the sensor has stabilised.

- The stabilised, long-term drift of the SD1000 and SD1100 sensors is approximately 1 psi per month. This shows an improvement of almost an order of magnitude on the Spectran coated sensor. All sensors continue to be monitored to assess the long-term reliability.
- The drift curves for the SD1000 and SD1100 sensors are almost identical over the duration of the experiment.

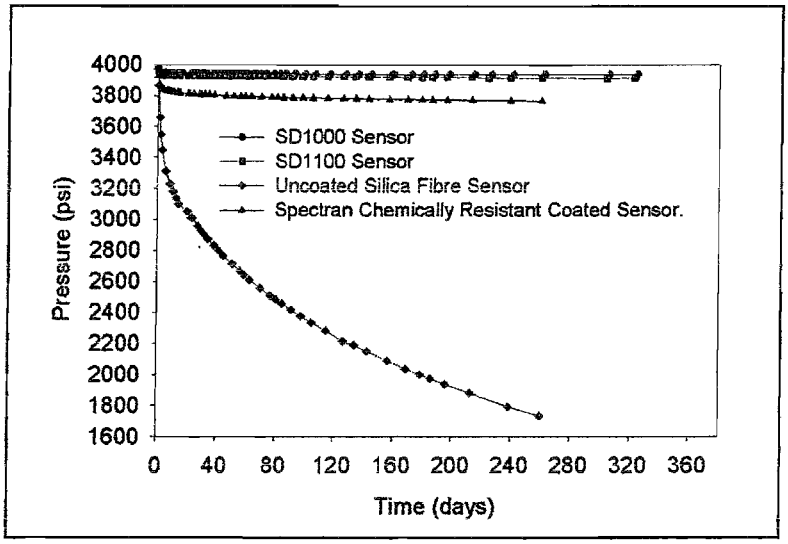

Figure 6.3.1: Plots of the stability of SD1000, SD1100, uncoated-silica and Spectran chemically-resistant-coated sensors in polysiloxane oil at 155°C under 4000psi pressure.

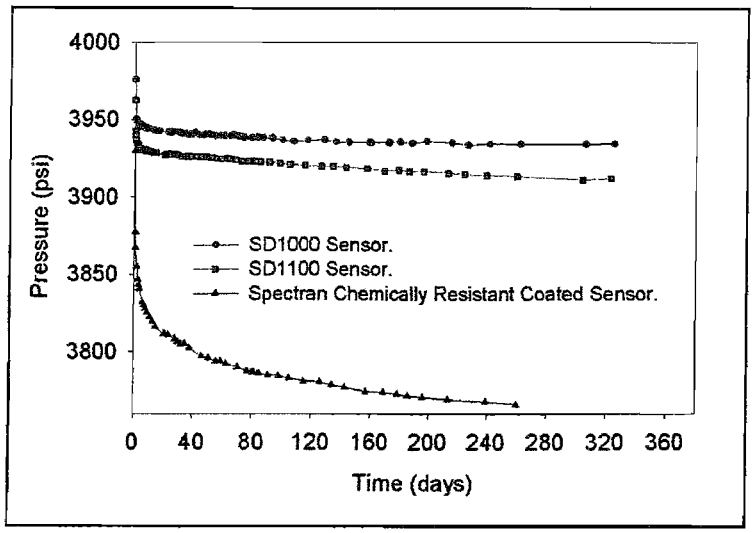

Figure 6.3.2: Expanded view of figure 6.3.1 showing the stability curves of SD1000, SD1100 and Spectran chemically-resistant-coated sensors in polysiloxane oil at 155°C

6.3.2 Polysiloxane Oil at 200°C.

Figure 6.3.3 shows plots for an SD1000 sensor and an SD1200 sensor in polysiloxane oil at 200°C and under 4000psi over a period of approximately 200days.

- The tantalum-doped side-hole fibre sensor (SD1200 sensor) shows a drift of over 100psi in the first day of operation compared to approximately 40 psi for the germanium-doped, side-hole-fibre sensor (SD1000 sensor).
- After the first day, the two sensors track each other extremely closely (ignoring the offset between the two sensor readings).
- Neither of these sensors shows the high level of stability observed at 155°C, discussed in the previous section. This may have been due to errors in fabrication; contamination of the sensor surface or imperfect coverage of the sensor in liquid metal.

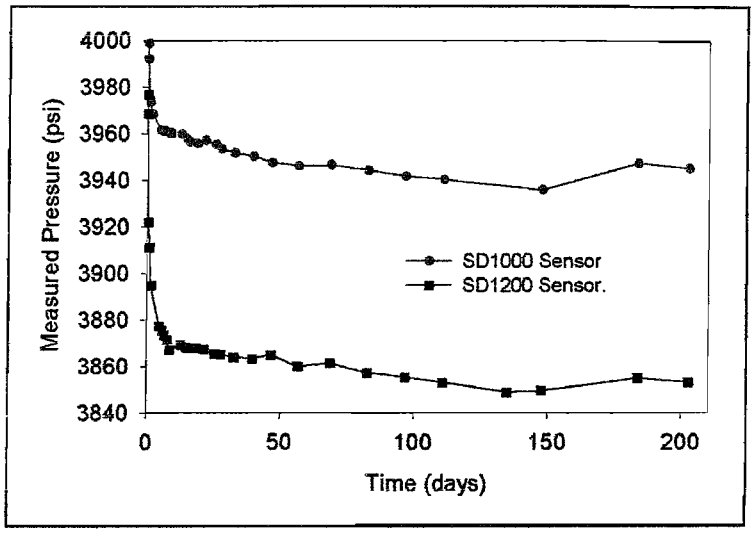

Figure 6.3.3: Plots of the stability of SD1000 and SD1200 sensors in polysiloxane oil at 200°C and under 4000psi pressure.

6.3.3 Polysiloxane Oil at 250°C.

Figure 6.3.4 shows plots for an SD1000 sensor, a Spectran Chemically Resistant coated sensor and an unprotected, silica-fibre pressure sensor monitored over time at 250°C and 4000psi in polysiloxane oil.

- The SD1000 sensor curve shows an initial drift of approximately -130psi over the first 8 or 9 days. This is larger than observed at 155°C and 200°C.
- The SD1000 sensor drift curve settles down very quickly after the initial 8 day drift. Stability is achieved much faster than at 155°C or 200°C.
- The stabilised, long-term drift of the SD1000 sensor is approximately 1 psi per month.
- The control sensor shows a drift of approximately 1000psi over a one month period.
- The Spectran coated sensor shows a positive drift of approximately +180 psi per month.
- The SD1000 sensor failed after approximately 45 days. On retrieval from the test chamber, the sensor package appeared to be in excellent condition. However, the downlead cable was damaged at the high-pressure seal.

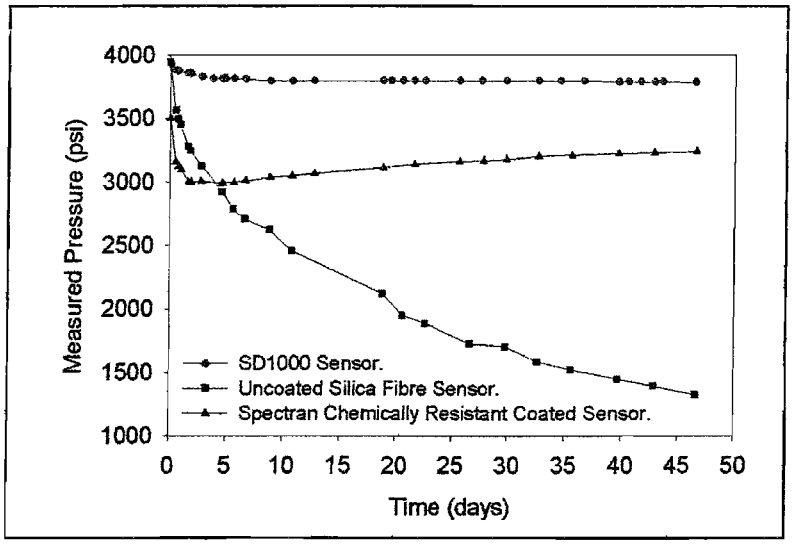

Figure 6.3.4: Plots of the stability of SD1000, uncoated-silica, and Spectran Chemically-Resistant-coated sensors in polysiloxane oil at 250°C and under 4000psi.

6.3.4 Water at 155°C and 200°C.

SD1000 sensors have been tested in water at 155°C and 200 °C and under 4000psi pressure.

Sensors showed similar stability curves to those observed in polysiloxane oil at 155°C during the initial period of the measurements. However, the signals began to fade in all water measurements resulting in sensor failures after approximately 110 days at 155°C and 12 days at 200°C.

On retrieval from the test chamber, the sensor package showed clear signs of damage:

- From the mirror end of the capillary, the package had turned white in colour and was no longer flexible but extremely brittle. This region extended along the package past the mirror region of the sensor.
- The remainder of the package was in good condition with no signs of reaction.

Where it was assumed that gallium is an un-reactive material, these results show clear signs of reaction between liquid gallium and high-temperature, high-pressure water. The reaction occurs at the interface between the metal and the water and progresses along the package with time. The rate of the reaction increases with increasing temperature.

6.4 Pre-Treatment of Sensors to Improve Stability.

SD1000 sensors and SD1100 sensors both showed an initial drift during the first 5 to 10 days at both 155°C and 250°C before becoming more stable. The stability after several months is approximately 1psi per month although this value is observed to improve with time. This drift, whilst extremely small, is not acceptable to the oil industry and needs to be further improved.

If the small drift was due to minute quantities of water dissolved in the gallium, one would expect the SD1100 sensor, with the additional carbon layer around the sensor, to show a much lower drift than the SD1000 sensor. This is not the case.

The cause of the initial short-term drift and long-term 1psi per month drift in the SD1000 sensor is therefore inherent to silica optical fibres but appears to reduce with increasing time when exposed to elevated temperatures.

Although not fully understood, possible explanations of the initial drift, and its reduction with time at elevated temperature have been considered:

- One possible explanation is that stress relaxation of the side-hole fibre results in a slow reduction of the fibre intrinsic birefringence towards zero. The relaxation is unlikely to be linear with time or temperature. One would therefore expect the drift to reduce with increasing time and temperature.
- Alternatively, a thin layer of absorbed water near to the silica-fibre surface (underneath the carbon layer in the SD1100 sensor) could cause the small initial drifts observed for the SD1000 sensors. With time, this small quantity of water would re-distribute itself through the fibre by diffusion. Diffusion of this water in the fibre would create stress and hence a drift of the sensor. With time, the water would become uniformly distributed and the sensor would return to a stress-free, stable state. Temperature would have a strong effect on the rate at which the stress-free condition was achieved.
- Similarly, moisture in the air contained within the side-holes of the side-hole fibre could have a similar effect on the sensor drift as it diffuses through the fibre. Again, this effect would reduce as the water re-distributed itself within the fibre. Temperature would also have a strong effect on the rate at which a stress-free condition was achieved.

One would expect that all three of these effects could be significantly reduced by pre-treatment of the sensor at elevated temperature for extended periods of time.

6.4.1 SD1010 and SD1210 Sensor Design and Fabrication.

The fabrication method used to make SD1000 and SD1200 sensors has been modified slightly to include a pre-treatment stage where SD1000 and SD1200 sensors are exposed to elevated temperatures in a nitrogen environment for extended periods of time. This additional stage to the sensor fabrication process was included in an attempt to pre-age the sensors to remove the initial drifts observed over the first few days of measurements.

A tubular, high-temperature chamber was designed in which sensors can be exposed to a controlled, uniform temperature whilst under a constant flow of nitrogen gas. Typically, a chamber temperature of 400°C has been used. At this temperature, with a slow flow of nitrogen, the polyimide coating of the capillary package does not burn and the sensor remains flexible after treatment. A temperature of 400°C was chosen in order to give the maximum rate of ageing, assumed to increase with increasing time, whilst operating within the safe limits of the furnace.

Following the high-temperature pre-treatment of the sensors, fresh gallium is injected into the capillary package to refill the annulus.

Sensors pre-treated at elevated temperature in this way are characterised as SD1010 (germanium-doped side-hole fibre) and SD1210 (tantalum-doped side-hole fibres) sensors.

6.4.2 SD1010 Sensor Stability in High-Temperature Fluids.

SD1010 sensors exposed to 400°C nitrogen for various lengths of time, have been measured in polysiloxane oils at 155°C and under 4000psi.

6.4.2.1 Polysiloxane Oil at 155°C.

Figure 6.4.1 shows plots for SD1010 sensors and an SD1000 sensor in polysiloxane oil at 155°C. Both of the SD1010 sensors were pre-treated at 400°C for approximately 8 days.

Figure 6.4.1: Plots of the stability of SD1010 sensors and an SD1000 sensor in polysiloxane oil at 155°C. SD1010 sensors have each been pre-treated at 400°C in nitrogen for 8 days.

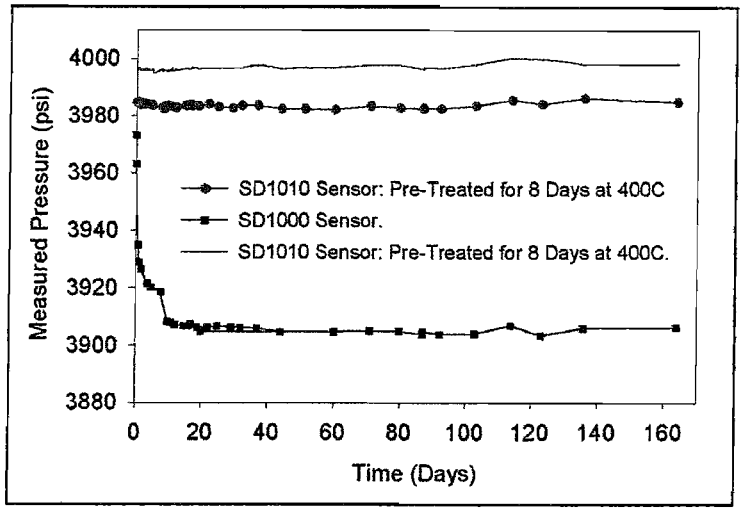

The SD1000 sensor shows the characteristic drift of approximately -80 psi over the first 10 to 20 days after which the stability approaches 1 psi per month.

- The SD1010 sensors exhibit a slight initial offset of between 5 psi and 15psi attributed to a combination of calibration errors, thermal cross-sensitivity of the sensor and temperature stabilisation of the test chamber.
- The SD1010 sensors show no measurable long-term drift.
- The SD1010 sensor shows a fluctuation as large as ± 1 psi over the duration of the measurement. The stability of this sensor is such that instabilities in the matched interferometer and instrumentation have been identified. The ±1psi fluctuations are attributed to the instrumentation.
- The stability of the SD1010 sensor is estimated to be better than 0.1psi per month although this value is difficult to ascertain using the current measurement approach.

6.4.2.2 Polysiloxane Oil at 200°C.

Figure 6.4.2 shows plots for an SD1010 sensor and an SD1000 sensor in polysiloxane oil at 200°C and under 4000psi. The SD1010 sensor was pre-treated at 400°C for approximately 14 days.

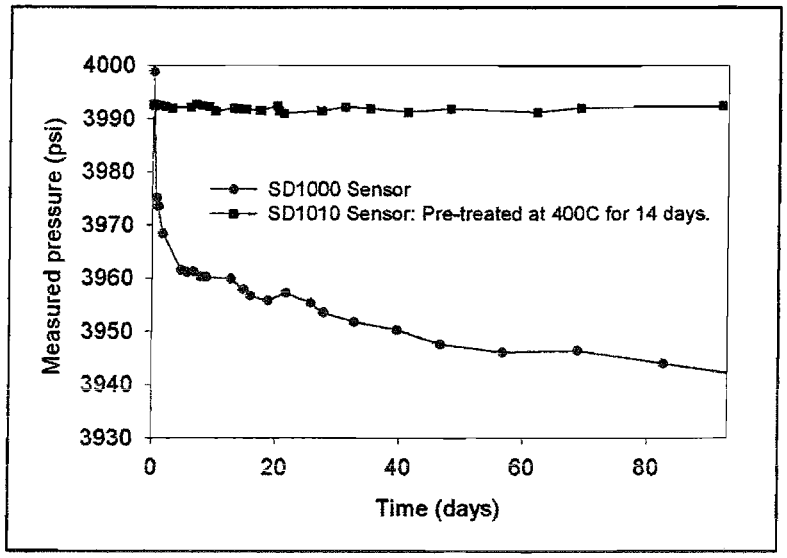

Figure 6.4.2: Plots of the stability of an SD1000 sensor and an SD1010 sensor in polysiloxane oil at 200°C. The SD1010 sensor was pre-treated at 400°C in nitrogen for 14 days.

- Over the 90 days measurement, the SD1000 sensor has drifted by over 50psi and continues to do so.
- Over the 90 days measurement, the SD1010 sensor has shown no measurable drift outside the ±1psi noise of the instrumentation and matched interferometer. The offset of approximately 7 psi, is attributed to a combination of calibration errors, thermal cross-sensitivity of the sensor and temperature stabilisation of the test chamber.

6.5 Robust Hermetic Packaging for Downhole Deployment.

Deployment trials of fibre-optic cables and sensors in the last 5 years has shown that the best cable for deployment and long-term survival, is a silica fibre coated with layers of carbon, polyimide, silicone and PTFE. The PTFE layer is extruded onto the cable in a process after the fibre is drawn. The overall dimension of the cable is generally governed by the thickness of the PTFE layer and is typically designed to be 300 to 500μm.

When fabricating an SD1 sensor using this cable as the downlead, or when splicing an SD1 sensor to this cable, a short, thin section between the cable and the sensor package is

introduced. This short section of thin cable provides a potential weakness, particularly during deployment.

Figure 6.5.1 shows a sketch of an SD1000 sensor that is attached to this cable. This consists of a long length of 500μm cable followed by a short length (20 to 50cm) of carbon and polyimide cable (approximately 180μm OD) followed by the SD1 sensor package, which has an outer diameter of approximately 320μm.

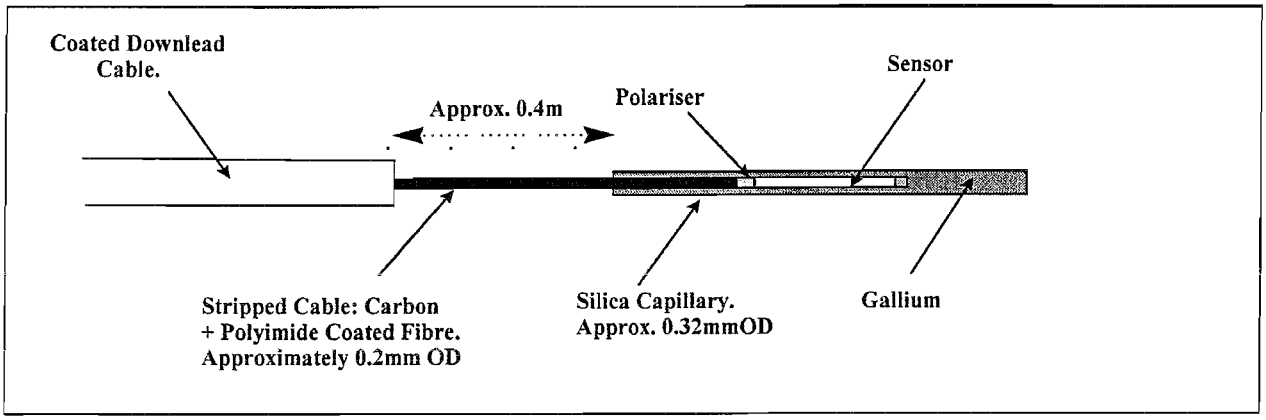

Figure 6.5.1: SD1000 sensor attached to a 500μm, teflon coated cable.

One method of overcoming the problem of attaching the sensor to 500μm cable is to use an additional capillary, made from PTFE, which covers the sensor package and exposed cable region.

Figure 6.5.2 shows a schematic of the robust sensor package intended for use in downhole deployment. The PTFE capillary has an inner diameter of approximately 400μm and an outer diameter of 600μm. This allows the PTFE to pass over the SD1 sensor but not the 500μm cable. Using a short length of high-temperature, PTFE heat-shrink, the cable and PTFE capillary are bonded together. This is repeated at the end of the PTFE capillary to produce a completely sealed unit. The sensor package in this design is sealed at the mirror end of the silica capillary by injecting a short plug of high-temperature epoxy into the capillary. Pressure is communicated to the fibre-sensor via the cable end of the silica capillary, which is left open.

The PTFE capillary is filled with polysiloxane oil prior to being sealed at both ends. This type of sensor is referred to as an SD2 sensor.

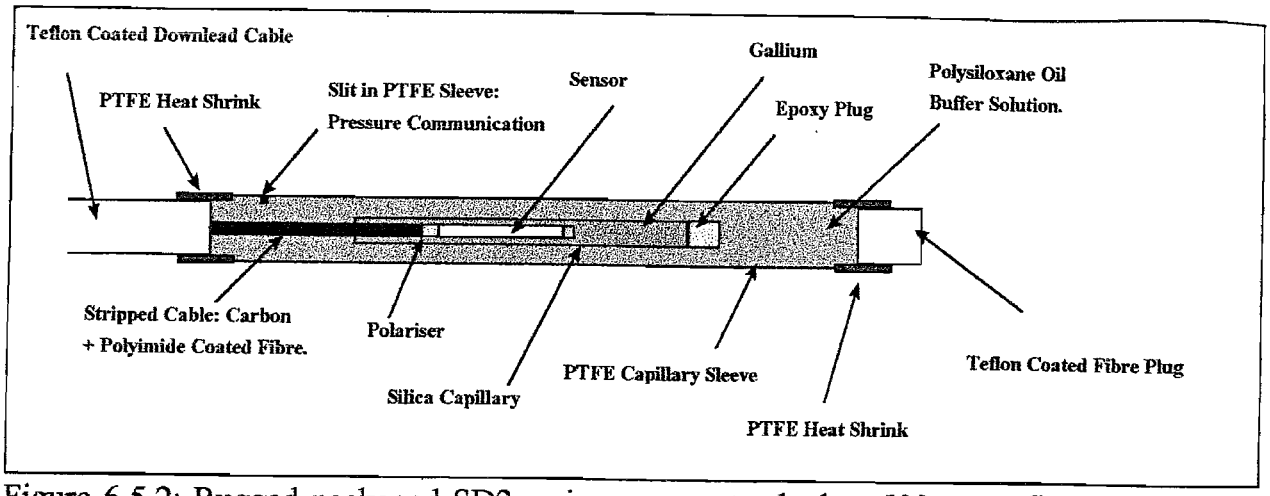

Figure 6.5.2: Rugged packaged SD2-series sensor attached to 500μm, teflon coated cable ready for deployment.

The SD2 sensor-package is extremely robust with no weak points and no uncoated, silica- fibre or splice regions. The maximum outer diameter of the package occurs at the two PTFE heat shrink sections.

6.5.1 SD2010 Sensor Stability in High-Temperature Fluids.

The SD2010 sensor should have the same long-term stability characteristics as the SD1010 sensor discussed in section 6.4. The only difference between the two sensors is the extra PTFE sleeve of the SD2010 sensor added for mechanical protection.

An SD2010 sensor and an SD1010 sensor were tested in polysiloxane oil at 200°C and under 4000psi pressure.

Figure 6.5.3 shows the plots for the two sensors over a period of approximately 90 days:

- The ±1psi noise error introduced by the matched interferometer and instrumentation is clearly shown by both of these plots.
- Both sensors show no measurable long-term drift outside the noise of the instrumentation.
- Measurements have been made up to January 2000. These sensors continue to be monitored.
- Measurements have started on SD2010 sensors in polysiloxane oil at 250°C and 300°C. Sensors show no signs of drift. Insufficient data is available at the time of publishing this thesis.

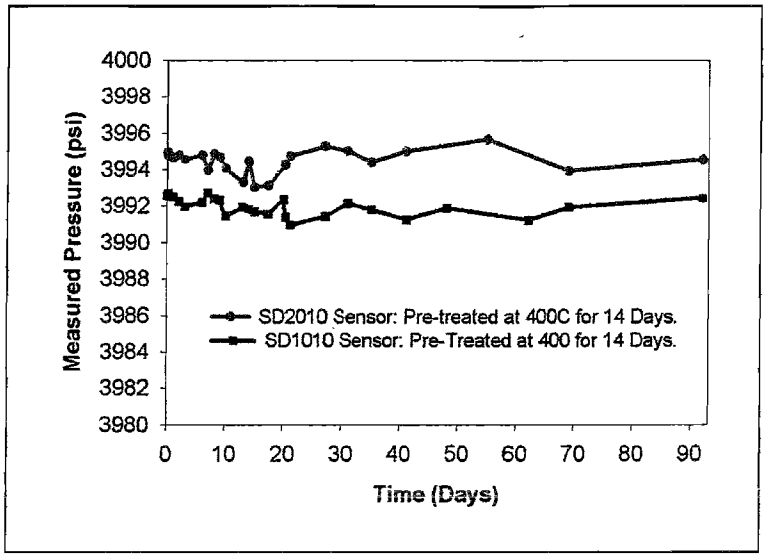

Figure 6.5.3: Plots of the stability of an SD2010 sensor and an SD1010 sensor in polysiloxane oil at 200°C. Both sensors were pre-treated at 400°C in nitrogen for 14 days.

6.5.2 SD2010 Sensor: Dynamic Pressure Sensor Performance.

The main worry of using an additional PTFE sleeve in the SD2010 sensor is the effect that this may have on the dynamic performance and resolution of the sensor.

6.5.2.1 Resolution of an SD2010 Sensor.

The response of an SD2010 sensor to very small changes in pressure has been monitored in order to estimate the resolution of the sensor and instrumentation.

Accurate application of very small changes in pressure has been achieved using a set up shown schematically in figure 6.5.4.

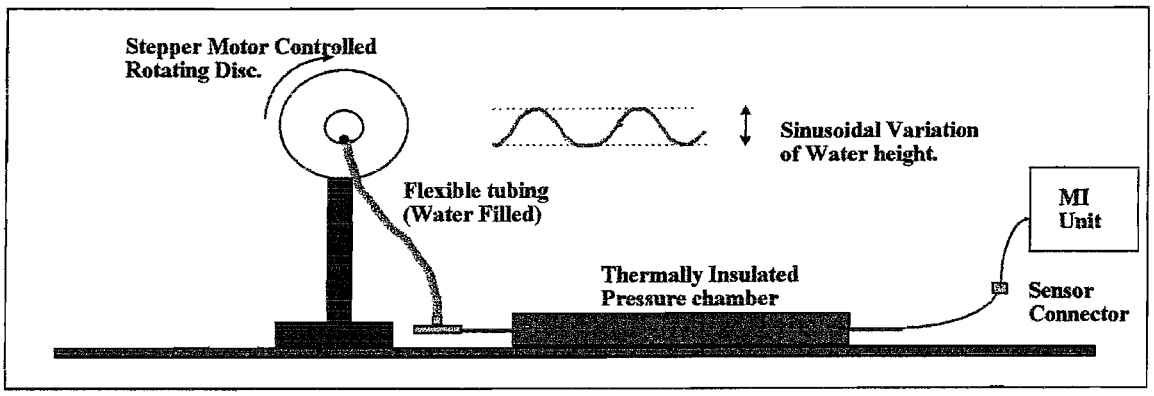

Figure 6.5.4: Set-up used to measure small a.c variations in hydrostatic pressure.

The measurements were made at low pressures. In this method, a head of water is contained in a length of flexible tubing fixed at an arbitrary position above the sensor. The sensor itself is contained in a pressure vessel, which is insulated to avoid thermal effects.

The top of the flexible water column is fixed to a disc, which can be stepper motor controlled to produce a sinusoidally-varying head of pressure.

Calculation of the pressure change exerted by a variable head of water is based on the equation:

$$\Delta P = \rho . g . \Delta h$$

Where ρ is the density of water, g is the acceleration due to gravity, and h is the height of the water column above the sensor. From this simple calculation, the pressure change created by a change in height of 1mm is expected to be approximately 0.0014psi.

The radius of rotation of the disc was approximately 13mm. Rotation of the disc therefore results in a sinusoidally-varying pressure of approximately 0.037 psi peak to peak.

Figure 6.5.5 shows the resulting 1 second and 10 second average responses of an SD2010 sensor to a 0.01 Hz variation in applied pressure, normalised around zero psi (ambient).

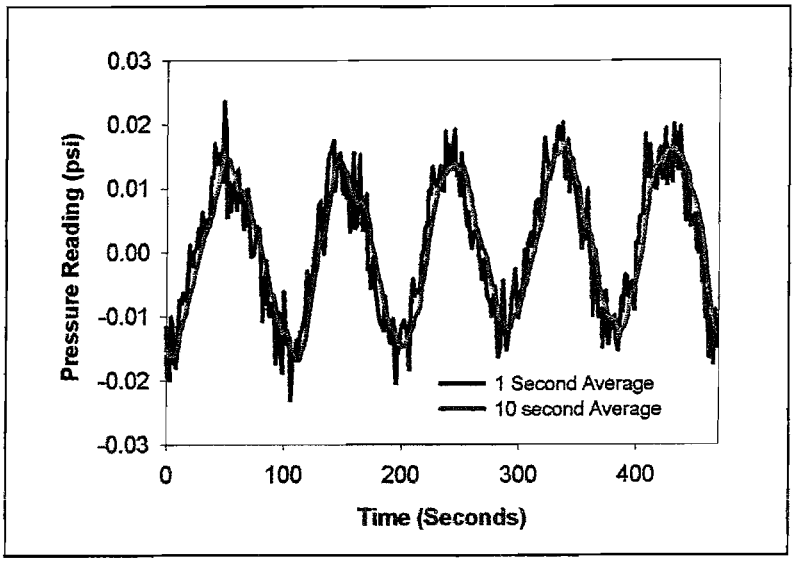

Figure 6.5.5: Plot of the 1 second and 10second averaged response of an SD2010 sensor to a 0.01Hz, 0.037psi peak-peak sinusoidal variation in pressure.

- The sensor clearly measures a sinusoidal pressure variation of approximately ±0.17psi.
- From the high signal-to-noise ratio of the 1 second response of the system, a resolution of better than 0.01 psi is predicted.
- The PTFE sleeving of the SD2010 sensor clearly has little effect on the resolution of the fibre-optic pressure sensor.

6.5.2.2 Dynamic Response of an SD2010 Sensor.

The response of an SD2010 sensor to pressure transients of 100psi, 500 psi and 1000psi has been measured. An SD2010 sensor and an electronic Druck gauge (used as a reference) were connected to a high pressure test chamber. Static pressures and pressure transients were applied to the chamber using a dead weight tester as described in chapter 2. The chamber throughout this measurement was maintained at ambient room temperature.

Figure 6.5.6 shows the 1 second average response of an SD2010 sensor and the response of the Druck gauge to various step changes in pressure. The curves show step responses at high pressure of 100, 500 and 1000psi with excellent agreement between the two gauges. The pressure steps correspond to ramp rates of approximately 3000psi / minute.

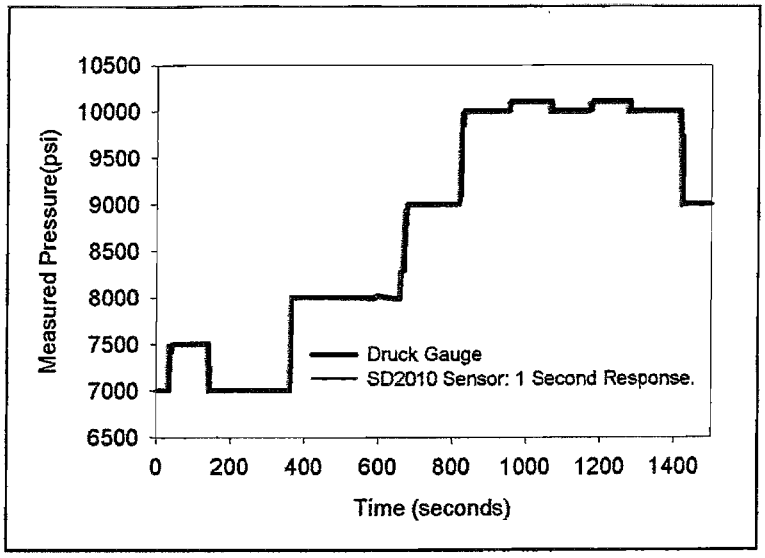

Figure 6.5.6: Response of an Sd2010 sensor and a Druck electronic pressure gauge to pressure transients of 100, 500 and 1000psi.

6.6 Discussion.

6.6.1 Protection of Optical Fibres and Sensors in Harsh Environments.

A novel hermetic-packaging for optical-fibre cables and sensors has been demonstrated and developed. The package consists of a cable, splice or sensor, coated with a liquid-metal, contained within a silica capillary.

The general benefits offered by an hermetic package over standard hermetic coatings are numerous:

- The hermetic package can be applied to any optical fibre sensor, device or cable after it has been fabricated offering:
  - hermetic protection of fragile splice regions.
  - hermetic protection of fibre Bragg gratings after they are UV written.
- For sensors requiring a mirror, this package provides high-reflectivity from a mirror formed between a cleaved fibre end-face and the liquid metal.
- The hermetic package does not affect the thermal sensitivity of fibre-optic sensors as liquids do not support shear stress.

The ability of the hermetic packages to protect optical fibres and sensors in high-temperature, high-pressure fluids has been demonstrated throughout this chapter with the use of side-hole-fibre pressure sensors.

Side-hole-fibre pressure sensors employing this packaging are referred to as SD sensors where a four-digit number following the SD, refers to characteristics of the optical fibre sensor, package-design and sensor pre-treatment.

Table 6.6.1 summarises these characteristics.

SD	*	*	*	*
Sensor Classification	**Package Details**	**Side-Hole Fibre Details**	**Sensor Pre-Treatment**	**Redundant: Future Classes**
SD1000	Silica Capillary	Ge Doped Core	N/A	
SD1100	Silica Capillary	Ge Doped Core. Carbon Coated.	N/A	
SD1200	Silica Capillary	Ta Doped Core	N/A	
SD1010	Silica Capillary	Ge Doped Core	400°C Nitrogen	
SD1210	Silica Capillary	Ta Doped Core	400°C Nitrogen	
SD2010	Silica Capillary & PTFE Sleeve.	Ge Doped Core	400°C Nitrogen	
SD2210	Silica Capillary & PTFE Sleeve.	Ta Doped Core	400°C Nitrogen	

Table 6.6.1: Summary of the details of various SD sensor designs.

The general structure of the sensor package, the fabrication technique and the treatment of sensors at elevated temperature have been developed to produce the following performance of SD pressure sensors:

1. An estimated stability of better than 0.1psi per month at 155°C and at 200°C in polysiloxane oil.
   - The same stability at 250°C. Measurements have recently started.(January 2000).
   - The same stability at 300°C. Measurements have recently started (January 2000).
   - This value is currently limited by the measurement instrumentation.
   - **No existing optical or electronic downhole gauge has this performance at 155°C.**
   - **No existing optical or electronic downhole gauge is reported for 200°C operation.**
2. SD1000 sensors have been in continuous operation at 155°C for over 13 months without degradation of signal. These measurements continue.

3. SD2000 sensors have been in continuous operation at 200°C for over 3 months without degradation of signal. These measurements continue.
4. SD2000 sensors are mechanically robust and are designed for deployment in the oil field.

6.6.2 Liquid-Metals as Hermetic Coatings.

The actual reason why gallium has offered such excellent protection of fibre-optic pressure sensors in high-temperature, high-pressure fluids is not fully understood and would therefore make an interesting area for future research.

Several potential reasons for the success of the gallium as a hermetic barrier have been considered:

- Gallium may be impervious to molecular water. This would make gallium an excellent barrier to water and would explain why sensors are so stable when protected by a layer of gallium.
- The solubility of molecular water in gallium may be so small that the drift effects are too small to be noticed. This would suggest that the molecular water content of gallium is much less than that of the polysiloxane oils used as HTHP fluids.
- Gallium may possess a "gettering" property where diffusing, molecular-water reacts with the gallium and becomes immobile, thus never reaching the silica fibre. This explanation is supported by the observations of a reaction between gallium and HTHP water (section 6.3.4).

Either one, or a combination of these reasons could explain why gallium provides such a high quality barrier against water diffusion into optical fibre sensor.

In order to gain a greater understanding of the role of gallium in the hermetic package, further research into the properties of liquid-metals is required.

6.6.3 Additional Applications of this Technology.

Whilst chapter 6 has focussed on the use of liquid metals, packaged inside silica capillaries, the hermetic properties are provided by the liquid metal itself. The package can be large or small and liquid metals can therefore be used to protect any type of optical or electronic sensor in harsh environments.

It should also be noted that this hermetic package could have far reaching applications

into the telecommunications market for protecting optical fibres and devices from harsh environments.

Any fibre-optic laser source, particularly those which utilise fibre Bragg gratings, will be subject to long-term instabilities when operating at elevated temperature in the presence of moisture. Such a hermetic package, involving liquid metals, could prevent this.

Furthermore, a liquid metal surrounding an optical fibre or device, could provide a thermal heat sink or source. Such an example is in the thermal stabilisation of fibre DFB (distributed feedback) lasers [72]. The liquid metal could also act as an electrode contact for an optical fibre or device.

The use of liquid metals also has potential for use in protecting downhole and surface electronic-pressure-gauges. Liquid metals may be utilised as a form of isolation or pressure communication between two reactive fluids [70].

6.7 Conclusions.

- A novel, hermetic-package for fibre-optic pressure sensors has been invented and developed.
- The resulting sensor, the SD-series pressure sensor has shown excellent dynamic response to pressure transients.
- The pressure sensor resolution has been measured. The sensor clearly measures a 0.037psi peak to peak sinusoidal pressure change. Estimated resolution of the device is better than 0.01psi.
- The SD2-series sensor shows excellent long-term stability in high-temperature, high-pressure fluid environments:
  - Better than 0.1 psi per month at 155°C
  - Better than 0.1 psi per month at 200°C
  - Early results predict better than 0.1 psi per month at 250°C and 300°C.
- The SD-series pressure sensor out-performs any other downhole, fibre-optic or electronic pressure sensor in the world.

Chapter 7

Field Test of the SD Fibre-Optic Pressure Sensor.

7.1 Introduction.

The SD2000 series fibre-optic pressure sensor, described in chapter 6, was field tested at Chevron's Fibre Optic Test Facility, Coalinga, California during the period of November 15th 1999 to December 4th 1999.

The purpose of this field trial was to investigate deployment issues of the new sensor design and to reproduce the laboratory, dynamic and long-term performance, achieved for the SD2000 sensor.

This chapter discusses the preparations, planned objectives and main achievements of the field trial.

The details of the deployment technique used to install fibre-optic cables and sensors in downhole hydraulic conduit (highways) are discussed.

7.2 Deployment of Optical Fibres by Fluid Drag.

7.2.1 Background.

The method of deploying optical-fibre transmission-lines into conduits using fluid drag was reported in 1982 [73]. The invention utilised the drag force generated by a high-velocity flow of gas passing over a fibre cable, contained within a flexible conduit.

Figure 7.2.1 summarises the forces that contribute to the deployment of fibres using viscous flow of a fluid.

The fluid-flow past the surface of the cable produces a drag force that largely depends on the velocity of the fluid relative to the cable surface. For deployment, the inlet bore ("stuffing box" or "lubricator") of the deployment system is made to be a close fit to the cable thus limiting flow in this direction (Vb is very small). The fluid-drag force therefore acts in the deployment direction and is dependent upon Vf, the forward flow velocity, and the surface area of the cable.

The forward flow velocity is found to be almost linearly dependent upon the pressure drop over the conduit length, dP [73]. For a given flow rate, dP is dependent upon the free cross sectional area of the bore.

Due to the pressure drop over the conduit length acting on the cross sectional area of the cable, a back force, F_B acts in the direction opposing deployment.

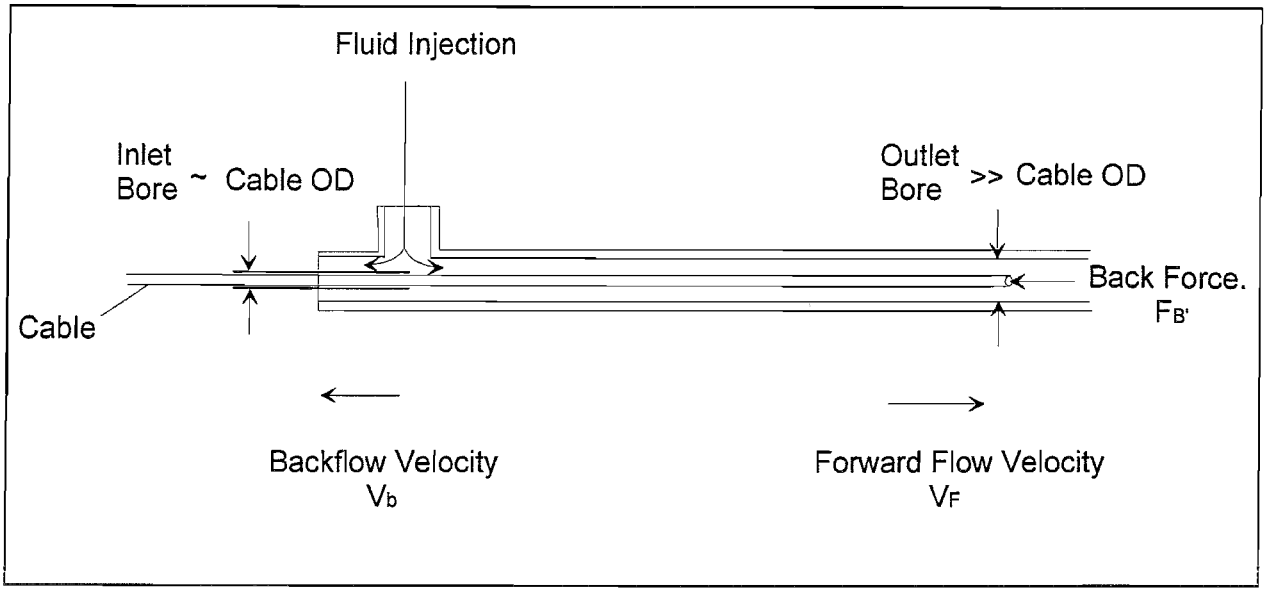

Figure 7.2.1: Summarising the forces involved in deployment by fluid drag.

The fluid drag of the gaseous medium produces a distributed pulling force on the fibre enabling the fibre to be pumped through routes containing bends. With other methods of fibre instalment into conduits, generally requiring a pulling cord, any deviation of the conduit pathway from a straight line increases friction between the fibre and the walls of the conduit.

7.2.2 Description of the Deployment Method.

The deployment method used at the field trial discussed in this chapter was developed during the period of 1994 to 1996 by Sensor Dynamics in conjunction with Chevron Research and Technology. The method is very similar to that used for transmission-line installation, previously described. However, for this deployment method, the fluid is in the liquid state. Originally the deployment fluid was water, however, for the reasons outlined in the previous chapters, a polysiloxane oil is now used both as the deployment fluid and as the high-pressure fluid medium. The polysiloxane oil is a commercially available heat transfer fluid supplied by Dow Corning: Syltherm 800 heat transfer fluid.

Syltherm 800 has a low viscosity, similar to that of water, is non-toxic and has the excellent thermal stability properties expected from a heat-transfer fluid.

Figure 7.2.2 is a schematic of the deployment system used in the field trial, showing the major components necessary for deployment. Figure 7.2.3 is a photograph of the actual deployment rig showing the deployment system hardware.

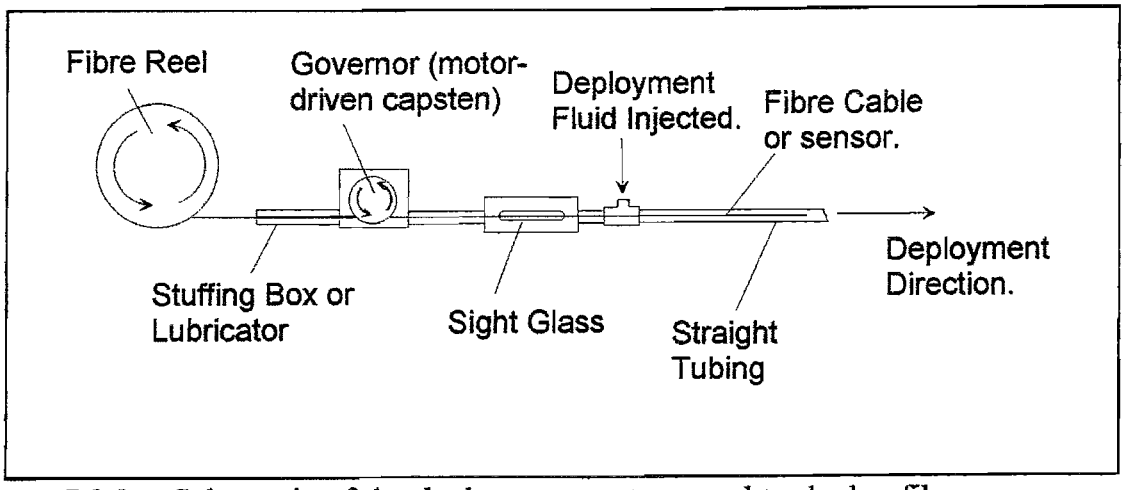

Figure 7.2.2: Schematic of the deployment system used to deploy fibre sensors and cables into downhole conduits.

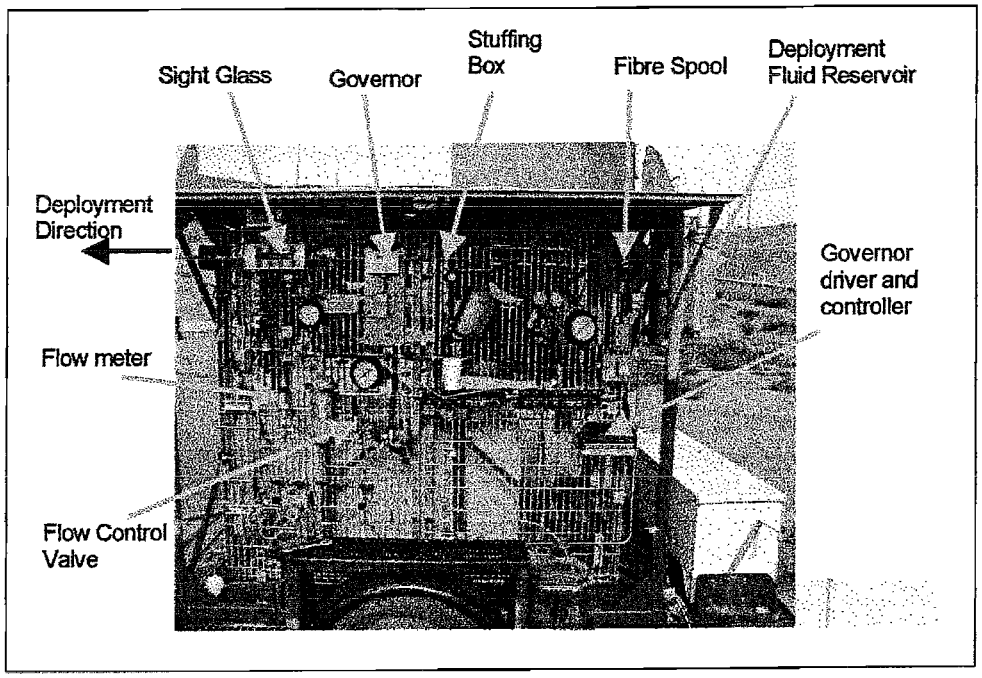

Figure 7.2.3: Photograph of the front panel of the deployment rig showing the main components of the deployment system.

The fibre cable is first fed through a "stuffing box", also referred to as a "lubricator". The stuffing box is fabricated from small-gauge, needle-stock tubing with an inner diameter slightly larger than the maximum outer diameter of the fibre downlead-cable. As described in the previous section, the stuffing box effectively eliminates any flow of deployment fluid

in the negative deployment direction.

The cable is then fed through a device called the "governor". The governor consists of a small, motor-driven wheel with a v-groove machined into it. With a single coil of cable wrapped around this wheel before being fed into the remainder of the system, this wheel acts as a capstan. The governor therefore serves two vital roles during deployment,

- Controlling the rate at which the fibre cable is fed into the conduit.
- Preventing the cable from being pushed out of the conduit in the event that the back force due to the highway pressure dominates the fluid drag force.

The sight glass is a non-essential part of the deployment system but allows the operator to visually monitor the cable during deployment to check for tension and motion.

The straight section after the sight glass joins the deployment system to the downhole conduit, the "highway". In the field-trial deployments, the straight section was made from narrow bore tubing (3/16" outer diameter) to increase the velocity of the fluid and hence the magnitude of the fluid drag acting to deploy the cable.

The remainder of the highway was fabricated from 1/4" outer diameter, stainless-steel tubing with a bore slightly larger than the first straight section.

The deployment rig also has a petrol-powered motor and a petrol-powered generator, not shown in figure 7.2.3. The motor powers a hydraulic pump to provide means of fluid flow, the rate of which is controlled using by the operator using the flow control valve shown in figure 7.2.3. The generator supplies the power needed to drive the governor-motor transformer and any additional electrical appliances needed at the deployment rig.

7.3 Field Trial Preparations.

7.3.1 Field Trial test Facility.

Chevron's fibre-optic test facility at Coalinga is based around observation well 4-4T1 in the Coalinga steam flood field. The site has been tailored to be the test facility for all future fibre-optic sensors intended for the oil industry.

Figures 7.3.1 to 7.3.4 are photographs of the test facility showing the major components. The site comprises; an air conditioned laboratory and workshop (iv), deployment rig (i), a high- pressure enclosure (iii) and the observation well itself (ii), fitted with two highways and a downhole pressure chamber.

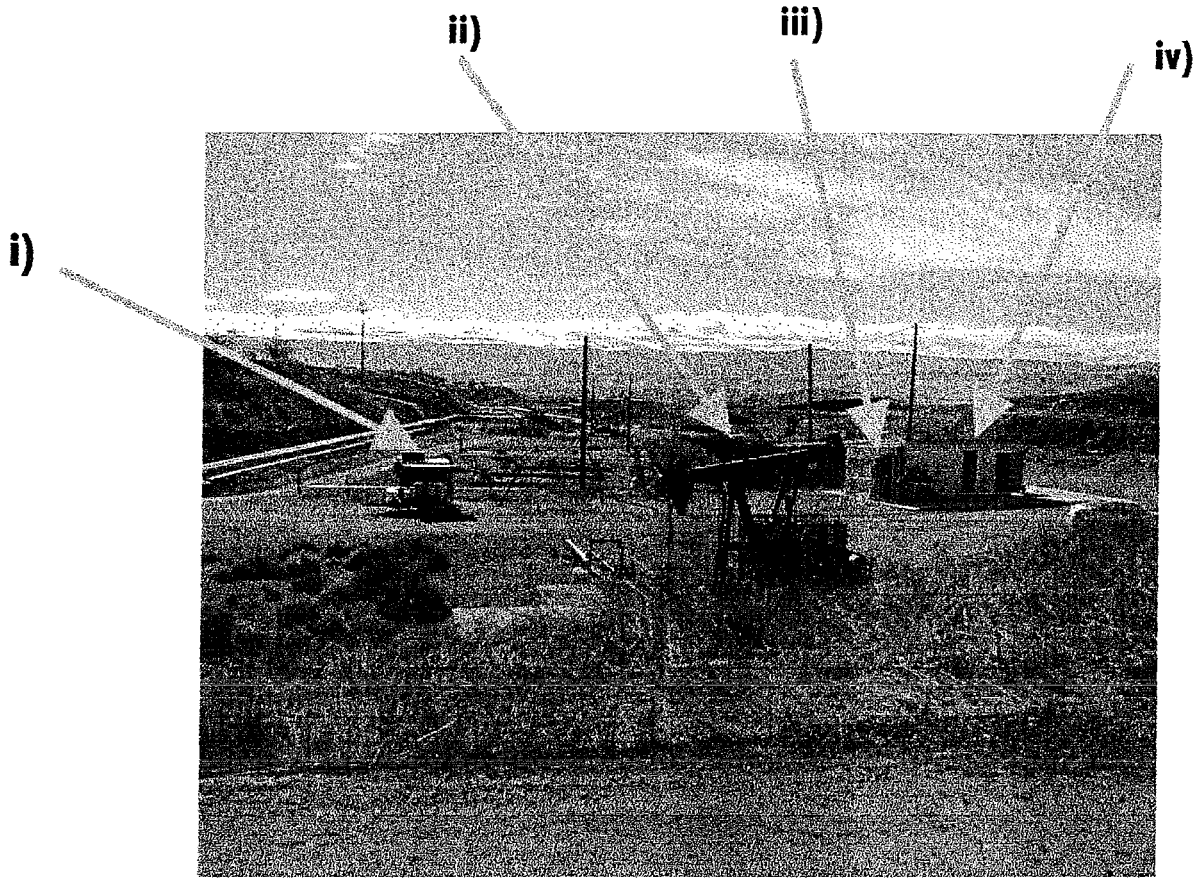

Figure 7.3.1: Photograph of the overall test site.

Figure 7.3.2 shows a cross section completion drawing of well 4-4T1. The well includes a temperature highway (shown in red), a pressure highway (green) and a fluid control line (blue). Both the pressure and temperature highways consist of U-shaped 1/4" outer diameter stainless steel tubing.

The pressure highway has a flow-activated valve, positioned at approximately 812.5' from the surface. This pressure port opens up into a specially-designed downhole pressure chamber which can be filled, emptied and pressurised via the 3/8" stainless steel fluid control lines (blue). The temperature highway has no downhole pressure- communication.

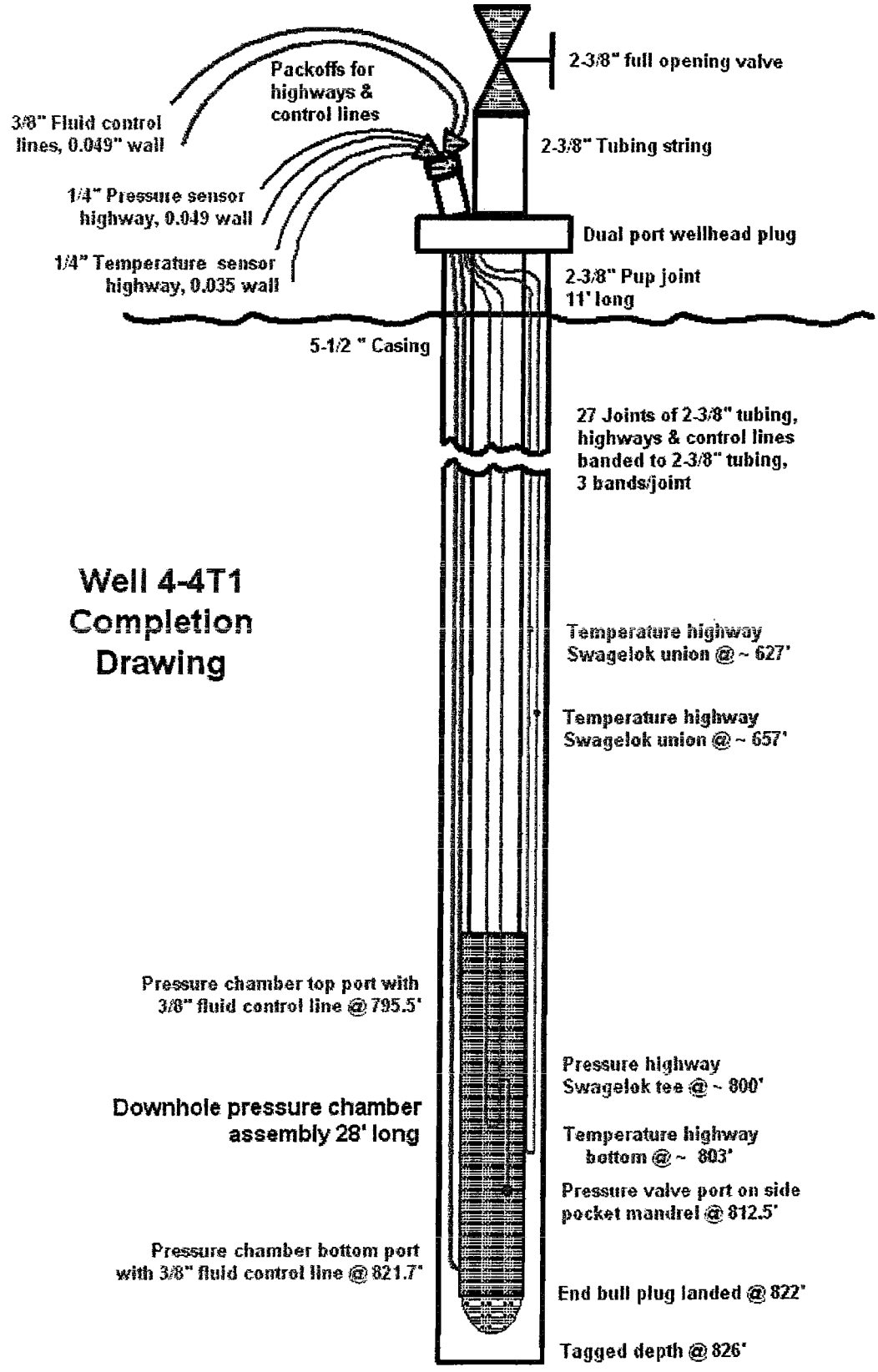

Figure 7.3.2: Cross section of Well 4-4T1 completion design.

Figure 7.3.3 shows a view inside the high-pressure enclosure attached to the side of the cabin. The enclosure contains all the means for filling, draining and pressurising the highways. Three splice chambers have been included on the front panel of the enclosure. Splice boxes provide the means for attaching fibre-optic, high-pressure seals (also referred to as penetrators) to pressure sensor downlead cables.

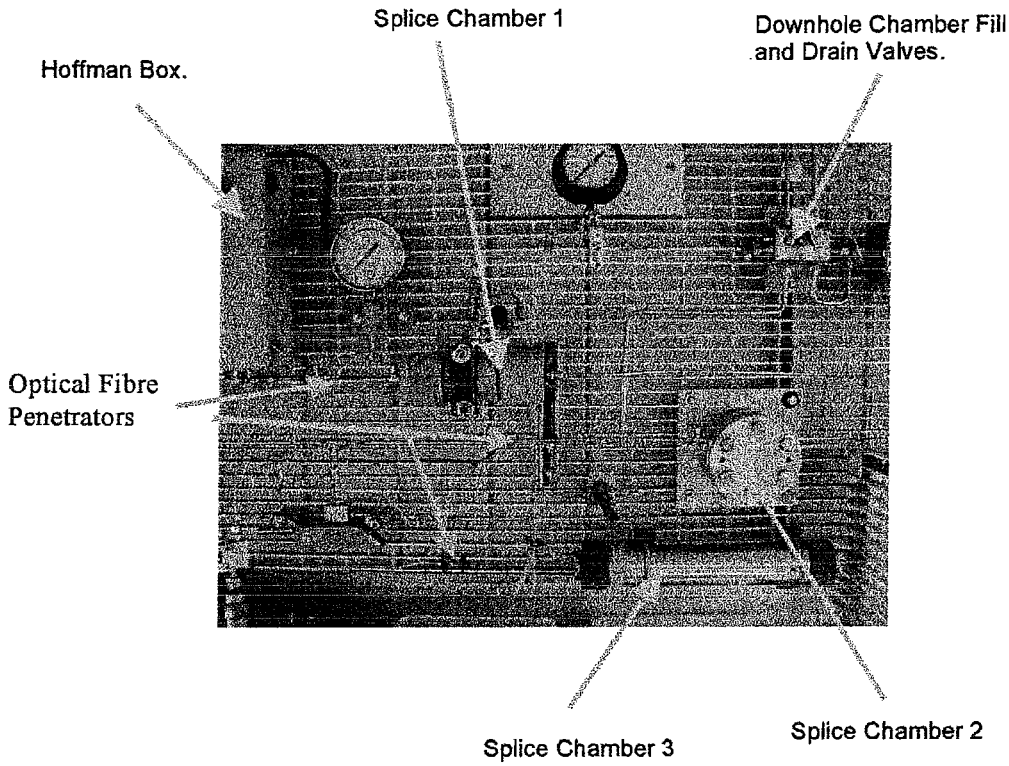

Figure 7.3.3: Photograph of part of the high-pressure enclosure showing the three splice chambers used during the field trial to splice fibre-optic, high-pressure seals (penetrators) to sensor cables.

Splice chambers are designed to withstand the high-pressure rating of the highway. The chambers must have sufficient inside volume to allow several metres of fibre to be coiled and contained after making a fusion splice between the penetrator and sensor-cable.

Two different types of splice chamber were made available at the test site. Splice chambers 1 and 3 are both "end-loading " designs while splice chamber 2 is a "front-loading" design. The benefit of the front-loading version is that the fibres and splice can be accessed by removing the front cover without actually interfering with the fibre or

penetrator.

The enclosure also contains a Hoffman box, which is a water-tight enclosure providing protection to electronic devices and fibre cables. The Hoffman box contains a Quartz and a Druck reference gauge and readout electronics. It also serves the purpose of routing the fibre-optic penetrator cables into the cabin to the measurement instrumentation (figure 7.3.4).

Surface valves, hand pumps, air activated hydraulic pumps and an old, dead-weight-tester are also contained within the enclosure. These instruments provide the means for pressurising the downhole chamber and highway.

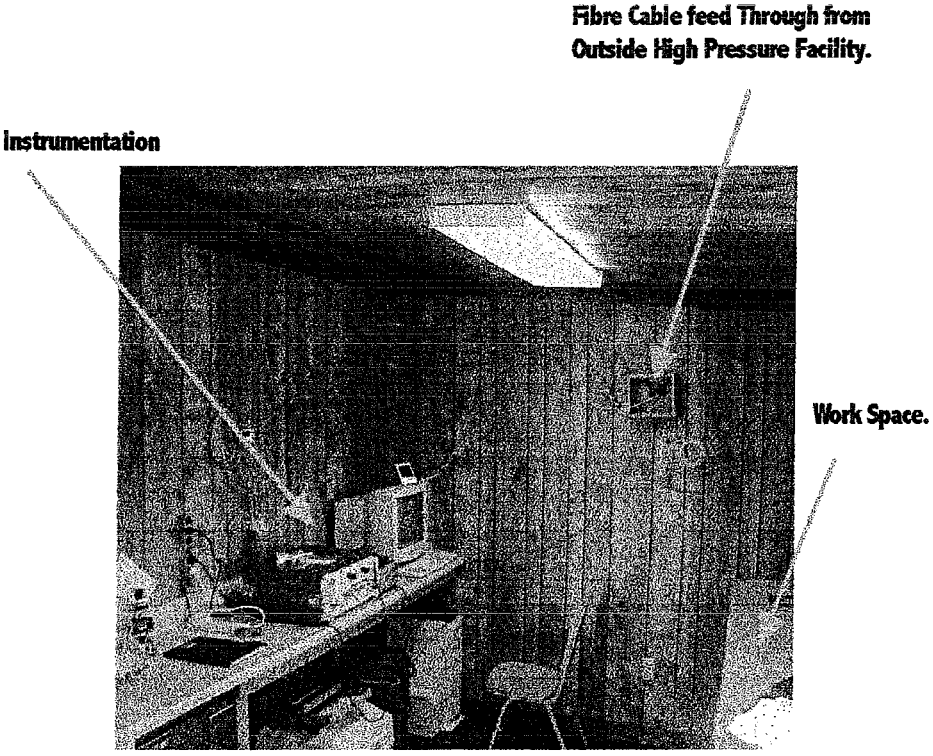

Figure 7.3.4: Photograph of part of the laboratory including the Sensor Dynamics Pressure-Sensor Instrumentation. Optical cables are fed from the high-pressure enclosure through a Hoffman box and into the cabin.

7.3.2 Preparations of Fibre-Optic Sensors and Components.

Figure 7.3.6 is a photograph of an SD2000 sensor-assembly supplied for the trial. The figure shows the single-mode cable on the spool. The cable passed through a closely fitting stuffing box and is eventually spliced to the pressure sensor. This method of shipment does not require any form of field splicing. The splice between the sensor and cable is contained within the SD2000 package and is protected from the downhole fluids.

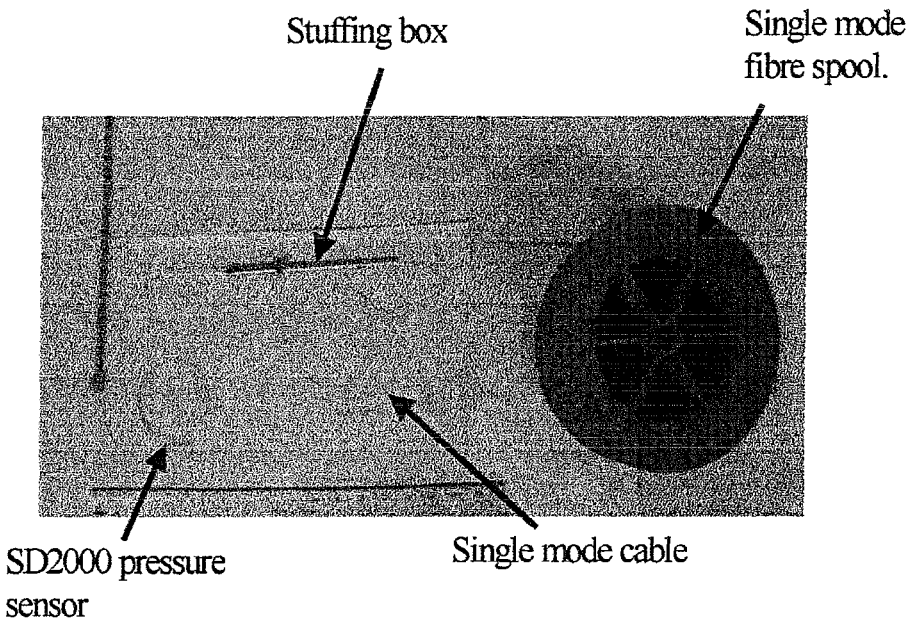

Figure 7.3.6 Photograph of a packaged SD2000 series sensor attached to a spool of Spectran single-mode fibre cable via a stuffing box.

7.4 Field Trial Objectives and Achievements.

7.4.1 Field Trial Objectives.

The overall objective of this field trial was to deploy an SD2000-series sensor into a downhole highway and reproduce the long-term stability and dynamic performance that have been observed in laboratory trials.

A secondary objective was to attempt dual deployment of two fibre sensors, either simultaneously or sequentially, into a single highway. Dual deployment has not previously been demonstrated in the laboratory or in the field.

7.4.2 Sensor Deployments.

7.4.2.1 Pressure Sensor Deployment 1.

The first pressure-sensor deployment attempt used one of the sensor and spool packages shown in figure 7.4.6. The sensor was deployed to a depth of approximately 235m from the well head. The deployment rate was carefully controlled to be slow (approximately 5 m /min) until the sensor was beyond the well head. The deployment rate was increased and controlled to be approximately 12m / min for the remainder of the deployment.

A single mode fibre penetrator, fabricated at Sensor Dynamics from 1/4" tubing, fittings and epoxy, was spliced to the sensor cable in splice chamber 1. .

7.4.2.2 Sequential DTS and Pressure Sensor Deployment.

A secondary objective of this field trial was to try to perform a dual deployment of sensors, sequentially at first and simultaneously if possible. This has not been previously demonstrated.

In order not to jeopardise the sensor in the pressure-highway, additional deployment trials used the temperature-highway. The decision was made to deploy both a pressure sensor and a multi-mode fibre cable for distributed-temperature measurement, into the same highway. The DTS fibre was required for a field trial later in December 1999 and it was also felt that the continuous availability of temperature data for this well would be valuable.

For the forth-coming field trial, access was required to both ends of the DTS multi-mode cable.

The multi-mode cable was based on the Spectran Chemically-Resistant fibre used for the pressure sensor. However, the teflon outer coating was slightly thinner, approximately 400μm.

The multi-mode fibre was the first to be deployed in the sequence. Deployment of the DTS fibre was successfully achieved.

The DTS cable was tethered in the splice chamber during the deloyment of the pressure sensor. Sequential deployment of a pressure sensor and DTS was successfully demonstrated

The pressure sensor was deployed to a depth of approximately 232m. Deployment was controlled at a rate of approximately 10 m /min.

A dual, high-pressure penetrator, incorporating one single mode and one multi-mode fibre, was fabricated from 1/4" tube, fittings and epoxy. The single-mode cable was spliced

to the pressure sensor downlead and the multi-mode penetrator fibre was spliced to the DTS fibre.

A multi-mode penetrator was spliced to the other end of the DTS fibre inside splice chamber 3. Penetrator cables were passed through the Hoffman box and into the cabin.

The DTS cable ends were connectorised with Diamond E2000 connectors and fixed at a bulkhead inside the cabin. The pressure sensor cables were routed through to the instrumentation.

7.4.3 Temperature Profiling of the Well.

A wireline temperature-measurement of well 4-4T1 was made on the 11th November 1999 by Pruett industries. This procedure involves lowering a temperature probe down into the well through the production tubing.

Figure 7.4.1 shows the plot of temperature versus depth from the top of the well head.

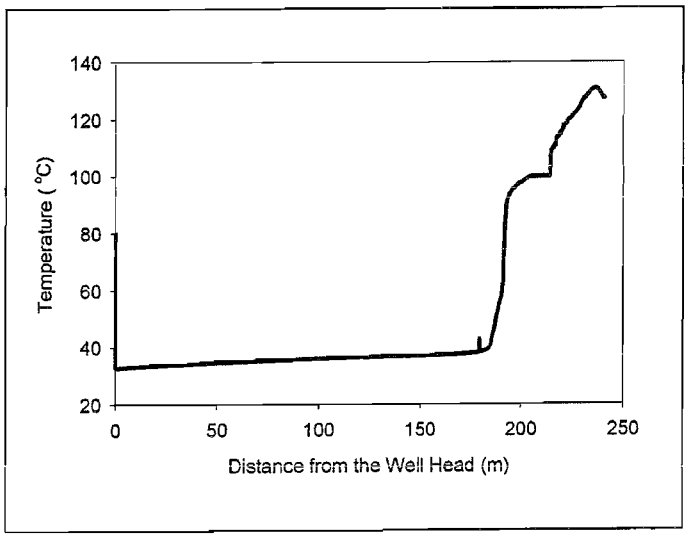

Figure 7.4.1: Temperature in °C plotted against depth (from the well-head) for well 4-4T1. Measurement made by wireline, 11th December 1999.

The wireline measurement shows that the maximum well-temperature occurs at a depth of approximately 236 metres. The temperature at this depth is approximately 131°C.

The expected temperature of this well should be closer to 155°C, the temperature used in the lab to test the stability of the SD2000 sensor.

Chevron were asked if the steam injection could be increased to this area of the field. Work took place on the steam-injector-well on the 23rd November 1999 to increase steam injection into this region of the oil field.

Due to the geology of the Coalinga oil field, the time expected before the effects of the steam injection increase are observed at well 4-4T1 is of the order of months. However, using the DTS installed in the temperature highway, these changes can be tracked over the first months of the year 2000.

The first DTS measurement was made by Pruett Industries on the 2nd December 1999. Figure 7.4.2 shows the plot of temperature in °C against depth in metres for the whole highway. Note that the depth scale does not coincide with that of figure 7.4.1 for the wireline measurement. The DTS measurement includes the penetrator-cable, spare cable in the splice chamber and the fibre in the highway between the splice chamber and the well head.

The curve shows a maximum temperature of 134°C at a distance of 151m from the fibre connector. The plot is symmetrical due to the highway being U-shaped. The curve shows a dip in the temperature to approximately 128°C at 157m from the fibre bulkhead connector.

Use of the DTS over several months should show changes in this profile as the downhole temperature changes.

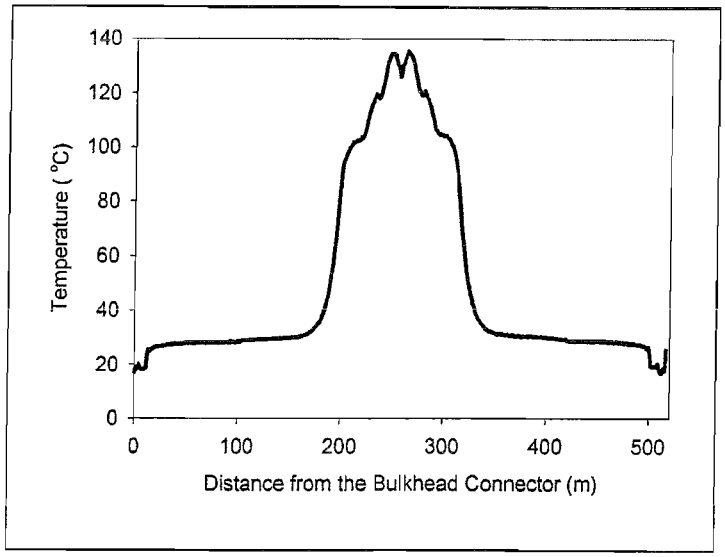

Figure 7.4.2: DTS temperature profile plot of well 4-4T1. Taken on the 2nd December 1999.

7.4.4 Pressure Sensor Performance.

In order to calibrate, measure and monitor the fibre-optic, downhole pressure-sensors, reference gauges are required. Available at the test site were two surface gauges, a Druck electronic gauge and a quartz pressure gauge. The outputs of these gauges were interfaced

into the pressure-sensor monitoring-equipment such that the data from the fibre and reference gauges could all be stored in the same files.

The Druck gauge measured gauge pressure (ie. atmospheric pressure is read as zero) and the quartz gauge measured absolute pressure. The Druck gauge resolution was limited by a 1psi quantisation level. The Quartz gauge resolution was not stated but the measurement reading was given to four decimal places (0.0001psi).

For the downhole, fibre-optic pressure-sensor, the head of polysiloxane oil in the highway above the sensor (approximately 230m) provides an additional static pressure of approximately 300psi.

For this field trial, the static-pressure offset of the head of oil in the highway was ignored and the downhole sensor was calibrated against one of the surface gauges. It was therefore necessary to approximate the contribution of the static head of pressure to be constant. This will inevitably lead to errors as the static head of pressure depends on the density of the polysiloxane oil in the highway. The temperature dependence of the polysiloxane oil, highway-fluid is approximately -1kg m^{-3} $°C^{-1}$. An average change of 1°C over the highway corresponds to a pressure change of approximately 0.33psi in the static-pressure head.

For pressure testing, figure 7.4.3 shows a schematic of the high-pressure configuration of the pressure highway. Pressure is applied to the highway with the hydraulic pump, via the downhole pressure-chamber. The pressure source is located at the surface, close to the Druck and the quartz gauges.

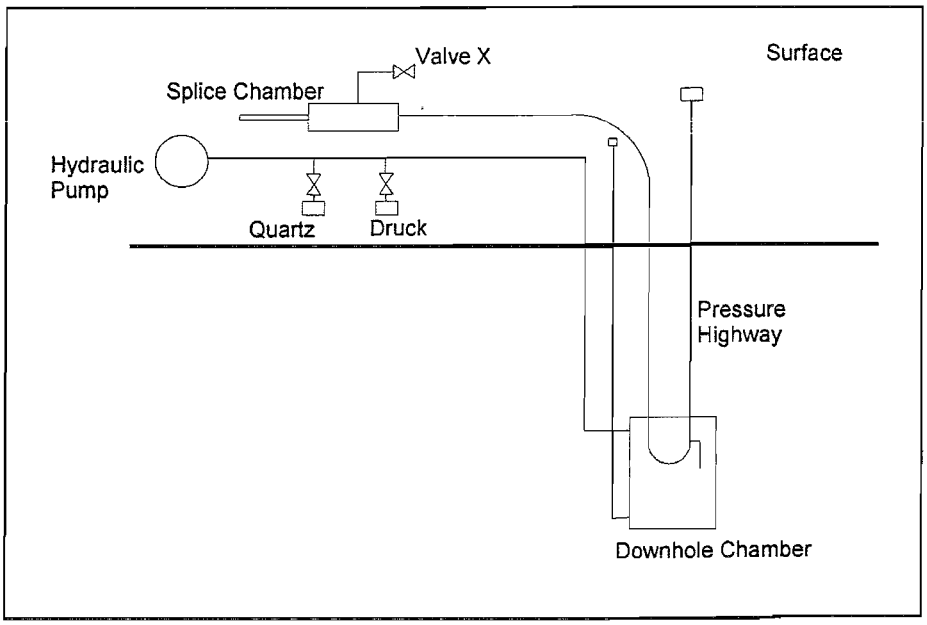

Figure 7.4.3: Schematic of the high pressure set-up for the pressure highway.

7.4.4.1 Long-term Stability.

In laboratory experiments, the long-term stability of pressure sensors is monitored using an accurate Dead Weight Tester (DWT). Using the DWT, a known pressure (accurate to 0.1psi) can be applied to the chamber and consistency can be achieved over extended test periods.

For this field trial, the available DWT was old and in need of a service having only recently been acquired. A consistent, accurate pressure could not therefore be achieved.

The only method available for monitoring the stability of the downhole sensor is to compare it to the surface gauges over extended periods of time.

For the short duration of the field trial, the fibre-optic pressure sensor showed excellent stability, consistent with laboratory observations. Continued monitoring through into 2000 will further test this stability.

7.4.4.2 Dynamic Response to Pressure Transients.

Figures 7.4.4 to 7.4.6 show examples of the responses of the fibre-optic, Druck and quartz pressure gauges to pressure ramps of different magnitudes. Generally, ramp rates of 1000psi in 1 to 2 minutes were achieved using the hydraulic pump at the surface.

From figures 7.4.4 to 7.4.6, the SD2000 pressure sensor and instrumentation tracks the Druck and quartz gauges extremely well. The responses of the three gauges are identical and it is therefore difficult to distinguish between the traces. However, as shown by figure 7.4.5, there is a time delay between the responses of the Druck and quartz and that of the SD2000 sensor. This time delay is demonstrated by the plots of "quartz - SD2000 1 second" and "Druck - SD2000 1Second". During each pressure ramp, there is a step in the difference between surface and downhole gauges. The position of the three gauges with respect to the pressure source (figure 7.4.3) is assumed to be the cause of this. This may also explain the small overshoots in response seen by the quartz gauge but not the SD2000

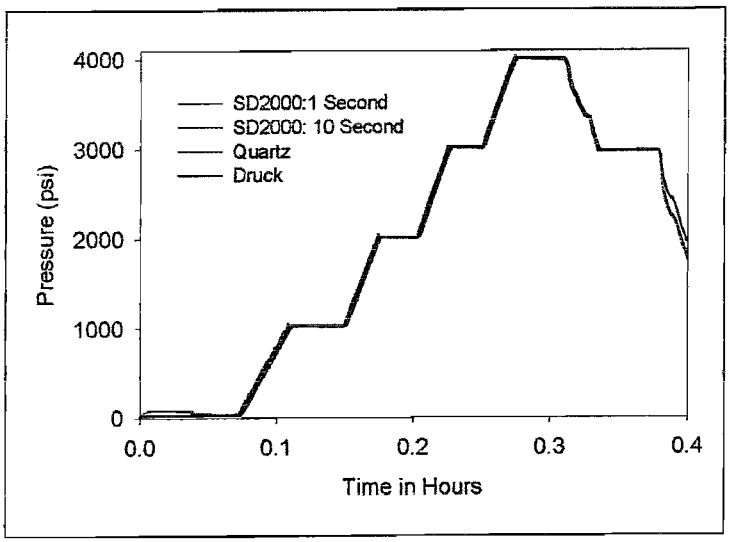

sensor during pressure steps. These overshoots are not shown very clearly in the figures.

Figure 7.4.4: Plot of the measured-pressure against time for surface electronic-gauges and a downhole, fibre-optic pressure sensor during ramps in pressure.

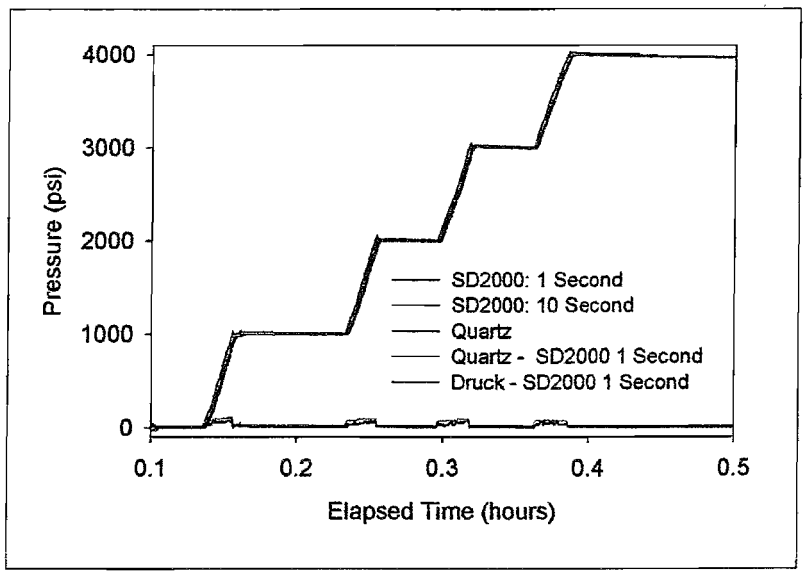

Figure 7.4.5: Plot of the measured-pressure against time for surface electronic-gauges and a downhole fibre-optic pressure sensor during pressure steps. Also shown are the plots of the difference between surface and downhole gauges showing delays in pressure communication.

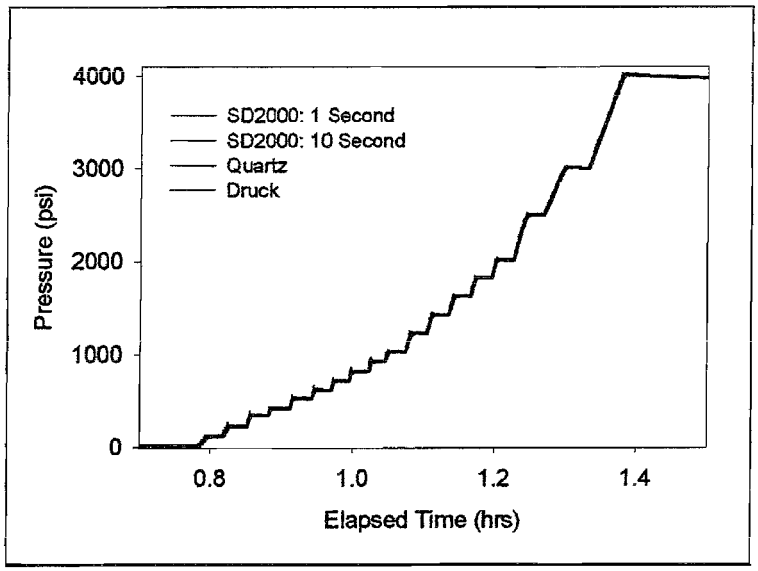

Figure 7.4.6 Plot of the measured-pressure against time for surface electronic-gauges and a downhole fibre-optic pressure sensors during steps in pressure of increasing magnitude.

7.4.4.3 Resolution.

Resolution measurements in the field were difficult to achieve. The apparatus required to produce the small sinusoidal pressure signal shown in chapter 6 was not available. The only measurement that was achieved was a step-change measurement of approximately 0.32 psi. The highway was opened up to ambient surface-pressure and a flexible tube was attached to valve X (figure 7.4.3) and taken to the roof of the cabin to make this the highest point of the pressure circuit. The flexible tubing was filled with oil and all air was removed.

Variation of the height of this column of oil was calculated to cause a pressure dependence of approximately 0.0013psi per mm. The column of oil was mounted on a plate and lifted on and off a box of height 255mm every 60 seconds. Figure 7.4.7 shows the measurement of these pressure changes for the quartz and the SD2000 pressure sensor. The slow DC drift of the quartz gauge is assumed to be due to a long-term stabilisation of pressure in the system due to a previous pressure event. This drift is seen in the quartz gauge but not in the SD2000 sensor. The high signal-to-noise on the step profiles indicates that the true resolution of the SD2000 sensor is much better than 0.3psi.

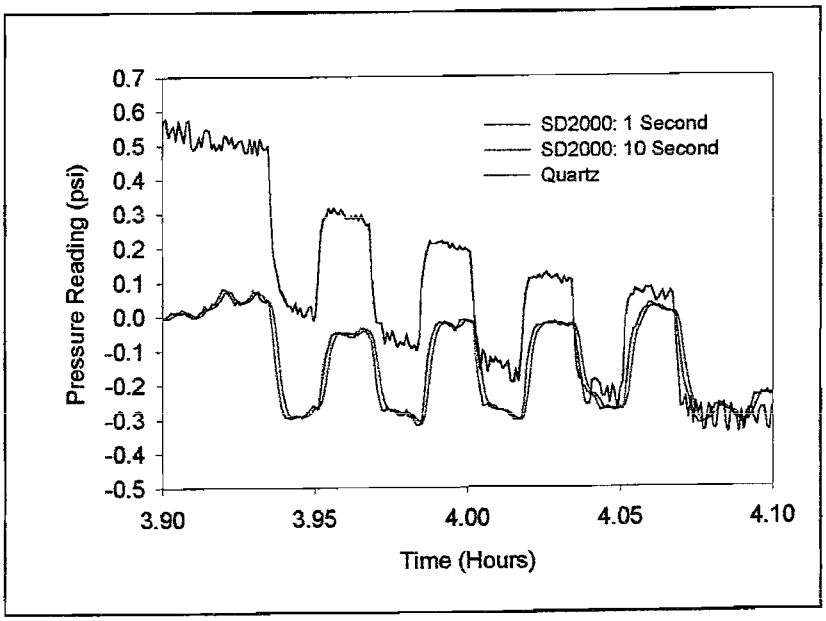

Figure 7.4.7:Response of the Surface Quartz-gauge and Downhole SD2000 fibre-Optic pressure sensor to steps in pressure of approximately 0.32 psi.

Figure 7.4.8 compares Quartz gauge and SD2000 pressure sensor responses to random pressure events during an overnight reading. The offset between the two gauges has been

removed to place both curves within the same pressure scale.

The two gauges track each other extremely well, even down to the smallest of pressure change events. The signal to noise of the fibre-optic sensor is clearly better than that of the Quartz gauge indicating superior resolution. Qualitatively, these results confirm that the SD2000 fibre optic pressure sensor is an extremely high-resolution device.

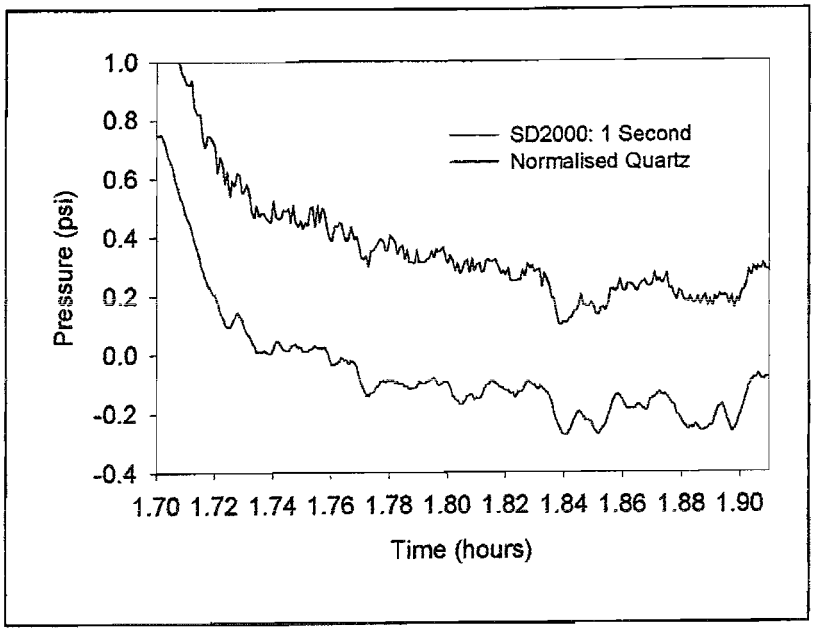

Figure 7.4.8: Sample data taken from an overnight measurement. Quartz and SD2000 pressure sensor responses to natural pressure events during the overnight measurement (at ambient surface pressure) are plotted against time.

7.5 Conclusions.

- Pressure sensors were successfully deployed and the major performance parameters monitored
- The deployment technology was extended in the field with the first ever sequential deployment of two different sensor types within the same highway.
- Temperature and pressure monitoring of well 4-4T1 will continue throughout the year 2000 using fibre-optic sensors.

Chapter 8

Downhole Fibre-Optic Pressure Sensing in the Oil Industry: Discussion

8.1 Introduction

The availability of permanent, real-time, downhole information is seen to be the key to improved oil and gas recovery efficiency.

Existing, electronic, downhole gauges are unable to survive the increasingly high-temperature conditions experienced in modern, deep, offshore oil-wells.

Fibre-optic sensors offer many advantages over existing, downhole electronic gauges and silica, as a base material, was considered to offer the stability required for high-temperature, high-pressure operation.

This thesis has documented a long-term investigation of the effects of high-temperature, high-pressure fluids on silica optical-fibre pressure sensors.

A review of the progress and discoveries that have been made in the topics described in this thesis is presented in this chapter, along with concluding remarks.

8.2 Effects of High-Temperature, High-Pressure Fluids on Fibre-Optic Polarimetric Pressure Sensors.

A polarimetric, fibre-optic pressure sensor has been extensively tested at high-temperature and high-pressure to simulate the downhole conditions in oil wells.

Chapter 2 presented the key results of this study into the effects that high-temperature, high-pressure fluids have on the long-term stability of the pressure sensor.

All uncoated, side-hole-fibre, pressure sensors show a long-term "drift" in measured pressure when exposed to high-temperature, high-pressure fluids. The characteristics of the sensor drift are summarised:

- The sensor drift is permanent, in that the side-hole fibres are transformed from low-birefringence fibres into highly birefringent fibres by the high-temperature, high-pressure treatment. Exposure to water at 300°C for as little as 2 days can produce a side-hole fibre with a beat length of only 2.4mm (measured at 633nm).
- The magnitude and rate of the sensor drift increases disproportionately with increasing

temperature.

- The sensor drift is dependent upon the fluid medium.
  - Water produces the highest drift rate in pressure sensors.
  - Polysiloxane oils caused the lowest drift rate, one sixth as high as water (at 300°C).
- The sensor drift curve of sensors in water and in polysiloxane oil at 300°C changes in drift direction ("Turns Over") between 2 and 4 days.
- Filling the side-holes with water increases the drift rate by a factor of approximately 9.
- The sensor drift is dependent upon the fibre outer diameter and is shown to be proportional to 1/r, where r is the fibre radius.
- The sensor drift is not dependent on applied pressure.
- The sensor drift is not dependent on fibre geometry or composition.

It was concluded that the cause of pressure-sensor drifts in high-temperature, high-pressure fluids was a reaction between the high-temperature, high-pressure fluid and the silica at the fibre surface.

8.3 Stressy Surface Layers in Side-Hole-Fibre Pressure Sensors Exposed to High-temperature, High-Pressure Fluids.

A finite element model was developed and used to investigate the relationship between the pressure sensitivity of a side-hole-fibre and its cross-sectional geometry.

The results of the model show a linear relationship between the pressure sensitivity of a side-hole fibre and the square of the angle φ, between the core-centre to side-hole-centre axis and the core to side-hole tangent. The model was shown to agree very closely with the measured pressure sensitivities of side-hole fibres used to fabricate pressure sensors.

The finite element model was modified to include stressed surface layers within the fibre, at the surface and around the side-holes. The thickness of the layers and the magnitude of the volume expansion (uniform over the layer) were varied. The introduction of stressed surface-layers in side-hole fibres causes a change in the fibre birefringence, which acts in the opposite direction to applied hydrostatic pressure. The magnitude of the birefringence change is proportional to both the thickness of the swollen layer and the magnitude of the swell.

Extending the stressed surface layer into the fibre, beyond the side-holes, causes a "turn

over" in the direction of the resulting fibre birefringence change.

The drift curve of a side-hole-fibre pressure sensor in water at 300°C was qualitatively modelled. The drift is modelled by a uniformly swollen, surface layer that propagates into the fibre with increasing time.

The existence of stressed surface layers in side-hole-fibre pressure sensors exposed to high-temperature, high-pressure water was experimentally demonstrated.

Sensors exposed to water at 300°C and 4000psi for up to 2 days were subsequently etched in hydrofluoric acid to remove the "permanent" effects of the high-temperature water. The results showed the presence of stressed surface layers as deep as 33μm into the silica cladding.

The results of this chapter suggest that any silica, optical-fibre pressure sensor will suffer from drift when exposed to high-temperature, high-pressure fluid environments.

8.4 Effect of Stressed Surface Layers on Other Fibre-Optic Pressure Sensors.

In chapter 4, the optical-path-lengths of silica fibres, and the Bragg wavelengths of fibre Bragg gratings were both shown to increase due to exposure to high-temperature, high-pressure fluids.

When normalised to pressure, both the fibre path-length and the Bragg grating wavelength show drifts of approximately -32,000psi in only 2 days in water at 300°C and 4000 psi. This is compared to a drift of -6000psi shown for side-hole-fibre pressure sensors in chapter 2.

The long-term measurement of optical-path-lengths of cables in high-temperature, high pressure fluids was used as a means for assessing the quality of commercially-available fibre coatings.

A carbon and polyimide dual coating supplied by Spectran has been identified as a suitable coating for cable protection in polysiloxane oil up to 250°C. This coating process is now used commercially to protect multi-mode DTS (distributed temperature sensor) cables for downhole, temperature profiling.

The Spectran coating was applied to side-hole fibres used to fabricate pressure sensors. The coatings significantly improved the sensor stability compared to uncoated-silica pressure sensors. However, the results of long-term measurements at high-temperature and high-pressure show:

- Inadequate stability, outside the specifications of the oil industry.
- High and unpredictable temperature cross-sensitivity of sensors due to the polyimide coating layer.
- The coatings provide no protection of splice regions of which there are 3 in the side-hole-fibre pressure sensor.

8.5 Water Diffusion into Silica Optical Fibres.

In chapter 5, the diffusion of water into silica optical fibres under high-temperature, high-pressure conditions has been considered as a potential cause of fibre pressure sensor drifts.

The spectral loss peaks at 1250nm and 1385nm, corresponding to OH absorption bands, have been monitored in fibres exposed to high-temperature, high-pressure water. Results of the real-time loss-measurements have shown the build-up of hydroxyl due to water diffusion into the optical fibre. In water at 300°C, the loss at 1250nm and 1385nm increased beyond the dynamic range of the measurement indicating that large quantities of molecular water had diffused into the silica fibre.

Loss measurements made on fibres in polysiloxane oil at 300°C and 4000psi showed that water diffuses into the fibre from the fluid medium. Low levels of OH loss were observed in comparison to the measurements made in high-temperature, high-pressure water. The OH loss reached saturation point after long-term exposure.

Comparisons have been made between the experimental results of this study and predicted water diffusion-profiles from diffusion coefficients calculated by other authors. A large discrepancy is shown between the results of this study and those of other authors. The rates of diffusion into silica fibres in this study are significantly greater than those reported for water diffusion into bulk-silica samples.

The discrepancy suggests that there may be different water-diffusion processes involved for glasses in high-temperature gases and high-temperature fluids. Furthermore, the fabrication method of optical fibres may also contribute to the unexpectedly high rates of water diffusion.

The results of this study have only been treated qualitatively. However, the real-time measurement of water diffusion into optical fibres could possibly lead to future research opportunities in the area of glass material-science.

8.6 Novel Hermetic Packaging to Protect Fibre-Optic Cables and Sensors in Downhole Environments.

A novel, hermetic packaging technique was reported in chapter 6. The packaging technique uses liquid metals as the hermetic barrier between high-temperature, high-pressure fluids and silica, fibre sensors and cables. A flexible, silica capillary provides the means for containing the liquid metal and the silica-fibre pressure sensor.

The hermetic package offers many advantages over conventional hermetic coatings:

- The hermetic package is a post-fabrication process enabling:
  - Hermetic protection of the whole sensor assembly including splice regions.
  - Hermetic protection of fibre Bragg grating sensors and devices after the UV writing of the device.
- Liquid metals do not support shear stress and hence provide no additional temperature cross sensitivity to a fibre-optic pressure sensor.
- The liquid metal, in contact with a cleaved fibre or sensor end face, provides a highly reflective, stable mirror. Mirrors relying upon evaporation or electroless deposition of metals onto fibre end faces have been a continuous source of sensor failures in high-temperature, high-pressure environments.

The first sensors protected with the hermetic packaging have been referred to as SD1-series sensors. SD1-series sensors have been shown to operate in polysiloxane oil at 155°C for over 13 months without signal degradation. These sensors show a long-term drift of approximately 1 psi / month. This is an improvement of approximately 1 order of magnitude on carbon-coated pressure sensors and over 200 times improvement on uncoated, silica, pressure sensors.

Chapter 6 described the various steps taken to further improve the SD1-series pressure sensor fabrication method and long-term stability. The resulting sensor design, the SD2-series pressure sensor, included an oil-filled, PTFE sleeve around the hermetic package for additional mechanical protection.

The SD2-series pressure sensor has shown an approximate stability of better than 0.5 psi over 5 months at 155°C and over 3 months at 200°C, in polysiloxane oil. This is an

improvement of 3 orders of magnitude over uncoated, silica pressure sensors.
Recent results up to mid January 2000 (less than one month) suggest the same stability is achieved at 250°C and 300°C. The stability value is currently limited by the measurement instrumentation.

The additional mechanical protection of the PTFE sleeve makes the SD-series sensor suitable for deployment into oil wells. When attached to a mechanically-robust, downlead cable, there are no unprotected or weak points to the whole sensor assembly.

Excellent dynamic response to pressure transients has been shown by this sensor and instrumentation. Furthermore, a resolution of better than 0.01 psi is estimated for the device.

8.7 Oil Field Testing of the Low-Drift Fibre-Optic Pressure Sensor Design.

Chapter 7 reported on the preparations, planned objectives and main achievements of a field trial of SD2-series pressure sensors in Chevron's Coalinga test facility in California.

- SD2-series sensors were successfully deployed into downhole highways to depths of approximately 230m.
  - The SD2-series pressure sensors showed high stability over the field test duration, consistent with the laboratory data presented in chapter 6.
  - Dynamic response and resolution of the sensor was demonstrated in the field trial.
- The first ever sequential deployment of a pressure sensor and DTS (distributed temperature sensor) cable into a single highway was demonstrated.
  - Real time, downhole pressure and temperature data has been captured and will continue to be monitored throughout the year 2000 from these sensors.

8.8 Conclusions.

An understanding of the effects of high-temperature, high-pressure fluids on silica, optical-fibre pressure sensors has been developed.

Experimental results suggest that the diffusion of molecular water into silica optical fibres is the root cause of drifts in fibre-optic pressure sensors and failures of fibre-optic cables.

Diffusion of molecular water and the subsequent reaction with the silica network of the fibre can create highly-stressed layers within optical fibres and pressure sensors. These stressed layers manifest themselves as increases in physical and optical-path-lengths of

fibre cables, increases in the Bragg wavelength of fibre Bragg gratings and changes in the birefringence of side-hole-fibre pressure sensors.

A novel protective packaging technique has been developed which offers hermetic protection to the pressure sensor cable and assembly. This sensor design, the SD2-series pressure sensor has shown an estimated stability of better than 0.1 psi per month at 155°C and 200°C in polysiloxane oil (similar 250°C and 300°C performance are also expected.).

Figure 8.1 summarises the advances that the author has made throughout this investigation. It plots the evolution of pressure sensor coating technology during the course of this PhD between 1996 and 2000.

The SD2-series pressure sensor shows long-term stability and high-temperature performance that out-performs any other downhole pressure-gauge currently available in the world.

Sensor Dynamics are in the process of raising funding for the pressure sensor, developed in this thesis, and make it available to the global oil industry.

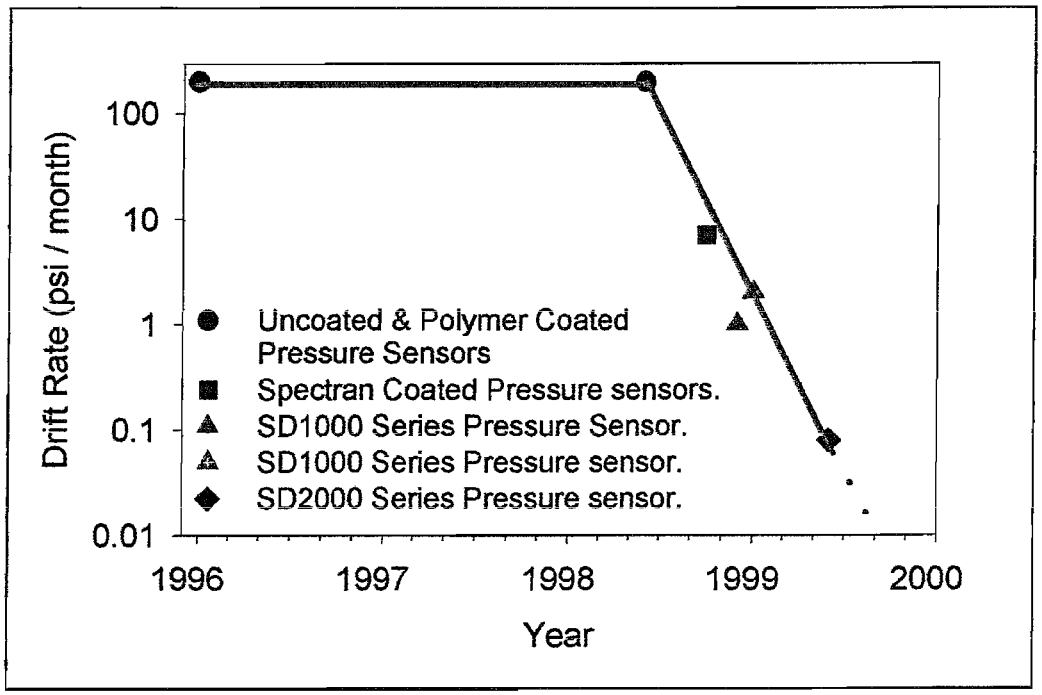

Figure 8.1: Plot of the improvements made to the side-hole-fibre pressure sensor stability between 1996 and 2000.

8.9 Potential Future Research Areas

The main result of this PhD programme has been the development of a stable optical fibre pressure sensor, capable of excellent performance in high-temperature, high-pressure environments. However, in developing this sensor, some of the fundamental properties of silica, fibre-optic coatings and liquid metals have been investigated. In addition to this, the stability of the fibre-optic pressure sensor has asked questions about the performance of the instrumentation used to interrogate the sensor, and improvements in this instrumentation are now required.

Potential areas for new research have therefore resulted from this PhD program. In the area of materials research, a greater understanding of the process of water diffusion in silica is required. Many researchers have published work on water diffusion in glass, and this work continues in laboratories around the world. The results in this thesis suggest a novel method of studying water diffusion into silica. Measurements made at high pressure and at various temperatures could accurately plot the diffusion rates, and diffusion coefficients of water in glass as a function of temperature and pressure.

The investigation of water diffusion in glass can also extend to a study of various glasses, with different thermal and physical properties. Indeed the Optoelectronics Research Centre at Southampton University, in collaboration with Chevron, Sensor Dynamics and EPSRC are in the process of writing a research proposal in this area. The new research will focus on water diffusion in different glasses and the development of novel coatings for hermetically protecting optical fibre cables and sensors.

Further research, directed at understanding the role of gallium in protecting fibres in HTHP fluids, would be a worthwhile study. The reason why the SD series pressure sensor is so stable is not fully understood. The results described in this thesis suggest that gallium may be impervious to molecular water but may also act as a "getter" of molecular water. If gallium does have a gettering property, then it may also have much further reaching implications in devices and applications where extremely low water content fluids are required.

For the SD pressure sensor, further developments are required in order to improve the consistency of the fabrication process. Experiments will also continue to attempt to optimise the pre-treatment process for different operational temperatures of the sensors.

The current instrumentation has instabilities that mask the true performance of the SD

pressure sensor. Ideally, an instrumentation set is required that can be highly multiplexed and that can scan several sensors at high frequency. This development is under way and will involve the use of modern digital demodulation techniques.

Appendix A:

Cross-sectional photographs of each of the side-hole fibres referenced in this thesis are presented in this appendix along with relevant information about the fibres concerning; material composition and geometry.

All fibre claddings are pure silica.

Fibre A:

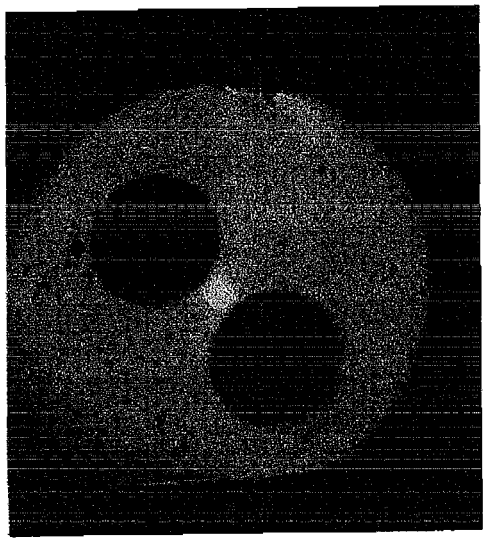

fibre radius r_{cl} (μm)	62.5
side-hole radius r_{SH} (μm)	16.8
core centre to side-hole centre separation (μm)	23.6
Measured fibre pressure sensitivity. (mrad. $psi^{-1}.m^{-1}$)	264.4
Measured fibre offset birefringence ($rad.m^{-1}$)	126.0
fibre core dopant.	Germanium

Fibre B:

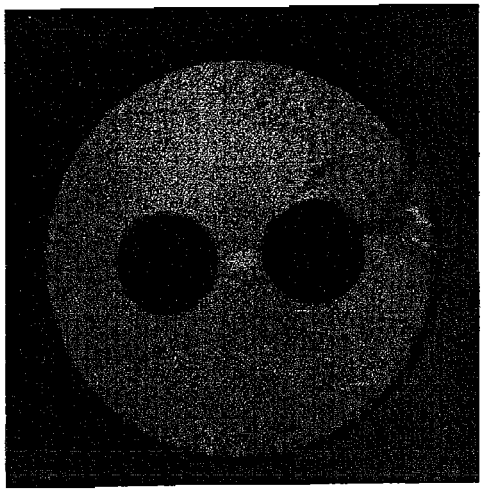

fibre radius r_{cl} (μm)	55.0
side-hole radius r_{SH} (μm)	14.7
Core centre to side-hole centre separation (μm)	21,2
Measured fibre pressure sensitivity. (mrad. $psi^{-1}.m^{-1}$)	241.7
Measured fibre offset birefringence ($rad.m^{-1}$)	120.8
fibre core dopant.	Germanium

Fibre C:

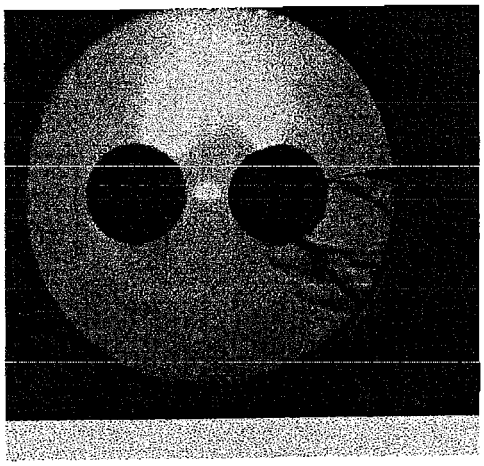

fibre radius r_{cl} (μm)	62.5
side-hole radius r_{SH} (μm)	16.0
core centre to side-hole centre separation (μm)	23.4
Measured fibre pressure sensitivity. (mrad. $psi^{-1}.m^{-1}$)	229.6
Measured fibre offset birefringence ($rad.m^{-1}$)	123.9
fibre core dopant.	Germanium

Fibre D:

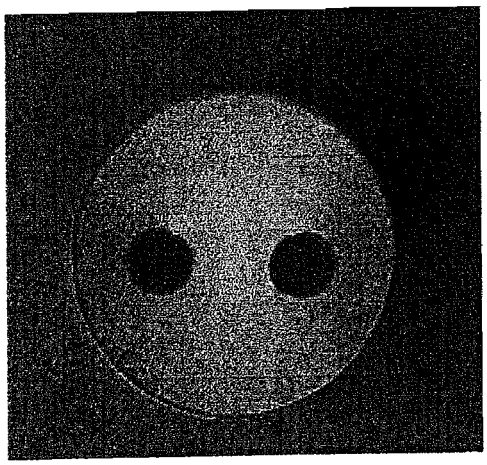

fibre radius r_{cl} (μm)	87.5
side-hole radius r_{SH} (μm)	17.5
core centre to side-hole centre separation (μm)	39.4
Measured fibre pressure sensitivity. (mrad. $psi^{-1}.m^{-1}$)	87.2
Measured fibre offset birefringence ($rad.m^{-1}$)	-14.7
fibre core dopant.	Tantalum

Fibre E:

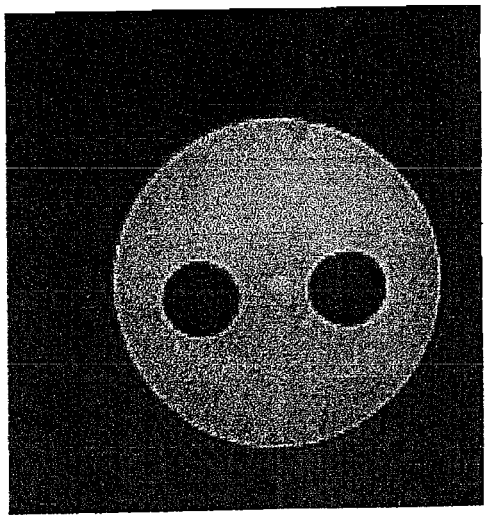

fibre radius r_{cl} (μm)	65.0
side-hole radius r_{SH} (μm)	13.0
core centre to side-hole centre separation (μm)	29.3
Measured fibre pressure sensitivity. (mrad. $psi^{-1}.m^{-1}$)	104.5
Measured fibre offset birefringence ($rad.m^{-1}$)	-6.3
fibre core dopant.	Tantalum

Fibre F:

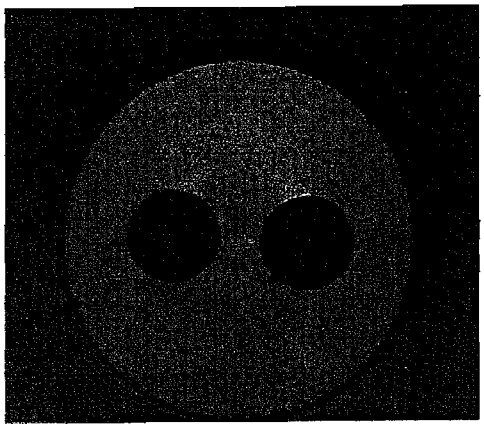

fibre radius r_{cl} (μm)	62.5
side-hole radius r_{SH} (μm)	14.0
core centre to side-hole centre separation (μm)	20.0
Measured fibre pressure sensitivity. (mrad. $psi^{-1}.m^{-1}$)	238.0
Measured fibre offset birefringence ($rad.m^{-1}$)	102.3
fibre core dopant.	Germanium

Fibre G:

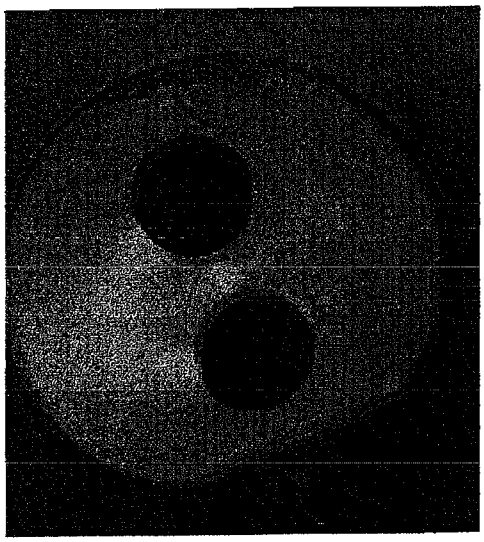

fibre radius r_{cl} (μm)	62.5
side-hole radius r_{SH} (μm)	16.5
core centre to side-hole centre separation (μm)	24.5
Measured fibre pressure sensitivity. (mrad. $psi^{-1}.m^{-1}$)	244.1
Measured fibre offset birefringence ($rad.m^{-1}$)	104.9
fibre core dopant.	Germanium

Fibre H:

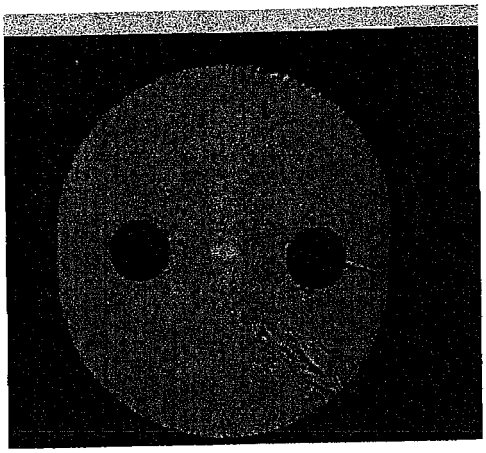

fibre radius r_{cl} (μm)	57.5 to 62.5
Side-hole radius r_{SH} (μm)	9.5
core centre to side-hole centre separation (μm)	30.0
Measured fibre pressure sensitivity. (mrad. $psi^{-1}.m^{-1}$)	40.8
Measured fibre offset birefringence ($rad.m^{-1}$)	139.0
fibre core dopant.	Germanium

Fibre I:

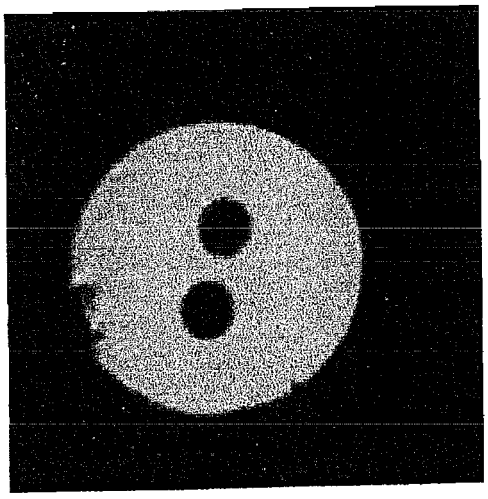

fibre radius r_{cl} (μm)	62.5
side-hole radius r_{SH} (μm)	14.1
core centre to side-hole centre separation (μm)	19.6
Measured fibre pressure sensitivity. (mrad. $psi^{-1}.m^{-1}$)	279.3
Measured fibre offset birefringence ($rad.m^{-1}$)	268.1
fibre core dopant.	Germanium

Fibre J:

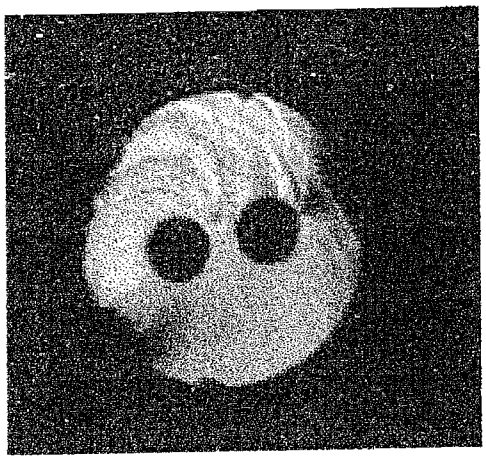

fibre radius r_{cl} (μm)	62.5
side-hole radius r_{SH} (μm)	12.3
core centre to side-hole centre separation (μm)	17.4
Measured fibre pressure sensitivity. (mrad. $psi^{-1}.m^{-1}$)	275.6
Measured fibre offset birefringence ($rad.m^{-1}$)	264.3
fibre core dopant.	Germanium

Fibre K:

fibre radius r_{cl} (μm)	62.5
side-hole radius r_{SH} (μm)	11.9
core centre to side-hole centre separation (μm)	35.9
Measured fibre pressure sensitivity. (mrad. $psi^{-1}.m^{-1}$)	108.2
Measured fibre offset birefringence ($rad.m^{-1}$)	26.0
fibre core dopant.	Tantalum

Fibre L:

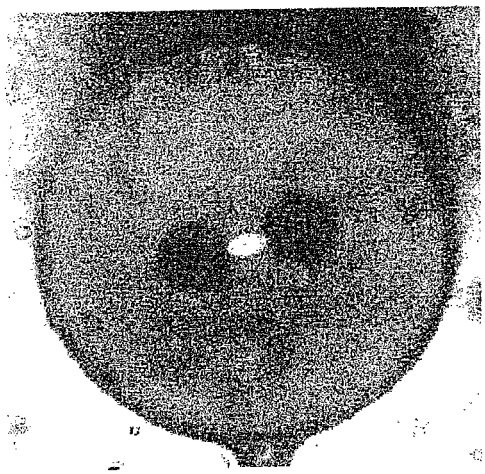

fibre radius r_{cl} (μm)	62.5
side-hole radius r_{SH} (μm)	10.0
core centre to side-hole centre separation (μm)	15.7
Measured fibre pressure sensitivity. (mrad. $psi^{-1}.m^{-1}$)	154.2
Measured fibre offset birefringence ($rad.m^{-1}$)	266.8
fibre core dopant.	Germanium

References:

[1] Anderson, R.N, Oil Production in the 21st Century, *Scientific American,* pp. 68 - 73, March 1998.

[2] Edwards, J.D, Crude Oil and Alternative Energy Production Forecasts for the Twenty-First Century: The End of the Hydrocarbon Era, *AAPG Bulletin,* Vol.81, No. 8, pp. 1292-1305, 1997.

[3] Seismic Technology: Evolution of a Vital Tool for Reservoir Engineers, *Journal of Petroleum Technology,* pp. 22 - 28, February 1999.

[4] Paton,S and Erratt,D, Rocks in a Hard Place, *New Scientist,* pp.34 - 36, 28 August 1999.

[5] Well Logging and Interpretation Techniques, Course for Home Study, Ed.3, Dresser Atlas, USA, 1982.

[6] Vella, M, Veneruso, T and Le Foll, P, The Nuts and Bolts of Well Testing, *Oilfield Review: Well Testing,* pp. 14 - 27, Elesvier, Netherlands, April 1992.

[7] Deruyck, B, Ehlig-Economides, C, Joseph, J, Testing Design and Analysis, *Oilfield Review: Well Testing,* pp. 28 - 39, Elesvier, Netherlands, April 1992.

[8] Humphrys, N.V, Myers, L.G, Pollin, A.G, Hill, S, Treheme, I, Using Interference Tests During Field Startup to Solve Critical Reservoir Management Issues at the Zafiro Field, Offshore Equatorial Guinea, *SPE Production and Facilities,* pp.205 - 211, November 1997.

[9] Vella, M, Veneruso, T and Le Foll, P, Gauges Through the Ages, *Oilfield Review: Well Testing,* p.23 , Elesvier, Netherlands, April 1992.

[10] Unneland, T, Haugland, T, Permanent Downhole Gauges Used in Reservoir Management of Complex North Sea Oil Fields, *SPE Production and Facilities,* pp. 195 - 203, August 1994.

[11] Bezerra, M.F.C, DaSilva, S.F, Thueveny, B.C, Permanent Downhole Gauges: A Key to Optimise Deepsea Production, *Presented at 24th Offshore Technology Conference,* Houston, Texas, 4 -7 may 1992.

[12] Botto, G, De Ghetto, G, Using Downhole Pressure Gauges in Hostile Deep Wells, Villafortuna-Trecate Field, *Journal of Petroleum technology,* pp. 594 - 598, July 1994.

[13] Unneland, T, Manin, Y, Kuchuk, F, Permanent Gauge Pressure and Rate Measurements fir Reservoir Description and Well Monitoring: Field Cases, *SPE Reservoir Evaluation and Engineering,* pp. 224 - 230, June 1998.

[14] Lumsden, P.J, Batten, A.H, Phillips, H.T, Nonintervention Solutions to the Loss of Downhole Data in a Subsea Field, SPE 50672, *Presented at SPE European Petroleum Conference*, The Hague, 20-22 October 1998.

[15] Tetlow, J, Wingate, P, The Britannia Field Development, *Journal of Petroleum Technology,* pp. 40 - 44, August 1999.

[16] Hartog, A.H, Leach, A.P, Gold, M.P, Distributed Temperature Sensing in Solid Cored Fibres, *Electronics Letters,* V.21, pp.1061 - 1062, 1985.

[17] Horiguchi, T, Kurashima, T, Koyamada, Y, Measurement of Temperature and Strain Distribution by Brillouin Frequency Shift in Silica Optical Fibres", *SPIE Proceedings OE/Fibers 1992,* Fiber Optic Sensors II Session, pp.2-13, 1992.

[18] Davis, A. R, Kirkendall, C. K, Dandridge, A, Kersey, A. D, 64 Channel All Optical Deployable Acoustic Array, *Proceedings of the 12th International Conference on Optical Fiber Sensors,* OFA6- 1 to 4, 1997.

[19] Hurtig, E, Grosswig, S, Kuhn, K, Distributed Fibre Optic Temperature Sensing: A New Tool for Long-Term and Short-Term Temperature Monitoring in Boreholes, *Energy Sources,* 19:55-62, 1997.

[20] Karaman, O.S, Kutlik, R.L, Kluth, E.L, A Field Trial to Test Fiber Optic Sensors for Downhole Temperature and Pressure Measurements, West Coalinga Field, California, *Society of Petroleum Engineers (SPE) 35685,* 1996.

[21] Bjornstad, B, Kvisteroy, T, Sensoner, A.S, Eriksrud, M, Fibre Optic well Monitoring System, SPE 23147, Presented at *The Offshore European Conference*, Aberdeen, Uk, 3-6 September 1991.

[22] Bjornstad, B, A Fibre-Optic System for Downhole Monitoring, presented at an *SUT/Inst MC Conference on "Subsea Control and Data Acquisition"*, London, 20-21 April 1994.

[23] Kvisteroy, T, Gusland, O,H, Stark, B, Nakstad, H, Eriksrud, M, Bjornstad, B, Optically Excited Silicon Sensor for Permanently Installed Downhole Pressure Monitoring Applications, *Sensors and Actuators A,* V.31, pp. 164 - 167, 1992.

[24] Kersey, A.D, Optical Fiber Sensors for Downwell Monitoring Applications in the

Oil and Gas Industry, *proceedings of the 13th International Conference on Optical Fiber Sensors*, pp. 326-331, Korea, 1999.

[25] P.Eigenraam, B.S.Douma, A.P.Koopman, Applications of Fibre Optic Sensors and Instrumentation in the Oil and Gas Industry, *proceedings of the 13th International Conference on Optical Fiber Sensors,* pp.602-607, Korea,1999.

[26] Jouve.P, Cretenet, A, Pouleau, J, Optical Sensor for Downhole Applications (translation), *Mesucore,* pp 93 - 102, November 1991.

[27] Lequime, M, Fiber Sensors for Industrial Applications, OtuD1-1, *proceedings of the 12th International Conference on Optical Fiber Sensors,* Williamsburg, Virginia, 28/31 October 1997.

[28] Schroeder, R.J, Yamate, T, Udd,E, High Pressure and Temperature Sensing in the Oil Industry Using Fiber Bragg Gratings Written onto Side Hole Single Mode Fiber, Tu2-3, *OFS 13*, pp. 42 - 45, Korea, April 1999.

[29] Kringlebotn, T.T, Optical Fiber Distributed Feedback Laser, *US Patent 5844927*, 1998.

[30] Kluth, E.L.E, Remotely Deployable Pressure Sensor, *United States Patent 5582064, 1996.*

[31] Xie, H, M, Dabkiewicz, Ph, Ulrich, R, Okamoto, K, Side-Hole Fiber for Fiber-Optic Pressure Sensing, *Optics Letters,* Vol.11, No.5, pp.333-335, 1986.

[32] Jansen, K & Dabkiewicz, Ph, High Pressure Fiber-Optic Sensor With Side-Hole Fiber, Fiber Optic Sensors II, *SPIE Vol.798*,(1987), pp.56-61.

[33] Croucher, J, A, Gomez-Rojas, L, Kanellopoulos, S, Handerek, V, A, Approach to Highly Sensitive Pressure Measurements Using Side-Hole Fibre, *Electronics Letters*, V.34, No.2, (1998), pp.208-209.

[34] Yoshida, K, Morikawa, T, Fabrication and Characterisation of Side-Hole Single-Mode Optical Fibers, *Optical Fiber Technology 2,* Vol.2, pp.285-290, 1996.

[35] Xu, M, G, .Johnson, M, Fahradiroushan, M, Dakin, J, P, Novel Polarimetric Fibre Device for Interrogating 'White Light' Interferometers, *Electronics Letters*, V.29, No.4, (1993), pp.378-379.

[36] Lemaire, P, J, Atkins, R, M, Mizrahi, V, Reed, W, A, High Pressure H_2 Loading as a Technique for Achieving Ultrahigh UV Photosensitivity and Thermal Sensitivity in GeO_2 Doped Optical Fibres, *Electronics Letters,* Vol.29, N0.13, pp. 1191-1193,

1993.

[37] ANSYS User's Manual for Revision 5.1 - Volumes I-IV, Swanson Analysis Systems, Housten, Pennsylvania, 1994.

[38] Snyder, A, Love, J, D, Optical Waveguide Theory, Chapman and Hall, London, 1983.

[39] Bansal, N, P, Handbook of Glass Properties, Academic Press Inc, London, 1986.

[40] Yariv, A,Yeh, P, Optical waves in Crystals: Propagation and Control of Laser Radiation, Wiley Interscience, New York, 1984.

[41] Neumann,E, G, Single-Mode Fibers: Fundamentals, Springer-Verlag, London, 1988.

[42] Clowes, J, Syngellakis, S, Zervas, M, N, Pressure Sensitivity of Side-Hole Fibers, *Photonics Technology Letters*,V.10, N0.6, (1998)., pp.857-859.

[43] Huff, R.G, Diamarcello, F. V, Hart, A. C, Amorphous Carbon Hermetically Coated Optical Fibers, *Technical Digest for Optical Fiber Communication Conference,* Paper TUG-2, 1988.

[44] Dong, L, Cruz, J. L, Reekie, L, Archambault, J. L, Tuning and Chirping Fiber Bragg Gratings by Deep Etching, *IEEE Photonics Technology Letters,* Vol.7, No.12, pp.1433-1435, 1995.

[45] B.J.Todd, Outgassing of Glass, *Journal of Applied Physics,* V.26,No.10,(1955),pp 1238-1243.

[46] B.J.Todd, Equilibrium between Glass and Water Vapour at Bake-Out Temperatures, *Journal of Applied Physics,* V.27,No.10,(1956), pp 1209-

[47] E.N.Boulos, N.J.Kreidl, Water in glass: a Review, *Journal of the Canadian Ceramic Society,* V.41,(1972),pp 83-90.

[48] H.Scholze, Gases and Water in Glass. Part One, *The Glass Industry,* October 1966, pp 546-551.

[49] H.Scholze, Gases and Water in Glass Part Two, *The Glass Industry,* November 1966, pp 622-628.

[50] H.M.Doremus, Internal Hydroxyl Groups Near the Surface of Silica, *J.Phys. Chemistry,*V.75, No.20, (1971).

[51] A.J.Moulson, J.P.Roberts, Water in Silica Glass, *Trans. Faraday Soc.,* 57,(1961),pp 1208-1216.

[52] F.M.Ernsberger, Molecular Water in Glass, *Journal of the American Ceramic Society- Discussions and Notes,* V.60, No.1-2,(1977),pp 91-92.

[53] R.F.Bartholomew, High Water Containing Glasses, *Journal of Non-Crystalline Solids,* 56(1983), pp331-342.

[54] R.Pfeffer, M.Ohring, Network Oxygen Exchange During Water Diffusion in SiO_2, *Journal of.Applied.Physics.*, V52 (2), (1981), pp.777-784.

[55] Helmich, Rauch, On the Mechanism of Diffusion of Water in Silica Glass, *Glastesche. Berichte,* No8, (1993).

[56] H.Wakabayashi, M. Tomozawa, Diffusion of Water into Silica Glass at Low Temperature, *Journal of the American Ceramic Society,* V.72, No.10,(1989).pp 1850-1855.

[57] M.Nogami, M.Tomozawa, Effect of Stress on Water Diffusion in Silica Glass, *Journal of the American Ceramic Society,* V.67,No.2,(1984), pp 151-154.

[58] M.Tomozawa, H.Li, K.M.Davis, Water Diffusion, Oxygen Vacancy Annihilation and Structural Relaxation in Silica Glasses, *Journal of Non-Crystalline Solids,* 179,(1994)pp 162-169.

[59] H.Wakabayashi, M. Tomozawa, Diffusion of Water into Silica Glass at Low Temperature, *Journal of the American Ceramic Society,* V.72, No.10,(1989).pp 1850-1855.

[60] R.H.Doremus, Diffusion of Water in Silica Glass, J.Mat.Res.,V.10, No.9, (1995), pp. 2379-2389.

[61] G.J.Roberts, J.P.Roberts, Influence of Thermal History on the Solubility and Diffusion of 'Water' in Silica Glass, *Phys.Chem.Glasses*, V.5, No.1, (1964), pp.26-32.

[62] Agarwal, M.Tomozawa,W.A.Lanford, Effect of Water Diffusion in Silica Glass at Various Temperatures, *J.Non-Cryst.Solids*, V.167, (1994), pp.139-148.

[63] I.Burn, J.P.Roberts, Influence of Hydroxyl Content on the Diffusion of Water in Silica Glass, *Phys.Chem. Glasses*, V.11, No.4, (1970), pp.106-114.

[64] M.Tomozawa, Concentration Dependence of the Diffusion Coefficient of Water in SiO_2 Glass, *Comms. Am.Ceram.Soc.*, V.68(9), (1985), C-251-C-252.

[65] G.Hetherington, K.H.Jack, Water in Vitreous Silica: Part 1. Influence of 'Water'Content on the Properties of Vitreous Silica, *Physics and Chemistry of Glasses,* V.3, No.4,(1962), pp 129-133.

[66] O.Humbach, H.Fabien, U.Grzesik, U.Haken, W.Heitmann, Analysis of OH Absorption Bands in Synthetic Silica, *J. Non-Cryst. Solids*, V203, (1996), pp.19-26.

[67] D.B.Keck, R.D.Maurer, P.C.Schultz, *Appl.Phys.Lett*, V.22, (1973), pp.307-

[68] P.Kaiser, A.R.Tynes, *Appl. Opt.* V.11, (1972), pp.1502-

[69] J.Crank, Mathematics of Diffusion, Clarendon Press, Oxford, (1975).

[70] Clowes, J.R, Kluth, E.L.E, Varnham, M.P.V, Rutt, H, Crawley, C.M, Apparatus for Measuring Pressure, *GB Patent Application GB9900739.2*, December 1998.

[71] CRC handbook of Chemistry and Physics, 73rd Edition, CRC Press Inc, 1992, London.

[72] Hadeler, O, Ronnekleiv, E, Berendt, M, Zervas, M, Temperature Distribution Along DFB Fibre Lasers, *IEE Colloquium on Optical Fibre Gratings,* pp.15/1-15/6, 1999.

[73] Spicer, L.R, Laying Cables, *United Kingdom Patent GB2171218*, Filed 6/5/1982.

[74] Kluth, E.L.E, Varnham, M.P, Apparatus for the Remote Measurement of Physical Parameters, *United States Patent 5,570,437*, October 1996.

Publications.

[1] Clowes, J, R, McInnes, J, Zervas, M.N, Payne, D. N, Effects of High-Temperature and Pressure on Silica Optical Fiber Sensors, *IEEE Photonics Technology Letters,* Vol.10, No.3, pp. 403 - 405, 1998.

[2] Clowes, J. R, Syngellakis, S, Zervas, M. N, Pressure Sensitivity of Side-Hole Optical Fiber Sensors, *IEEE Photonics Technology Letters,* Vol 10., No. 6, pp.857 - 859, 1998.

[3] Clowes, J. R, Edwards, J, Grudinin, I, Kluth, E. L. E, Varnham, M. P, Zervas, M. N, Crawley, C. M, Kutlik, R. L, Low Drift Fibre-Optic Pressure Sensor for Oil Field Downhole Monitoring, *Electronics Letters,* Vol35, No. 11, pp.926 - 927.

[4] Clowes, J.R, Kluth, E.L.E, Varnham, M.P.V, Rutt, H, Crawley, C.M, Apparatus for Measuring Pressure, *GB Patent Application GB9900739.2*, December 1998.

Conferences.

[1] Clowes, J. R, McInnes, J, Zervas, M. N, Payne, D. N, Effects of High Temperature and Pressure on Silica Optical Fibre Sensors, *presented at the 12th International Conference on Optical Fibre Sensors,* Williamsberg, Virginia, USA, 28 - 31 October 1997.

[2] Kluth, E. L. E, Varnham, M. P, Clowes, J. R, Kutlik, R. L, Upgradable sensing systems for the oil and gas industry, *presented at the SPIE International Symposium on Environmental and Industrial Sensing, 19-22 September 1999.*

[3] Kluth, E.L.E, Varnham, M.P, Clowes, J.R, Kutlik, R.L, Crawley, C.M, Heming, R.F, Advanced Sensor Infrastructure for Real-Time Reservoir Monitoring, ***Presented at the SPE Europec 2000 conference on Integrated Reservoir Management,*** Paris, Oct 2000.

Acknowledgements

I would like to thank my supervisors, at the Optoelectronics Research Centre, Prof. Michalis Zervas, and at Sensor Dynamics Ltd, Dr. Erhard Kluth and Dr. Malcolm Varnham, for their help and guidance throughout this PhD and in writing this thesis.

I am grateful to all the staff at Sensor Dynamics Ltd, both past and present. I would particularly like to thank Jim McInnes for his help in introducing me to the practical side of fibre-optics, Irina Grudinina and Jeanie Edwards for their help in carrying out experimental work included in this thesis, and Geoff Gamble for getting me, and the field trial hardware, to California in one piece.

I would also like to thank Dr. Stavros Syngellakis of the Mechanical Engineering department at the University of Southampton for his work on the finite element model used in this study.

The assistance of Malcolm Varnham and Roy Kutlik (of Chevron Research and Technology) during the field trial deployments is greatly appreciated.

The work was carried out under a case studentship supported by Sensor Dynamics Ltd and EPSRC. I would like to thank them and also Chevron research and Technology for financial support during this PhD.

Finally, I would specially like to thank Rachel Fisher for her love, support and patience over the last 4 years.